UNIVERSITY OF CALIFORNIA

Santa Barbara

Ruthenium Nitrosyl Salen and Salophen PhotoNORMS: Biological Studies and Applications towards Small Molecule Delivery Platforms

A dissertation submitted in partial satisfaction of the

requirements for the degree Doctor of Philosophy

in Chemistry

by

Meredith Anne Crisalli

Committee in charge:

Professor Peter C. Ford, Chair

Professor Trevor Hayton

Professor Norbert Reich

Professor Ram Seshadri

December 2014

The dissertation of Meredith Anne Crisalli is approved.

_____

Prof. Trevor Hayton

_____

Prof. Norbert Reich

_____

Prof. Ram Seshadri

_____

Prof. Peter C. Ford, Committee Chair

November 2014

Ruthenium Nitrosyl Salen and Salophen PhotoNORMS: Biological Studies and Applications towards Small Molecule Delivery Platforms

by

Meredith Anne Crisalli

ACKNOWLEDGEMENTS

I would like to thank my advisor, Dr. Peter C. Ford for his many years of support and encouragement in completing work at UCSB and abroad at USP. He has given me invaluable advice on research, publications, and presentations. Thank you to my research group members for the hours of research talks, inside jokes, working together on projects, and supporting each other at conferences. A huge thank you to Agustin Pierri, Po-Ju Huang, Tony DeMartino, and Megan Chui for years of coffee and candy trips.

At the Universidade de São Palo, I am very grateful for the support of Dr. Roberto Santana de Silva and his lab members for their encouragement in learning Portuguese and training at USP. A special thank you to Dr. Maurico Boscolo, Dr. Clayston Pereira, and Dr. Lilian Franco for helping me practice Portuguese prior to my research trip to Brazil.

I am very thankful for my close friends at UCSB. Hannah Kallewaard, my amazing roommate for over three years, and Sara Nownes, who kept me sane through entrance exams, orals, proposal writing, and running buddies. You are both amazing women who have helped keep me motivated as well as laugh during our weekends with David Lum and Josh Kelley.

I have a lot of love and thanks to give to my family. My parents for raising me to be inquisitive and siblings, Alycia, Evan, and Lyndsay along with their spouses Nicholas, Christina, and Matt, all of whom have supported me through many years of school and very bad chemistry jokes. Finally, thank you to my wonderful husband Pete who has always been encouraging. Even though we were 300 miles away you have always been supportive, shared your humor, and made me strive to be a better researcher and scientist.

Vita of Meredith Anne Crisalli
May 2014

EDUCATION

2009- 2014	Ph.D. Candidate, Inorganic Chemistry, University of California, Santa Barbara
2004-2008	B.A. Chemistry, Willamette University, Salem, Oregon

PUBLICATIONS

- **Crisalli, M. A.**; Franco, L. P.; Silva, B. R.; Bendhack, L. M.; Santana da Silva, R.; Ford, P.C.; "The Photoactive Release of Nitric Oxide from a Water Soluble Ruthenium Nitrosyl Complex, Photochemical and Biological Studies", *In Preparation.*

WORK EXPERIENCE

- Research Associate, LS9, Inc. (REG Life Sciences, LLC) August 2008- September 2009
  Analytical Chemist with Research and Development – Main duties; sample quantification of organic compounds on a Thermo GC-FID, method development in ChromQuest software, gas management and ordering for the analytical laboratory, head of maintenance for GCMS, data entry software, and GC-FID maintenance

SCIENTIFIC EXPERIENCE

- 2009- Present – Ph.D. Research, Lab of Dr. Peter C. Ford.
  Research centered on the synthesis, characterization, and purification of photosensitive ruthenium nitrosyl complexes for use in biological systems. Studies centered on the controlled release of nitric oxide as a radiation sensitizer.
- 2013 April-June – Universidade de São Palo in Rieberião Preto, Brazil.
  International internship including language immersion and research completed in Portuguese. Cell viability studies with drug administration and myograph studies with rat aortas. A continuation of doctoral research.
- 2007-2008 – Willamette University, Lab of Dr. Karen McFarlane Holman.
  Senior Thesis Research on the interactions of glutathione with the ruthenium centered anti-cancer drug, NAMI-A.
- 2006 – Otago University, Lab of Dr. Rex T. Weavers.
  Synthesis of radio labeled flavonoids under the direction of Benjamin T. Compton.

PRESENTATIONS

- 2014 – "Release of nitric oxide from ruthenium centered PhotoNORMs and their use as small molecule delivery platforms", **Crisalli, M. A.**; Franco, Lilian P.; Pierri, Agustin E.; Huang, Po-Ju; Santana da Silva, Roberto; Ford, Peter C.; Abstracts of Papers, 248th ACS National Meeting & Exposition, San Francisco, CA, United States, August 10-14, 2014, INOR-118.
- 2013 – "Biocompatible ruthenium nitrosyl synthesis and biological studies" Southern California Inorganic Photochemistry Conference, Catalina Island, September
- 2012 – "Photolyzed nitric oxide release from ruthenium scaffolds" Southern California Inorganic Photochemistry Conference, Catalina Island, September

- 2011 – "Photolyzed nitric oxide release with ruthenium metal centers" Southern California Inorganic Photochemistry Conference, Catalina Island, September
- 2010 – "Photochemical nitric oxide release by ruthenium salen derivatives" Southern California Inorganic Photochemistry Conference, Catalina Island, September

POSTER PRESENTATIONS

- 2013 – "Quantum yields of nitric oxide production from photoactive ruthenium nitrosyls and their covalent attachment to nanoparticle antennas", **Crisalli, M. A.**; Bordini, J.; Tfouni, E.; Ford, P. C. From Abstracts of Papers, 245th ACS National Meeting & Exposition, New Orleans, LA, 2013, INOR-221
- 2012 – "Modifying photoactivate ruthenium salen nitrosyls for covalent attachment to QDs and quantum yield studies of NO release", **Crisalli, M. A.**; Works, C. F.; Ford, P. C.; 243rd ACS National Meeting & Exposition, San Diego, CA, 2012, INOR-865 and selected for SciMix
- 2008 – "IR spectroelectrochemical investigations of the anticancer drug, NAMI-A", R**oberts, Meredith A.**; Fryd, Rachelle L.; Witkowsky, Lea B.; McFarlane Holman, Karen L.; 235th ACS National Meeting, New Orleans, LA, 2008, INOR-789

RECOGNITIONS

- 2012 – 2014 UCSB ConvEne IGERT Fellow
- 2012 – ConvEne IGERT Associate
- 2009 – Elected, Phi Lambda Upsilon, Chemical Honor Society, UCSB
- 2007-2008 – William B Webber Scholarship, faculty selected award for one chemistry major to create and present lesson plans and activities for 5th grade classes to increase the love of science in youth

TEACHING EXPERIENCE

2012 – Mentored visiting undergraduate, Emma Norman, from the University of Southampton, UK and designed a project for her master's thesis research.

- 2011 – Mentored incoming graduate students, Ellie Pedrick and Susan Rich
- 2009-2011 – UCSB Introductory Chemistry Laboratory TA (6 quarters)

SKILLS

- Organic and Inorganic synthetic techniques
- AT-IR
- Fluorescence and Emission Spectrometer
- Gas Chromatography
- Column Chromatography
- Thin Layer Chromatography
- Solvent distillation techniques
- Schlenk line techniques
- HPLC
- Varian FT-IR
- Inert glove box techniques
- 400 mHz and 500 mHz Varian NMR
- Thermo GC-FID
- UV-Vis Spectrophotometer
- Sievers Nitric Oxide Analyzer 280i
- Liquid
- Cell plating and incubation
- MTT assay
- Chromquest
- ChemDraw
- Magnetic Susceptibility Balance
- SciFinder
- Excel
- Prism
- Igor

ABSTRACT

Ruthenium Nitrosyl Salen and Salophen PhotoNORMS: Biological Studies and Applications towards Small Molecule Delivery Platforms

by

Meredith Anne Crisalli

Nitric oxide (NO) is an endogenously produced small molecule involved in neural transmission, immune response, and blood pressure regulation. The radical nature of NO has also been studied for its ability to increase radiation damage in hypoxic cells, thus improving radiation chemotherapy. In this vein, we are committed to generating molecules that utilize an external trigger to allow for controlled release of NO in biology.

Photochemical release of NO allows for specific location, timing, and dosage of a drug and has the potential to limit wide spread side-effects common to chemotherapy treatments. Several novel ruthenium nitrosyls have been synthesized and studied for their photoactive nitric oxide release. Compounds were characterized by mass spectroscopy, NMR, UV-visible spectra, IR, elemental analysis, photochemical reactivity and ability to release NO. Quantum yields and efficiency measurements were conducted by monitoring the moles of NO produced due to light irradiation. The release of NO was detected by a Nitric Oxide Analyzer in real time.

Two major compounds will be discussed, a water soluble, water stable ruthenium nitrosyl for applications in biological systems and a hydrophobic ruthenium nitrosyl variant which was infused into a polymer matrix with up-converting nanoparticles (UCNP). The water soluble compound Ru(NO)(salen-CO_2H)Cl **1**, has been studied for its photochemistry, cytotoxicity on a murine melanoma cancer cell line, and vasodilation in murine aortic rings. The hydrophobic compound, Ru(NO)(salophen)Cl, was loaded into a polymer matrix with UCNP, utilizing unique properties of UCNPs to shift the excitation wavelength into the near infrared region, where there is better tissue penetration of light. This document contains the synthetic, photochemical, and studies on the efficiency of NO release for each compound.

Table of Contents

LIST OF FIGURES

LIST OF SCHEMES

LIST OF TABLES

Chapter 1. Introduction

1.1 NO in Biology

In 1987 nitric oxide (NO) was observed to be an endogenously produced small molecule for biological signaling.[1, 2] Once thought to solely be a toxic inorganic gaseous molecule, NO has now been found to possess a myriad of roles in biology, many of which are concentration dependent and closely regulated by the body. As a signaling molecule, NO is responsible for smooth muscle relaxation, vasodilation, and neurotransmission at nanomolar concentrations.[3] NO is also generated as an immune response to pathogens in much higher concentrations, inducing cell death.[4] NO can be generated and utilized in three separate regulatory roles, by three different nitric oxide synthase enzymes: iNOS (immune system), eNOS (endothelial tissue), and nNOS (nervous system).

One of the more pertinent biological applications of NO is vasodilation. NO is produced in endothelium cells from oxidation of *L*-arginine to *L*-citrulline, a process catalyzed by the P450 type enzyme eNOS.[5] The resulting NO then diffuses through smooth muscle tissue and binds to the iron heme of soluble guanylyl cyclase (sGC), the enzyme that catalyzes conversion from guanosine triphosphate (GTP) to cyclic guanosine monophosphate (cGMP). The net result is the NO-triggered induction of arterial vaso-relaxation.[6]

1.2 NO in Cancer

The rapid growth of tumors causes the formation of irregular blood vessels which leads to portions of a tumor being oxygen deficient. The lack of oxygen results in anaerobic respiration and the buildup of lactic acid within the tumor, lowering the pH.[7] Primary and metastatic tumors have both been shown to exhibit slightly acidic pH values relative to the pH

observed in normal, healthy tissue.[7] The acidic and hypoxic environments in tumors inhibits radiation induced apoptosis and the efficacy of radiation therapy.

NO has also been shown to modulate the growth of tumors, exhibiting both tumoricidal and tumor promoting behavior with strong dependence upon the concentration and location of up-regulation or release of NO. In low concentrations, NO helps cell proliferation and protects against apoptosis.[8 9] Alternatively, increased NO concentrations have been observed to suppress cellular respiration and DNA synthesis and shift metabolic pathways to remove iron storage in tumors through immune response.[10,11,12] The impacts of DNA synthesis suppression are attributed to either radical attack damaging DNA or binding to the DNA repair mechanisms, which can result in gene mutations or apoptosis at mM concentrations.[12]

The radical character of NO has proven useful as a γ-radiation sensitizer, a valuable feature in the radiotherapy of hypoxic tumors that have reduced radiation sensitivity as a result of their low oxygen concentrations.[13] The generation of NO at a hypoxic tumor site as both a vasodilator and a radiation sensitizer increases both the oxygen concentration and the concentration of radiation sensitizers, specifically NO and O_2. Owing to the fast diffusion and short lifetime of NO, radiation treatment and NO production would need to be administered simultaneously. The ability of photoactive releasing molecules to control location, timing, and dosage is ideal for this form of photo dynamic therapy (PDT).

1.3 Enemark-Feltham Notation

Nitric oxide as a free radical, depicted as NO• has the potential to either gain an electron to become NO^-, or lose an electron to form NO^+. With triple bond character, NO^+ will bind linearly to metals with an MNO bond angle of 180° while the valance bond structure for NO^- will exhibit a MNO bond angle of 120°, designated as bent. Upon binding with transition

metals however, the NO bond can be directed to a different binding mode due to ligand field effects changing the oxidation state of the metal.[14] The formal charge and electron assignments become more difficult when NO binds to a metal with several possible oxidation states and results in two isoelectronic designations, for example Ru(II)-NO^+ and Ru(III)-NO• as resonance forms.

Enemark and Feltham therefore devised a notation in order to simplify assignment of the oxidation state of both metal and NO ligand. Total electrons in the system are assumed to belong to the metal-NO conjugate and is depicted as $\{M\text{-}NO\}^n$ where *n* is equal to the total valance *d* electrons from the metal plus the π^* electron contribution from the nitrosyl. The example above can therefore be written as $\{Ru\text{-}NO\}^6$ where 6 electrons are shared between the metal and nitrosyl. Moreover, the Enemark-Feltham notation allows for the ambiguity of a metal nitrosyl bond angle (M-N-O) that is not completely linearly bound at 180° nor completely in the bent form at 120°.

1.4 Photochemistry of NO Releasing Complexes

Copious numbers of metal complexes have been studied for their NO releasing capabilities. The main thrust of the research has focused on a few metals capable of releasing NO photochemically known as photoactive nitric oxide releasing molecules or photoNORMs. Furthermore, the ideal wavelength for biological applications occurs where deoxygenated hemoglobin, melanin, and water do not absorb strongly and tissue penetration is deepest. This leaves a therapeutic window between 700-1100 nm.[15] Initial studies focused employing iron complexes, primarily due its earth abundance and common use in heme structures, followed by chromium, ruthenium, and more recently, manganese. The structures of several photoNORMs that have been well-studied are included in Figure 1.1.

The canonical NO releasing complexes were first reported in 1858 with the studies of M L. Roussin. Roussin prepared a new synthetic iron sulfur cluster by reacting nitroprusside with sulfur to produce an iron sulfur salt.[16] The resulting complexes, Roussin's Red Salt dianion $Fe_2S_2(NO)_4^{2-}$ (RRS) and Roussin's black salt $Fe_4S_3(NO)_7^-$ (RBS), were observed to release NO upon heating or photochemical excitation. They also possess the added advantage of water solubility.[17] The large number of NO ligands sequestered in the inactivated complex allows for multiple moles of NO to be released per mole of iron compound upon thermal heating or photochemical activation. In experiments with hypoxic V79 Chinese hamster lung fibroblast cancer cells, RRS was proven to increase the potency of gamma-radiation therapy when cells were exposed to light and NO was released.[18] Photoactivated release at 365 nm of NO is quite high for RBS, with quantum yields ranging from 0.09 when irradiated in pH 10 buffer to 0.40 in acetone.[19] Unfortunately, these compounds are thermally unstable and decompose over time at biological temperatures, and are unstable to oxygen which severely limits biological applications. With consideration of the instability of RRS and RBS, Roussin's red salt esters (RSE) were synthesized to help stabilize the Fe-S-Fe bonds while retaining photoactive NO releasing abilities.[20] The RSE complexes reported also retained partial oxygen and thermal sensitivity as the parent compounds with 10% decomposition in aerated solvent over 30 hours in the dark.[20] Chromium species have also displayed great ability to release NO. The most studied being $Cr(III)(cyclam)(ONO)_2^+$, ("CrONO"), which possesses a ligand field absorption band allowing for sufficient absorbance for photoactivation at 550 nm and a quantum yield for NO release of 27% upon irradiation at 436 nm.[21] It has been shown to induce vasodilation in porcine arteries when excited at 470 nm and has exceptional stability in the dark over time. Kinetic studies of the compound have shown that

the release of NO is dependent on the presence of oxygen or glutathione as a trapping agent, the highly reducing environment of tumors can therefore be used to trap the photoproduct and minimize recombination with NO.[7]

Mascharak and coworkers have been studying manganese nitrosyl derivatives with di-carboxiamine ligands. One such compound, with a quinolyl-carboxamide, $[(PaPy_2Q)Mn(NO)](ClO_4)$, displays an absorbance maxima at 670 nm in water and a molar absorptivity of 450 M^{-1} cm^{-1}, indicating valuable photochemical properties. Indeed, the improved extinction coefficient and lability of the manganese-NO bond afford a quantum yield of NO release at 69.4% when irradiated at 550 nm. However, it should be noted that these results were determined in extremely high concentrations with a high intensity of light, due to limitations in actinometry, therefore <99.999% of light was assumed to be absorbed for quantum yield calculations.[22] Moreover, the carboxamide manganese nitrosyl has not been exposed directly to cells but rather embedded into a polymer matrix to prevent complex release, indicating possible cytotoxicity of the free complex. Therefore continuing research has focused on the encapsulation of the compound within a porous Si-MCM-41 structure for the purpose of treating drug resistant bacteria with high concentrations of NO upon irradiation to induce apoptosis. This method of NO treatment has shown positive results in cell death when bacteria is exposed to 15-50 mg of the 2% wt loading MCM-41.[23]

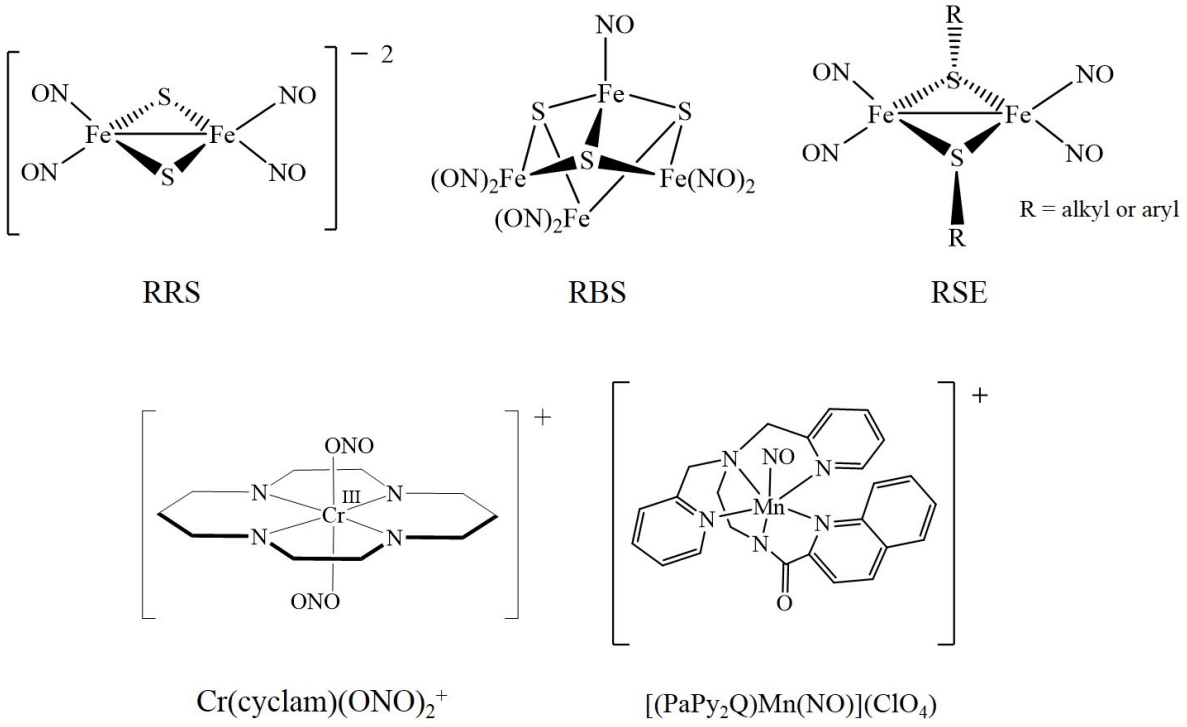

Figure 1.1. PhotoNORMs: Roussin's Red Salt (RRS), Roussin's Black Salt (RBS), Roussin's Red Salt Ester (RSE), $Cr(cyclam)(ONO)_2^+$, and $[PaPy_2Q)MN(NO)](ClO_4)$.

1.5 Ruthenium nitrosyls

Ruthenium centered nitrosyls have been extensively studied due to efficient release of NO upon light irradiation (reference). DFT calculations have shown the release of NO to be associated with excitation of the metal-to-ligand charge transfer (MLCT) which increases electron density in the π^*_{NO} orbital, effectively promoting NO release.[24] Initially synthesized as a pro-catalyst for the epoxidation of alkenes[25] and as Lewis acid catalysts that had to be shielded from light during experiments,[26] the Ru(NO)(salen)Cl [salen = N,N′-bis-(salicylidiene)ethylenediaminato] compound was studied in this laboratory as a photochemical NO precursor, informing possible therapeutic properties of such complexes.

Chelating ligands with donor atoms of nitrogen, oxygen, phosphorus, and sulfur help to stabilize the ruthenium compounds in the Ru(II) oxidation state. Therefore ligands such as

Schiff bases, porphyrins, and di-carboxiamines have been studied as stable NO releasing molecules.[27] Di-carboxiamines have shown great promise with quantum yields for NO release ranging from 5% up to 18% with irradiation wavelengths below 400 nm (ultraviolet excitation), however these compounds are not water soluble.[27]

Efforts have been made to append a fluorescent dye tether to the axial position of carboxiamine ligands to allow for metal-nitrosyl complex tracking.[28] While adding such approaches have shown potential promise, the dye dissociates in cell cultures by approximately 5% within an hour, losing fluorescence and destabilizing the metal-nitrosyl compound. The more acidic pH environments observed in live cells elicit greater loss (approximately 10%) of resorufin in live cell cultures over an hour, further limiting complex tracking for *in vivo* experiments.[28]

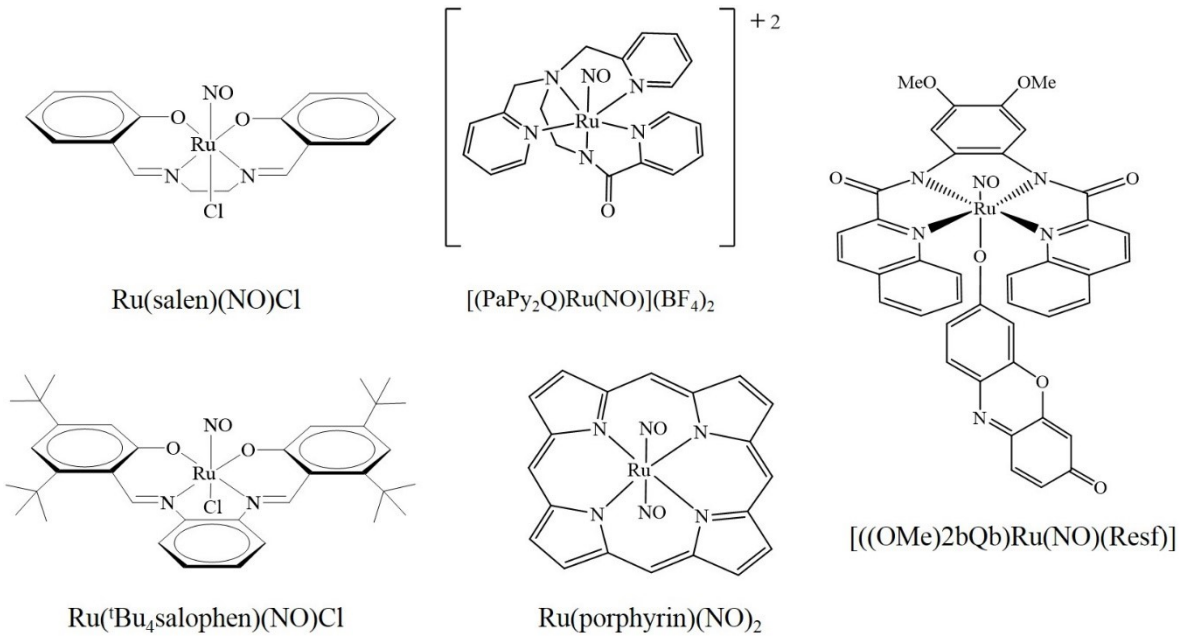

Figure 1.2. Ruthenium centered PhotoNORMs.

Porphyrins, commonly used for biological purposes in heme and oxygen transportation, was an ideal selection for a due to the presence of the ligand in biology where stability and water solubility are obviously not problematic. Unfortunately, porphyrin

ruthenium nitrosyls, while water soluble, have been shown to have a fast back reaction to reform the nitrosyl with a rate $k < 10^7 M^{-1}s^{-1}$.[29, 30] This rapid back reaction limits the application of this class of photoactive compounds as NO releasers, since the bound ruthenium-nitrosyl is too stable for the desired applications.

Schiff base ligands however, formed from the condensation of an aldehyde and amine, are easily modifiable. Ruthenium nitrosyl salen and salophen compounds are oxygen, water, and thermally stable while retaining photolability of the metal-NO bond upon excitation with the appropriate wavelength for the metal to ligand charge transfer band (MLCT). The initial catalyst, Ru(NO)(salen)Cl was studied by Carmen F. Works.[31] Dr. Works' research showed the ability of the ruthenium nitrosyl to release NO at several excitation wavelengths with photochemical activity up to 546 nm with a QY of 7% in acetonitrile .[31] Attempts to red-shift the absorbance have led to incorporation of salophen ligands, which afford an approximately 100 nm bathochromic shift in absorbance maxima and afford visible light excitation for metal-NO bond excitation. A representative example is the comparison of Ru(^{t}Bu$_4$salen)(NO)Cl with Ru(^{t}Bu$_4$salophen)(NO)Cl, where incorporation of the salophen ligand results in shift in maxima from 370 nm to 468 nm. Moreover, the quantum yield upon irradiation at 365 nm increasing from 0.030 for the salen complex to 0.055 for the salophen complex, with photoactivated NO release still being efficient for the salophen upon excitation at 546 nm (Φ = 0.011).[31]

1.6 Up-Converting Nano Particles

Nanoparticles (NPs), as the name describes, are defined as particles with a diameter equal to or less than 100 nm.[32] Presently, nanoparticles are being explored for a variety of purposes in medicinal chemistry, ranging from direct treatment to drug payload delivery.[33, 34,

[35, 36] In the context of photoactivated therapy, the photophysical properties of nanoparticles are most interesting, as interactions of light with certain nanoparticles can be employed to increase efficiency of photochemical processes at wavelengths were the photoactivated drug may not absorb light sufficiently. One process that is uniquely applicable is that of upconversion, when two or more photons of light are absorbed by a system and the resulting emitted wavelength of light is higher in energy than a single photon of absorbed light.[37] This can occur by two different mechanisms: simultaneous absorption or sequential absorption. Simultaneous absorbance of two (or more) photons requires excitation by a pulse laser with a high power density (~10^6 W/cm^2). [38] Sequential excitation however, involves long lived excited states that can absorb photons from a continuous wave (CW) lamp or LED to convert low energy light into high energy emission or higher energy anti-Stokes luminescence.[38]

The upconverting nanoparticles (UCNPs) used in the studies to follow undergo sequential absorbance in order to emit higher energy light. This is achieved when a photon of light is absorbed by a system, the excited state then undergoes intersystem crossing (isc) to an excited state with a long half-life.[38] A second photon is then absorbed and the electron excited into a higher occupied state, and the UCNP eventually relaxes via emission of a single photon. Once the photon is emitted, the energy released is then greater (lower wavelength) than one photon absorbed (higher wavelength) and is referred to as a two-photon or multi photon UCNP.

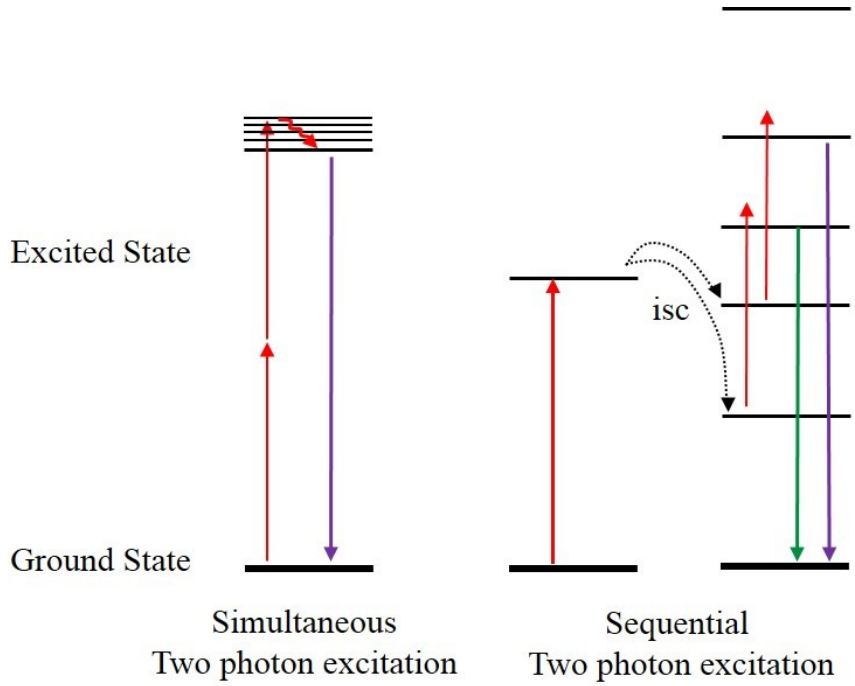

Figure 1.3. Simplified depiction of two-photon absorbance and emission of a higher energy light.

UCNPs have been explored heavily for uses in biolabeling, optical storage, solid state lasers, light emitting diodes (LEDs), display systems, and imaging.[39, 40] For bioimaging, the surface of particles is modified with PEG groups and can be circulated through a mouse system. The PEGylated particles collect within the tumor and low energy light is used to excite the UCNPs, where the emission is imaged and the tumor can be identified.[33, 34] More recently, UCNPs have been imbedded within a micelle that contains a drug payload. Upon irradiation, the high energy emission causes the micelle to break and the drug is released at a specified location.[35, 36] The work here will center on exploiting UCNPs for their use in drug delivery, particularly the encapsulation of the particles within close proximity of a photoNORM to produce NO release due solely to the emission from the UCNP and the absorbance of the photoNORM by trivial energy transfer.

1.7 Statement of Goals (research aims)

Photoactive drug delivery of caged compounds has been of great interest over the past two decades. Much focus has centered on delivering drugs that possesses a high degree of specificity such that the drug does not activate before it reaches the target location. A secondary approach to specificity is to design a drug that is photoactive; a compound that can passively travel through the body while retaining activity once it reaches the desired location and can be triggered externally, in this case with light irradiation. The photochemical release at a biological target would enable defined concentrations of that drug to be delivered locally and diminish systemic side-effects associated with overdosing. This method will potentially allow a caged drug to be administered without consequence until the photolysis is directed to a specific location. Thus one is able to specify the location, timing, and dosage of such an event.[41] In this context, we[42] and others[43] have been studying the photochemistry of ruthenium nitrosyl compounds owing to their thermal stability, low toxicity, and the photolability of the Ru-NO bond with light to release nitric oxide.

Many current techniques of chemotherapy and anti-cancer treatments have extremely negative side effects, such as nausea, anemia, blood disorders, nerve damage, and irreversible damage to internal organs such as the heart and liver.[44] Consequently, research is ongoing to develop better drug delivery methods and drugs with greater specificity and leaving healthy cells unharmed. Due to the wide variety of roles that NO can play, it is extremely important to control the concentration released in any therapeutic application.[45] With such considerations, there are continuing efforts to make photoactive nitric oxide donors with high biological stability,[46, 47, 48, 49 , 50] and ruthenium nitrosyls are of particular interest owing to the photolability of the otherwise very stable Ru-NO bond.

Traditional drug delivery methods consist primarily of oral delivery, intravenous delivery, inhalation or topical application of drugs. Probably the most coming drug delivery method, oral delivery consists of simply swallowing the drug followed by uptake to the bloodstream in the intestine and systemic transport as opposed to specific regionalization.[51] If the drug is intended for use past the stomach, the pills are coated with sodium alginate, calcium chloride, or various polymers to survive the stomach acid.[51] Inhalation therapy is utilized for the administration of lung specific drugs through aerosol sprays such as asthma inhalers and topical creams such as steroids, are absorbed through the skin at the intended site.[51] Intravenous drug delivery is utilized heavily in hospitals and chemotherapy applications. Water solubility can limit IV delivery and therefore, water insoluble drugs are commonly dissolved in a DMSO/ water mixture, additionally drug uptake is highly concentrated at the lining of the endothelial cells.[52] Drug specificity is controlled with targeting utilizing specific ligands, hormones, vitamins, growth factors, or peptides.[51] However, the release and uptake of drugs is highly dependent on an individual's metabolic systems and release of the active pharmacokinetic drug is often non-specific.

In this context, we have prepared several ruthenium nitrosyl compounds that will be discussed over the next several chapters. Each of these compounds are water, oxygen, and thermally stable while retaining the photolability of NO release. Each compound has been characterized by NMR, IR, UV-visible spectra, mass spectroscopy, and their ability to release nitric oxide upon photolysis (quantum yield). I also report the activity of Ru(NO)(salen-CO_2H)Cl (**1**) (salen-CO_2H = N,N'-ethylenebis(3,3'-bis-carboxyl-salicylidene-iminato) in cell toxicity and vascular reactivity studies.

To limit the potential toxicity, we will also discuss encapsulation of the pro-drug, Ru(NO)(salophen)Cl, into biocompatible polymers poly(lactic-co-glycolic acid) (PLGA) and Polydimethylsiloxane (PDMS). These polymers are FDA approved for biological use and have been greatly studied.[53, 54] Additionally, PLGA and PDMS are both hydrophobic and can be synthesized to encapsulate both hydrophobic UCNPs and photoNORMs concurrently, therefore these matrices have the ability to induce NO release from near infra-red photolysis (falling within the therapeutic window of 700-1100 nm[15]).

1.8 References

[1] Ignarro, L. J.; Buga, G. M.; Wood, K. S.; Byrns, R. E.; Chaudhuri, G., "Endothelium-derived relaxing factor produced and released from artery and vein is Nitric-oxide", *Proc. Natl. Acad. Sci. U.S.A.*, **1987,** *84* (24), 9265-9269.

[2] Palmer RMJ, Ferrige AG, Moncada S; "Nitric oxide release accounts for the biological activity of endothelial-derived relaxing factor", *Nature,* 1987, **327,** 524-526.

3 Feldman, P. L.; Griffith, O. W.; Hong, H.; Stuehr, D. J.; "Irreversible inactivation of macrophage and brain nitric oxide synthase by L-NG-methylarginine requires NADPH-dependent hydroxylation", *J. Med. Chem.*, **1993**, 36 (4), 491-496.

[4] (a)Wink, D. A.; Mitchell, J. B.; "Chemical biology of nitric oxide: Insights into regulatory, cytotoxic, and cytoprotective mechanisms of nitric oxide", Free Radical Biol. Med. **1998**, 25, 434−456. (b) Nitric Oxide: Biology and Pathobiology, 2nd ed.; Ignarro, L. J., Ed.; Elsevier Inc.: Burlington, MA, **2010**. (c) Wink, D. A.; Hanbauer, I.; Grisham, M. B.; Laval, F.; Nims, R. W.; Laval, J.; Cook, J.; Pacelli, R.; Liebmann, J.; Krishna, M.; Ford, P. C.; Mitchell, J. B. "Chemical biology of nitric oxide: regulation and protective and toxic mechanisms." Curr. Top. Cell. Regul. **1996**, 34, 159-187.

[5] Moncada, S.; Palmer, R. M. J.; Higgs, E. A. Nitric Oxide: Physiology, Pathophysiology, and Pharmacology *Pharmacol. Rev.* **1991**, *43*, 109-142.

56. Marletta, M. A. "Nitric Oxide Synthase Structure and Mechanism", *J. Biol. Chem.* **1993**, *268*, 12231-12234.

[6] Palmer, R. M. J.; Ashton, D. S.; Moncada, S. Vascular endothelial cells synthesize nitric oxide from L-arginine *Nature* **1988**, *333*, 664-666.

[7] Gerweck, L. E.; Seetharaman, K.; "Cellular pH gradient in tumor versus normal tissue: potential exploitation for the treatment of cancer" Cancer Res, **56**, (1996), 1194-1198

[8] Olson, S. Y.; Garb·n, H. J., "Regulation of apoptosis-related genes by nitric oxide in cancer" *Nitric Oxide* **2008,** 19 (2), 170-176.

[9] Sagar, S. M.; Singh, G.; Hodson, D. I.; Whitton, A. C.; "Nitric oxide and anticancer therapy", *Cancer Treatment Reviews* **1995,** *21* (2), 159-181.

[10] Tomita, M.; Sato, E. F.; Nishikawa, M.; Yamano, Y.; Inoue, M.; "Nitric oxide regulates mitochondrial respiration and functions of articular chondrocytes", *Arthritis & Rheumatism*, 2001, **44**, 96–104

[11] Choudhari, S. K.; Chaudhary, M.; Bagde, S.; Gadbail, A. R.; Joshi, V.; "Nitric oxide and cancer: a review", *World Journal of Surgical Oncology,* **2013**, 11, 118

[12] Xu, W.; Liu, L. Z.; Loizidou, M.; Ahmed, M.; Charles, I. G.; "The role of nitric oxide in cancer", *Cell Research* (2002) **12,** 311–320.

[13] (a) Bourassa, J.; DeGraff, W.; Kudo, S.; Wink, D. A.; Mitchell, J. B.; Ford, P. C. "Photochemistry of Roussin's Red Salt, $Na_2[Fe_2S_2(NO)_4]$, and of Roussin's Black Salt, $NH_4[Fe_4S_3(NO)_7]$. In Situ Nitric Oxide Generation To Sensitize γ-Radiation Induced Cell Death", J. Am. Chem. Soc. 1997, 119, 2853−2860.

(b) Jordan, B. F.; Sonveaux, P.; Feron, O.; Gregoire, V.; Beghein, N.; Dessy, C.; Gallez, B. "Nitric oxide as a radiosensitizer: evidence for an intrinsic role in addition to its effect on oxygen delivery and consumption.", Int. J. Cancer 2004, 109, 768−773.

(c) Mitchell, J. B.; Wink, D. A.; DeGraff, W.; Gamson, J.; Keefer, L. K.; Krishna, M. C. "Hypoxic mammalian cell radiosensitization by nitric oxide", Cancer Res. 1993, 53, 5845−5848.

[14]Enemark, J. H.; Feltham, R. D.; "Principles of structure, bonding, and reactivity for metal nitrosyl complexes" *Coord. Chem. Rev.* 1974, **13**, 339-406

[15] König, K.; "Multiphoton microscopy in life sciences", *Journal of Microscopy*, 2000, **200**, 83-104.

[16] Roussin, M. L. "Recherches sur les nitrosulfures doubles de fer (nouvelle classe de sels)", Ann. Chim. Phys. **52**, (1858), 285–303.

[17] Bourassa, J.; Lee, B.; Bernard, S.; Schoonover, J.; Ford, P. C.; "Flash Photolysis Studies of Roussin's Black Salt Anion: $Fe_4S_3(NO)_7^-$" *Inorg. Chem.* **1999**, 38, 2947-2952

[18] Bourassa, J.; DeGraff, W.; Kudo, S.; Wink, D. A.; Mitchell, J. B.; Ford, P. C.; "Photochemistry of Roussin's Red Salt, Na2[Fe2S2(NO)4], and of Roussin's Black Salt, NH4[Fe4S3(NO)7]. In Situ Nitric Oxide Generation To Sensitize γ-Radiation Induced Cell Death", *J. Am. Chem. Soc.*, **1997**, 119, 2853-2860.

[19] Bourassa, J.; DeGraff, W.; Kudo, S.; Wink, D. A.; Mitchell, J. B.; Ford, P. C.; "Photochemistry of Roussin's Red Salt, Na2[Fe2S2(NO)4], and of Roussin's Black Salt, NH4[Fe4S3(NO)7]. In Situ Nitric Oxide Generation To Sensitize γ-Radiation Induced Cell Death", *J. Am. Chem. Soc.*, 1997, **119**, 2853-2860.

[20] Conrado, C. L.; Bourassa, J. L.; Egler, C.; Wecksler, S.; Ford, P. C.; *Inorg. Chem.* 2003, **42**, 2288–2293

[21] Ostrowski, A.D.; Deakin, S. J.; Azhar, B.; Miller, T. W.; Franco, N.; Cherney, M. M.; Lee, A. J.; Burstyn, J. N.; Fukuto, J. M.; Megson, I. L.; Ford, P. C.; "Nitric Oxide Photogeneration from trans-Cr(cyclam)(ONO)2^+ in a Reducing Environment. Activation of Soluble Guanylyl Cyclase and Arterial Vasorelaxation", *J. Med. Chem.*, 2010, **53**, 715–722

[22] Eroy-Reveles, A. A.; Leung, Y.; Christine M. Beavers, Marilyn M. Olmstead, and Pradip K. Mascharak. P. K.; "Near-Infrared Light Activated Release of Nitric Oxide from Designed Photoactive Manganese Nitrosyls: Strategy, Design, and Potential as NO Donors", *J. Am. Chem. Soc.*, **130** (2008), 4447-4458.

[23] Heilman, B. J.; St. John, J.; Oliver, S. R. J.; Mascharak, P. K.; "Light-Triggered Eradication of Acinetobacter baumannii by Means of NO Delivery from a Porous Material with an Entrapped Metal Nitrosyl", *J. Am. Chem. Soc.*, **134** (2012), 11573−11582

[24] Freitag, L.; Gonzalez, L.; "Theoretical Spectroscopy and Photodynamics of a Ruthenium Nitrosyl Complex", *Inorg. Chem.*, **53**, 6415-6426.

[25]Leung, W.-H.; Che, C.-M.; "Oxidation Chemistry of Ruthenium-Salen Complexes", *Inorganic Chemistry*, **28**, 1989, 4619-4622.

[26] Odenkirk, W.; Rheingold, A. L.; Bosnich, B.; "Homogeneous catalysis: a ruthenium-based Lewis-acid catalyst for the Diels-Alder reaction", *J. Am. Chem. Soc*, **1992**, *114, 6392-6398.*

[27] Rose, M. J.; Olmstead, M. M.; Mascharak, P. K.; "Photoactive Ruthenium Nitrosyls Derived from Quinoline- and Pyridine-based Ligands: Accelerated Photorelease of NO due to Quinoline Ligation" *Polyhedron*, **26** (2007), 4713.

[28] Rose, M. J.; Fry, N. L.; Marlow, R.; Hinck, L.; Mascharak, P.K.; "Sensitization of ruthenium nitrosyls to visible light via direct coordination of the dy resorufin: Trackable NO donors for light-triggered NO delivery to cellular targets", *J. Am. Chem. Soc.*, **2008**, 130, 8834-8846.

[29] Ford, P. C.; Laverman, L. E.; "Reaction mechanisms relevant to the formation of iron and ruthenium nitric oxide complexes", *Coord. Chem. Rev.* **249** (2005), 391.

[30] Lim, M. D.; Lorkovic, I. M.; Ford, P. C. ; *J. Inorg. Biochem.* 99, (2005), 151

[31] Works, C. F.; Jocjer, C. J.; Bart, G. D.; Bu, X.; Ford, P. C.; "Photochemical Nitric Oxide Precursors: Synthesis, photochemistry, and ligand substitution kinetics of ruthenium salen nitrosyl and ruthenium salophen nitrosyl complexes", *Inorg. Chem.*, **2002**, 41, 3728-3739.

[32] S. Horikoshi and N. Serpone *Microwaves in Nanoparticle Synthesis, First Edition. "Introduction to Nanoparticles"*, p. 1-24, Wiley-VCH Verlag GmbH & Co. KGaA. (2013)

[33] Liu, Q.; Yang, T.; Feng, W.; Li, F.; "Blue-Emissive Upconversion Nanoparticles for Low-Power-Excited Bioimaging in Vivo", *J. Am. Chem. Soc.*, **2012**, *134* (11), pp 5390–5397

[34] Dai, Y.; Xiao, H.; Liu, J.; Yuan, Q.; Ma, P.; Yang, D.; Li, C.; Cheng, Z.; Hou,Z.; Yang, P.; Lin, J.; "In Vivo Multimodality Imaging and Cancer Therapy by Near-Infrared Light-Triggered *trans*-Platinum Pro-Drug-Conjugated Upconverison Nanoparticles", *J. Am. Chem. Soc.*, **2013**, *135* (50), pp 18920–18929

[35]Yan, B.; Boyer, J.-C.; Branda, N. R.; Zhao, Y.; "Near-Infrared Light-Triggered Dissociation of Block Copolymer Micelles Using Upconverting Nanoparticles", *J. Am. Chem. Soc.*, **2011**, *133* (49), pp 19714–19717

[36] Yan, B.: Boyer, J.-C.; Habault, D.; Branda, N. R.; Zhao, Y.; **"**Near Infrared Light Triggered Release of Biomacromolecules from Hydrogels Loaded with Upconversion Nanoparticles", *J. Am. Chem. Soc.*, **2012**, *134* (40), pp 16558–16561.

[37] Ghosh, P.; Lorbeer, C.; Mudring, A. –V.; "Nanofluorides for Environmentally Benign Lighting and Energy Conversion in Solar Cells" *Fluorine-Related Nanoscience with Energy Applications,* Chapter 6, **2011,**pp 87-99 *ACS Symposium Series*, Volume 1064

[38] Chen, G.; Qiu,H.; Prasad, P. N.; Chen, X.; "Upconversion Nanoparticles: Design, Nanochemistry, and Applications in Theranostics", *Chem. Rev.*, **2014**, 114, 5161−5214

[39] Zhang, F.; Wan, Y.; Yu, T.; Zhang, F.;Shi, Y.; Xie, S.;Li, Y.; Xu, L.; Tu, B.; Zhao, Z.; "Uniform Nanostructured Arrays of Sodium Rare-Earth Fluorides for Highly Efficient Multicolor Upconversion Luminescence", *Angew. Chem. Int. Ed.*, **46**, 7976–7979.

[40] Kubacka, A.; Fernández-García, M.; Colón, G.; "Advanced Nanoarchitectures for Solar Photocatalytic Applications", *Chem. Rev.*, **2012**, *112* (3), pp 1555–1614

[41] (a) Ford, P. C. "Polychromophoric Metal Complexes for Generating the Bioregulatory Agent Nitric Oxide by Single- and Two-Photon Excitation" *Acc. Chem. Res.* **2008**, 41, 190–200.

(b) Ostrowski, A. D.; Ford, P. C. "Metal complexes as photochemical nitric oxide precursors: Potential applications in the treatment of tumors." *Dalton Trans.*, **2009**, 10660-10669.

[42] (a) Works, C. F.; Ford, P. C.; "Photoreactivity of the Ruthenium Nitrosyl Complex, Ru(salen)(Cl)(NO). Solvent Effects on the Back Reaction of NO with the Lewis Acid Ru^{III}(salen)(Cl)", *J. Am. Chem. Soc.*, 2000, *122* (31), pp 7592–7593

(b) Works, C. F.; Jocher, C. J.; Bart, G. D.; Bu, X.; Ford, P. C.; "Photochemical Nitric Oxide Precursors: Synthesis, Photochemistry, and Ligand Substitution Kinetics of Ruthenium Salen

Nitrosyl and Ruthenium Salophen Nitrosyl Complexes", *Inorg. Chem.*, 2002, *41* (14), pp 3728–3739.

(c) Carlos, R. M.; Ferro, A. A.; Silva, H. A. S.; Gomes, M. G.; Borges, S. S. S.; Ford, P. C.; Tfouni, E.; Franco, D. W.; "Photochemical Reactions of trans-[Ru(NH3)4L(NO)]3+ Complexes" *Inorg. Chem. Acta*, 2004, 357(5), 1381-1388.

(d) Tfouni, E.; Bordini, J.; Ford, P. C.; "Photochemical release of nitric oxide from a regenerable [Ru(salen)(H2O)(NO)]+ via sol-gel chemistry" *Chem. Commun.*, 2005, 4169-4171

(e) Bordini,J.;. Novaes, D. O.; Borissevitch, I. E.; Owens, B. T.; Ford, P.C.; Tfouni, E.; "Acidity and photolability of ruthenium salen nitrosyl and aquo complexes in aqueous solutions" *Inorganica Chemica Acta*, 2008, 361, 2252-2258

(f) Birkmann, B.; Bandyopadhyay, S.; Owens, B. T.; Wu, G.; Ford, P.C.; "Synthesis of a Nitro Complex of RuIII(salen): Unexpected Aromatic Ring Nitration by a Nitrite Salt", *J. Inorg. Biochem.* 2009, 103(2), 237-242.

(g) Oliveira, F. d. S.; Togniolo, V.; Pupo, T. T.; Tedesco, A. C.; Santana da Silva, R.; "Nitrosyl ruthenium complex as nitric oxide delivery agent: synthesis, characterization and photochemical properties", *Inorg. Chem. Comm.*, 2004, 160-164.

(h) Novais da Rocha, Z.; Galvao de Lima, R.; Doro, F. G.; Tfouni, E.; Santana da Silva, R.; "Photochemical production of nitric oxide form a nitrosyl phthalocyanine ruthenium complex by irradiation with light in the phototherapeutic window", *Inorg. Chem. Comm.*, **2008**, 737-740.

[43] (a) Tfouni, E.; Doro, F. G.; Figueiredo, L. E.; Pereira, J. C. M.; Metzker, G.; Franco, D. W.; "Tailoring NO donors metallopharmaceuticals: ruthenium nitrosyl ammines and aliphatic tetraazamacrocycles", *Current Med. Chem.*, **2010**, 3643-3657.

(b) Ghosh, K.; Kumar, S.; Kumar, R.; Singh, U. P.; Goel, N.; "Oxidative cyclization of a phenolic Shiff base and synthesis of a cyclometalated ruthenium nitrosyl comples: photoinduces NO release by visible light", *Inorg. Chem.*, **2010**, 7235-7237.

(c) Fry, N. L.; Heilman, B. J.; Mascharak, P. K.; "Dye-tethered Ruthenium Nitrosyls Containing Planar Dicaboxamide Tetradentate Ligands: Effects of In-Plane Ligand Twist on NO Photolability" *Inorg. Chem.*, **2011**, 50, 317-324.

(d) Fry, N. L.; J. Wei, J.; Mascharak, P. K.; "Triggered Dye Release via Photodissociation of Nitric Oxide from Designed Ruthenium Nitrosyls: Turn-ON Fluorescence Signaling of Nitric Oxide Delivery" *Inorg. Chem.* **2011**, 50, 9045-9052.

(e) Kumar, A.; Pandey, R.; Gupta, R. K.; Ghosh, K.; Pandey, D. S.; "Synthesis, characterization and photochemical properties of some ruthenium nitrosyl complexes", *Polyhedron*, **2013**, 837-843.

(f) Rose, M. J.; Mascharak, P. K.; "Photoactive ruthenium nitrosyls: Effects of light and potential application as No donors", *Coord. Chem. Rev.*, **2008**, 252, 2093-2114.

[44] Partridge, A. H.; Burstein, H. J.; Winer, E. P.; "Side Effects of Chemotherapy and Combined Chemohormonal Therapy in Women with Early-Stage Breast Cancer", *J. Nat Cancer Institute Mono.*, 2001, **30**, 135-142.

[45]Wink, D.A.; Hines, H.B.; Cheng, R. Y. S.; Switzer, C. H.; Flores-Santana, W.; Vitek, M. P.; Ridnour, L. A.; Colton, C. A.; "Nitric oxide and redox mechanisms in the immune response", *J. Leukoc Biol.*, 2001, **89**(6), 873-891

[46] Ostrowski, A. D.; Ford, P. C. "Metal complexes as photochemical nitric oxide precursors: Potential applications in the treatment of tumors", *Dalton Trans.*, **2009**, 10660− 10669.

[47] Rose, M. J.; Mascharak, P. K. "*Fiat Lux*: selective delivery of high flux of nitric oxide (NO) to biological targets using photoactive metal nitrosyls", *Curr. Opin. Chem. Biol.* **2008**, 12, 238−244.

[48] Sortino, S. "Photoactivated nanomaterials for biomedical release applications", *J. Mater. Chem.* **2012**, 22, 301−318.

[49] Burks, P. T.; Ostrowski, A. D.; Mikhailovsky, A. A.; Chan, E. M.; Wagenknecht, P. S.; Ford, P. C. "Quantum dot photoluminescence quenching by Cr(III) complexes. Photosensitized reactions and evidence for a FRET mechanism", *J. Am. Chem. Soc.* **2012**, 134, 13266−13275

[50] Burks, P. T.; Ford, P. C. "Quantum dot photosensitizers. Interactions with transition metal centers", *Dalton Trans.* **2012**, 41, 13030−13042

[51] " Tiwari, G.; Tiwari, R.; Sriwastawa, B.; Bhati, L.; Pandey, S.; Pandey, P.; Bannerjee, S. K.; "Drug delivery systems: An updated review", *Int. J. Pharm. Investig*., **2012**, 2, 2–11

[52] Misra, A.; Ganesh, S.; Shahiwala, A.; Shah, S. P.; "Drug delivery to the central nervous system: a review", *J Pharm Pharmaceut Sci*, **2003**, 6, 252-273, 2003.

[53] Baru, J. S.; Bloom, D. A.; Muraszko, K.; Koop, C. E. "John Holter's shunt", *J. Am. Coll. Surgeons*, **2001**, 192, 79. b.) Aschoff, A.; Kremer, P.; Hashemi, B.; Kunze, S.; "The scientific history of hydrocephalus and its treatment." *Neurosurg. Rev.*, **1999**, 22, 67.

[54] Danhier, F.; Ansorena, E.; Silva, J. M.; Coco, R.; Le Breton, A.; Préat, V.; "PLGA-based nanoparticles: An overview of biomedical applications", *J. Controlled Release*, **161** (2012) 505–522

Chapter 2. Experimental Section

2.1 Reagents, Solvents, and Gases

2.1.1. Reagents

Ruthenium(III) nitrosyl chloride mono hydrate was purchased from Strem Chemicals Inc. Remaining synthetic materials including trifluoroacetic acid, 4-hydroxybenzoic, hexamethylenetetramine, and laboratory solvents were purchased from Sigma-Aldrich. 95% sodium hydride was purchased from Sigma-Aldrich and store in an inert glove box and transferred into an inert reaction flask for use on the Schlenk line. Actinometry solvents were prepared according to the Calvert and Pitts[1] and potassium ferrioxalate was purchased from Strem Chemicals.

2.1.2. Cell media

Cell lines, media, and MTT assay reagents for cell toxicity studies were provided by the Faculdade de Ciências Farmacêuticas de Ribeirão Preto, Universidade de São Paulo.

2.1.3. Solvents

Solvents were purchased from Fisher Scientific. THF was distilled and stored in the glove box. Deuterated solvents for NMR were purchased from Cambridge Isotope Laboratories. All buffers used for quantum yield and fluorescent measurements were prepared in nanopure water at 50 mM concentrations. The exact pH was adjusted using dilute NaOH or HCl as required. Phosphate buffers were prepared for pH values 11.0, 7.4, 6.0, and 4.5 while a HCl/KCl buffer was used for pH 1.0 and tris(hydroxymethyl)aminomethane ("Tris") was used to prepare the pH 9.0 buffer. Standard Krebs buffer (mM): NaCl (130.0), KCl (4.7),

KH_2PO_4 (1.2), $MgSO_4$ (1.2), $NaHCO_3$ (14.9), glucose (5.5) and $CaCl_2$ (1.6) was made with sterile deionized water.

2.1.4. Gases

Argon for reactions under an inert atmosphere was purchased from Praxair and passed through a desiccant column to remove gaseous water before introducing to the reaction flask. Medical grade air and helium were purchased from Praxair and used on the Nitric Oxide Analyzer as carrier gasses.

2.1.5. Instruments

NMR spectra were collected on a 400 or 500 mHz Varian NMR. Absorbance spectra were taken on a Shimadzu UV-2401PC UV-visible spectrophotomer or a Stellar Net SL5-DH spectrophotometer over the wavelength range 800nm to 200 nm. Fluorescence and emission data were collected on a Photon Technology International fluorimeter with a model 814 PMT detection system at 1 nm resolution with an Ushio Xenon arc lamp and Hammamatsu R928P PMT. Infra-red spectra were recorded on a Mattson Research Series FTIR or a PerkinElmer UATR Two spectrometer. Nitric oxide production was monitored on a General Electric Sievers Nitric Oxide Analyzer NOA 1080i (NOA). Samples were irradiated by either a high-pressure Oriel Hg lamp with 365 nm interference filters or by a Lexion LED (470 nm) as specified.

2.2 Ligand Synthesis

2.2.1 Salicylaldehyde-4-carboxylic acid

The salicylaldehyde-4-carboxylic acid was synthesized according to published procedures[2] and is outlined in Scheme 1. An overview is detailed here: 4-hydroxybenzoic acid (15.0 g, 36.2 mmol) was dissolved in 30 mL triflouroacetic acid under argon atmosphere. A solution of hexamethylenetetramine (15.3 g, 36.4 mmol) dissolved in 48 mL of triflouroacetic acid was added drop-wise to the 4-hydroxybenzoic acid with rapid stirring over 40 minutes. The resulting mixture was then refluxed with rapid stirring under an inert atmosphere. Thin layer chromatography (TLC) was used to monitor the rate of the reaction with a chloroform: methanol 100:15 mobile phase. The solution was allowed to reflux for 4 h or until the 4-hydroxybenzoic acid was no longer observed by TLC.

The reaction mixture was removed from heat and allowed to cool to room temperature after which it was transferred into a flask containing 300 mL of aqueous 4 M HCl and stirred at room temperature for 3 h in the presence of air. The resulting yellow precipitate was filtered in air and washed with approximately 200 mL of nanopure water. Crude solid was recrystallized from ethanol, filtered and washed with cold ethanol and allowed to dry fully under vacuum. The product was confirmed by ^{1}H NMR in accordance to published work. ^{1}H

NMR (CD_3OD, 500 MHz): δ 10.15 (1H, s, HC=O), 8.44 (1H, d), 8.20 (1H, dd), 7.06 (1H, d) phenyl protons (Figure 1).

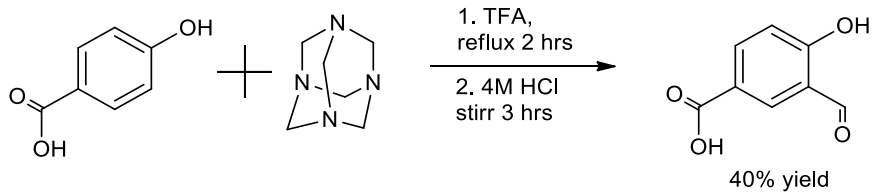

Scheme 1. Synthesis of salicylaldehyde-4-carboxylic acid according to published proceedures.[2]

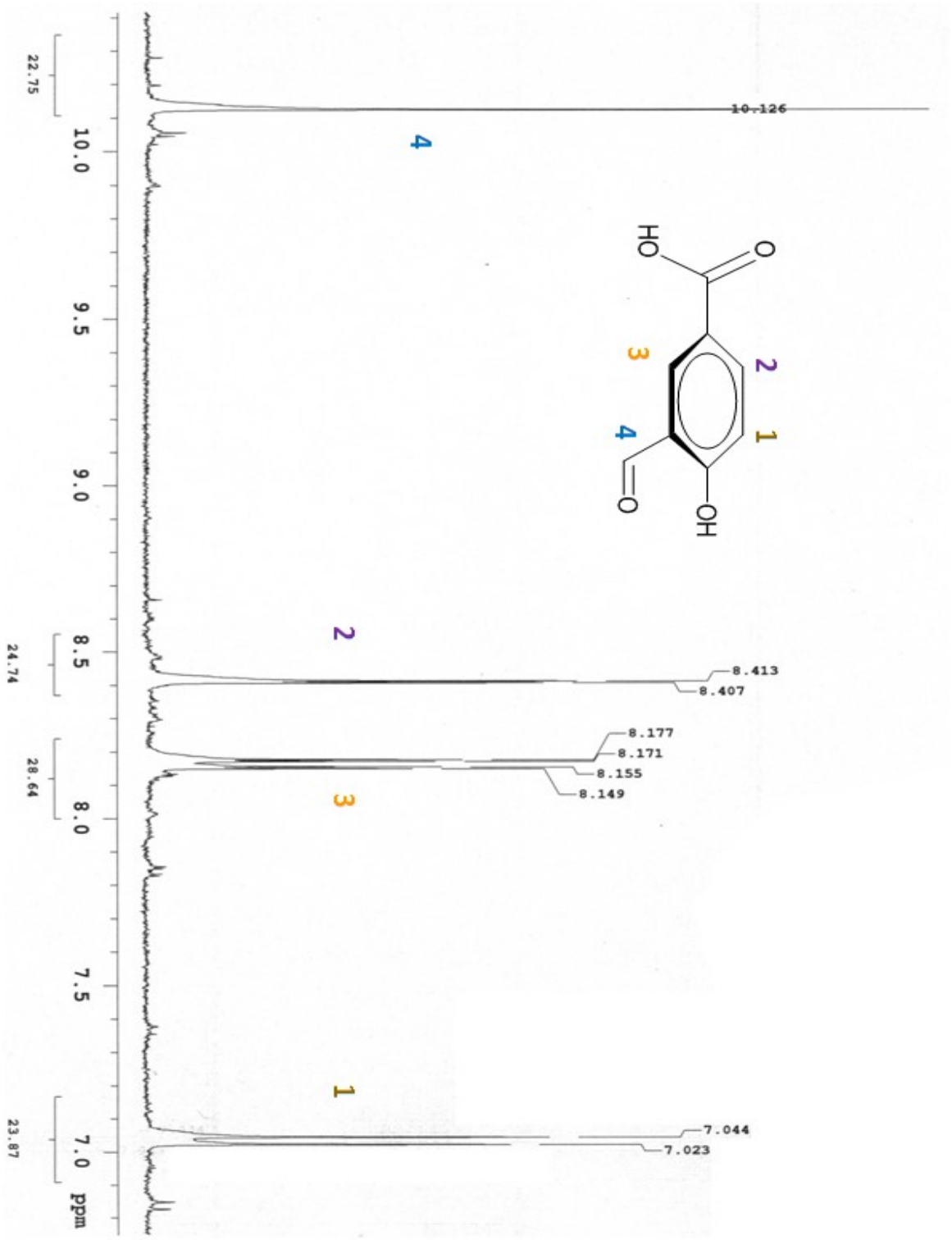

Figure 4. ^{1}H NMR spectra of salicylaldehyde-4-carboxylic acid in deuterated methanol at room temperature.

2.2.2 Salen-CO_2H

The carboxylic acid derivative of the salen ligand (3,3'-((1E,1'E)-(ethane-1,2-diylbis(azanylylidene))bis(methanylylidene))bis(4-hydroxybenzoic acid)) or "salen-CO_2H" was prepared according to the reaction sequence outlined in Scheme 2. The salen-CO_2H was synthesized by the condensation of salicylaldehyde-4-carboxylic acid with ethylenediamine. Briefly, salicylaldehyde-4-carboxylic acid (1.79 g, 10.8 mmol, 2 eq.) was dissolved in 15 mL of ethanol with mild heating and stirring. A solution of ethylenediamine (0.324 g, 5.39 mmol, 1 eq.) in 10 mL of ethanol was added to the salicylaldehyde solution causing an immediate formation of precipitates. The reaction was allowed to run to completion by heating at reflux for 1 h with stirring. The solution was removed from heat and the solid was allowed to precipitate. The yellow precipitate was collected by filtration, washed with cold ethanol and dried under vacuum. (**Scheme 2**) ^{1}H NMR (D_2O, 500 MHz): δ: 8.71 (1H, s) methane protons, 8.04 (1H, d), 7.84 (1H, d), 6.87 (1H, d) phenyl protons, 3.95 (2H, s) ethylene bridge (Figure 2). MS(FAB+): m/z 353.05 (M -3 H^+). Elemental Analysis C 57.80%, H 4.20%, N 7.90%. Theoretical C 60.67%, H 4.53%, N 7.86%.

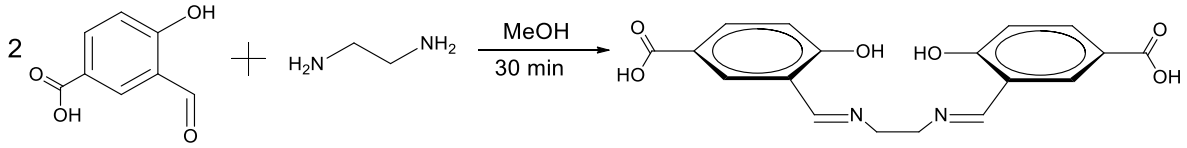

Scheme 2. Synthetic scheme of the condensation reaction to produce the carboxylic acid modified salen, salen-CO_2H.

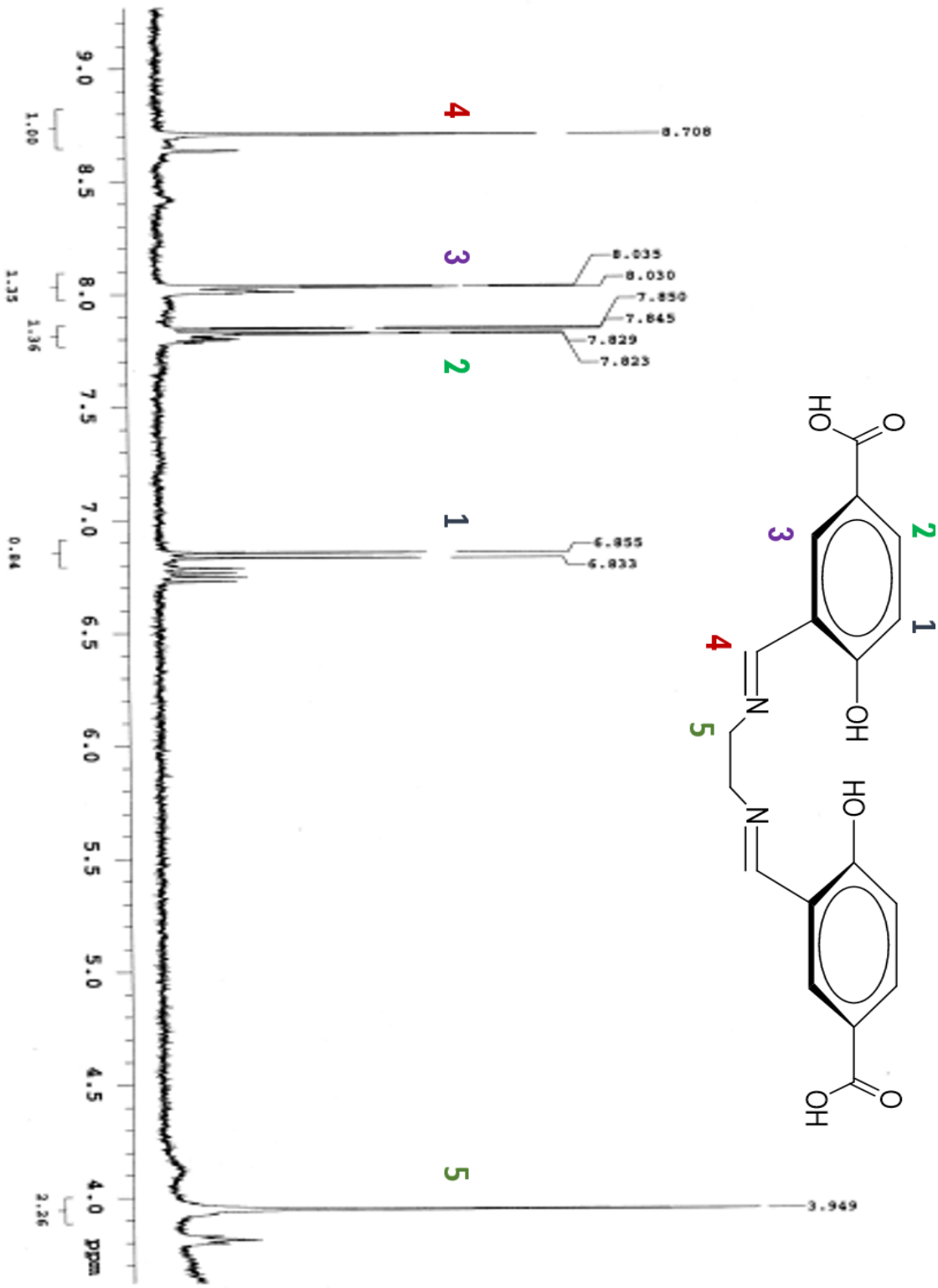

Figure 5. ^{1}H NMR spectra of salen-CO_2H in $(CD_3)_2SO$ at room temperature.

2.2.3 Salophen

Reagents to synthesize the salophen ligand were commercially available and used without further purification. Salicylaldehyde (2.10 mL of 19.8 mmoles, 2 eq.) was dissolved in approximately 100 mL of ethanol and heated with stirring (Scheme 3). To the hot solution, one equivalent of 1,2-phenylene diamine (1.0658 g, 9.86 mmoles.) was added and the solution was heated at reflux for 2 hours. The mixture containing this yellow precipitate was allowed to cool slowly and precipitate from the solution. Once at room temperature the solid was filtered and washed with cold ethanol to produce 2.5652 g of product. The ^{1}H NMR spectrum in acetonitrile (CD_3CN, 500 MHz) gave the following resonances: δ: 8.78 (2H, s) imine protons, 7.53 (2H, d), 7.40 (6H, m), 6.98 (4, d) phenyl protons (Figures 3 and 4). Elemental Analysis C 75.8%, H 4.70%, N 8.40%. Theoretical C 75.93%, H 5.10%, N 8.86%.

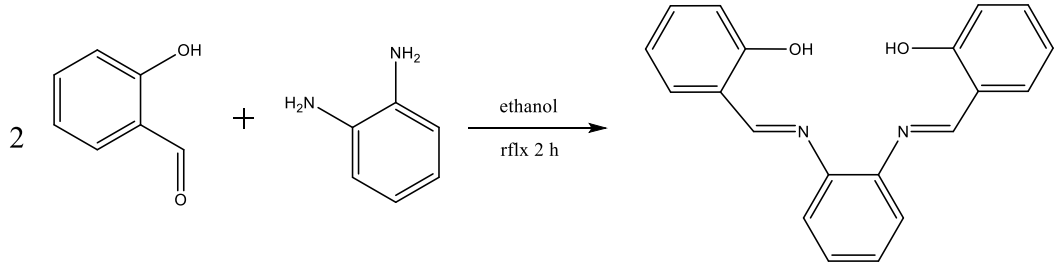

Scheme 3. Synthetic scheme of the condensation reaction to produce the salophen ligand.

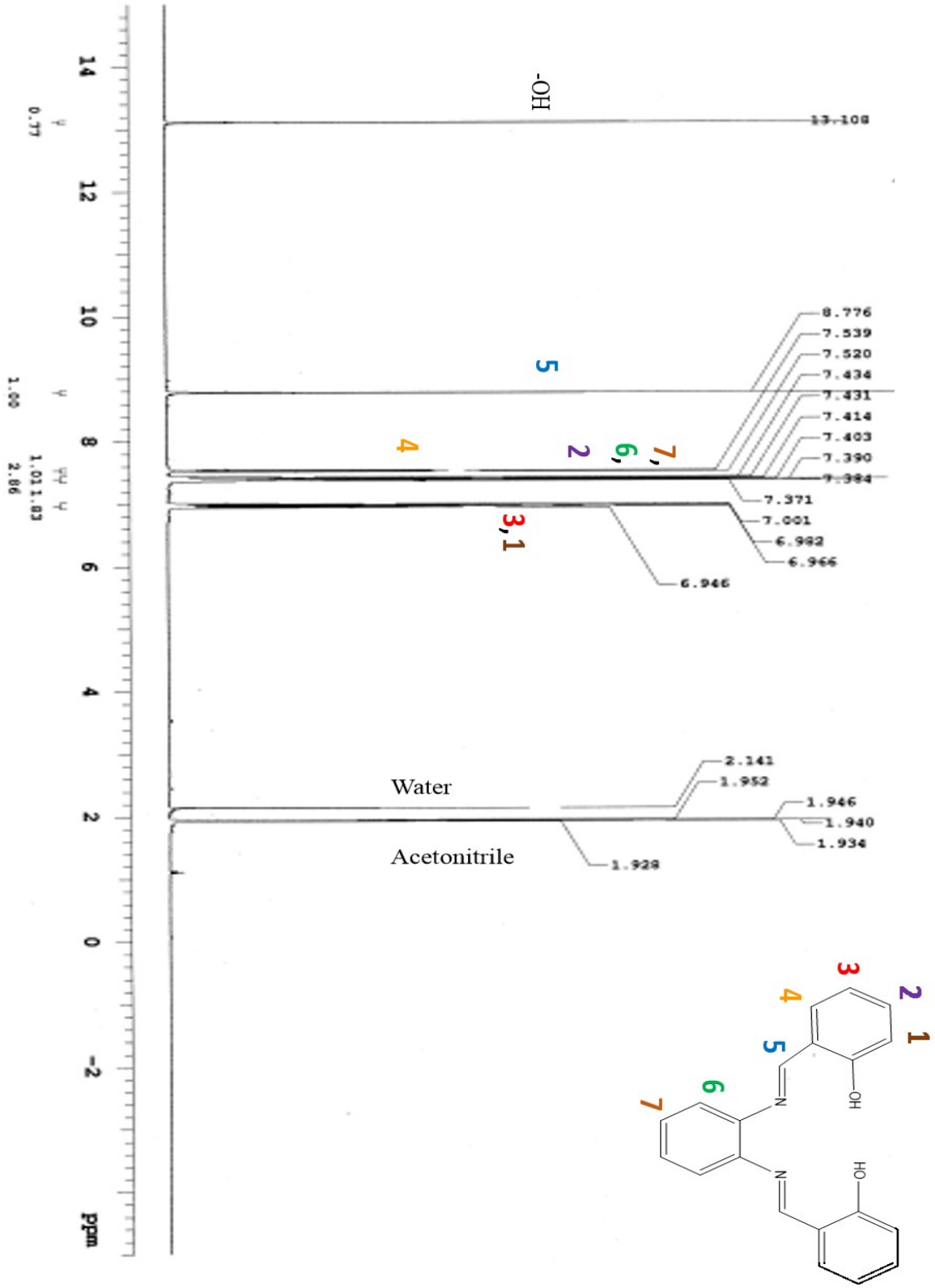

Figure 6. ^{1}H NMR spectra of the salophen ligand in deuterated acetonitrile at room temperature.

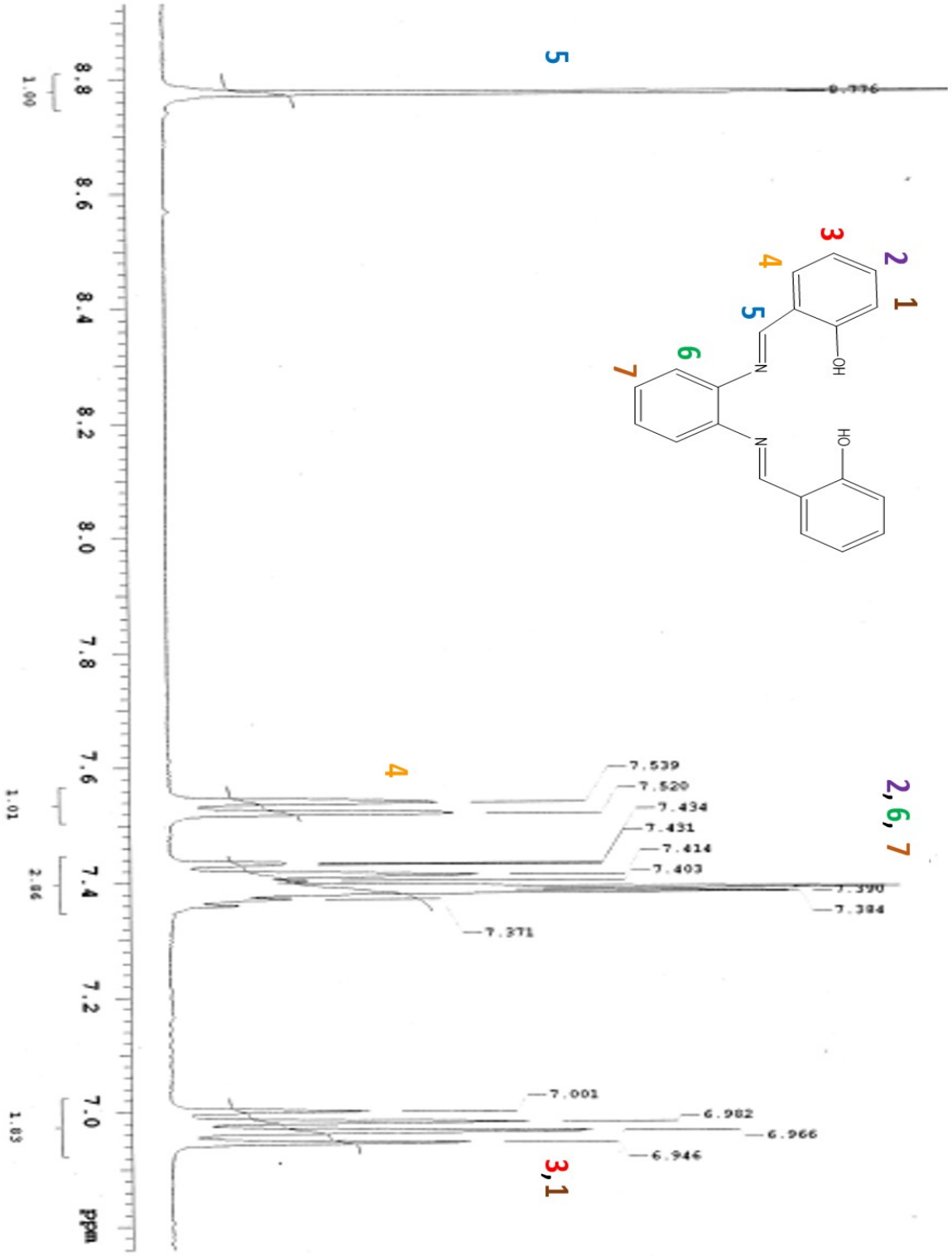

Figure 7. ^{1}H NMR spectra of the salophen ligand in deuterated acetonitrile at room temperature. Aromatic splitting pattern is highlighted.

2.3 Synthesis of Ruthenium Nitrosyls

2.3.1 Ru(NO)(salen-CO_2H)Cl

The nitrosyl complex chloridonitrosyl(N,N′-ethylenebis(3,3'-bis-carboxylsalicylidene-iminato)ruthenium(III), Ru(salenCO_2H)(NO)Cl (**1**) was prepared as follows. A mixture of salen-CO_2H (0.50 g, 1.41 mmol), sodium hydride (0.107 g, 4.45 mmol), and trichloridonitrosylruthenium(III) monohydrate, Ru(NO)Cl_3•H_2O, (0.317 g, 1.41 mmol) was added to a three neck 300 mL round bottom flask and placed under an argon atmosphere. Approximately 150 mL of deaerated ethanol was then transferred via cannula into the reaction flask. The resulting solution was then refluxed under argon in the dark for 4 h, after which the reaction solution was allowed to cool to room temperature and the ethanol was removed via rotary evaporation. The sodium chloride byproduct was removed from the desired product by washing the solid with water adjusted to pH 5 with dilute HCl. The remaining solid was dried under vacuum for several h (Scheme 4, step iii). ^{1}H NMR (DMSO-d_6): δ 8.69ppm (1H, s) methane protons, 8.02 (1H, s), 7.85 (1H, d), 6.83 (1H, d) phenyl protons, 3.94 (2H, s) ethylene bridge. Elemental Analysis C 37.04%, H 4.20%, N 7.98%. Theoretical [Ru(NO)(salen-CO_2H, CO_2Na)Cl•$2H_2O$], C 37.35%, H 2.96%, N 7.26%. (Figure 5). MS(FAB+): m/z 535.05 (M – NO^+). FTIR (KBr) ν_{NO} = 1865 cm^{-1}. UV-vis (pH 7.4 50 mM phosphate buffer) λ_{max} 248nm (ε = 3.8 x 10^4 M^{-1} s^{-1}), 359 (ε = 6.6 x 10^3 M^{-1} s^{-1}).

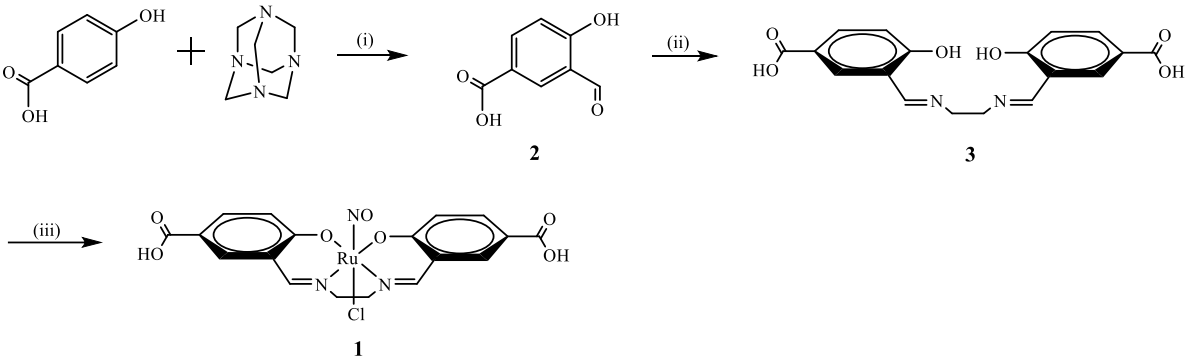

Scheme 4. Complete synthesis of Ru(salen-CO_2H)(NO)Cl: (i) triflouroacetic acid, under argon atmosphere, 4 h reflux; (ii) 0.5 equivalents of ethylenediamine refluxed in ethanol for 1 h; (iii) 2.3 equiv. NaH, 1 equiv. $Ru(NO)Cl_3 \bullet H_2O$, under argon, refluxed in ethanol for 4 h.

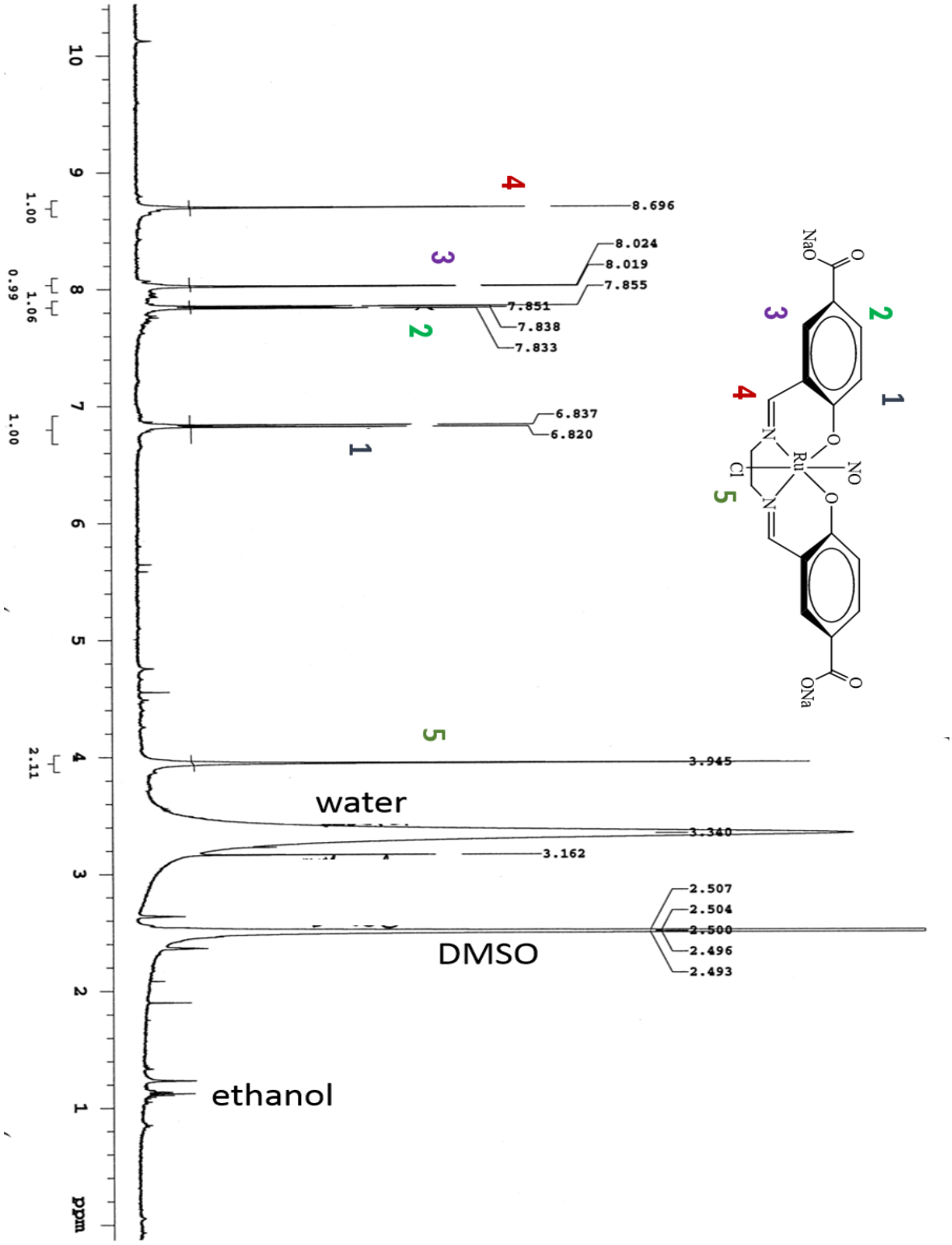

Figure 8. ^{1}H NMR spectra of the Ru(NO)(salen-CO_2H)Cl in d_6 DMSO at room temperature.

2.3.2 Ru(NO)(salophen)Cl

Salophen (0.0647g, 0.205 mmol, 1 eq.) and NaH (0.0083g, 0.35 mmol, 1.5 eq.) were combined in 20 mL of distilled THF and put under argon. The evolution of hydrogen gas was immediately observed once the solvent was added. The reaction was allowed to continue for 10 minutes with slight heating and stirring.

In the dark, $RuCl_3(NO)\cdot H_2O$ (0.0522g, 0.204 mmol, 1 eq.) was dissolved in ~15 mL of THF under argon and then cannula-transferred into the salophen reaction flask. The complete solution was refluxed under argon for 4 h before the solvent was removed by negative pressure (Scheme 5).

The product was chromatographed on a silica column with 99:1 chloroform: methanol to remove the excess ligand. The ratio was increased up to 3% methanol to remove the brown ruthenium band, which was collected and the sample was checked by ^1H NMR in acetonitrile. ^1H NMR (CD_3CN): δ 8.63ppm (1H, s) methane protons, 7.54 (1H, m), 7.36 (2H, m), 7.23 (1H, m), 7.02 (1H, m), 6.91 (1H, td) phenyl protons (Figures 6-8). Elemental Analysis C 51.3%, H 3.36 %, N 8.86 %. Theoretical [Ru(NO)(salophen)Cl], C 49.96%, H 2.93%, N 8.74%. MS(FAB+): m/z 504.03 ($M + Na^+$) (Figure 9). FTIR (KBr) $\nu_{NO} = 1882\ cm^{-1}$. UV-vis (toluene) λ_{max} 336 nm ($\varepsilon = 1.0 \times 10^4\ M^{-1}\ s^{-1}$), 465 ($\varepsilon = 2.7 \times 10^3\ M^{-1}\ s^{-1}$), (acetonitrile) λ_{max} 330 nm ($\varepsilon = 2.1 \times 10^4\ M^{-1}\ s^{-1}$), 440 ($\varepsilon = 5.2 \times 10^3\ M^{-1}\ s^{-1}$), (isopropyl acetate) λ_{max} 330 nm ($\varepsilon = 1.7 \times 10^4\ M^{-1}\ s^{-1}$), 450 ($\varepsilon = 4.6 \times 10^3\ M^{-1}\ s^{-1}$).

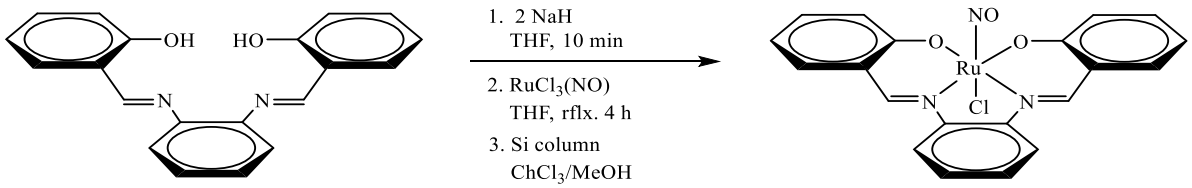

Scheme 5. Insertion of the ruthenium nitrosyl into the ligand structure.

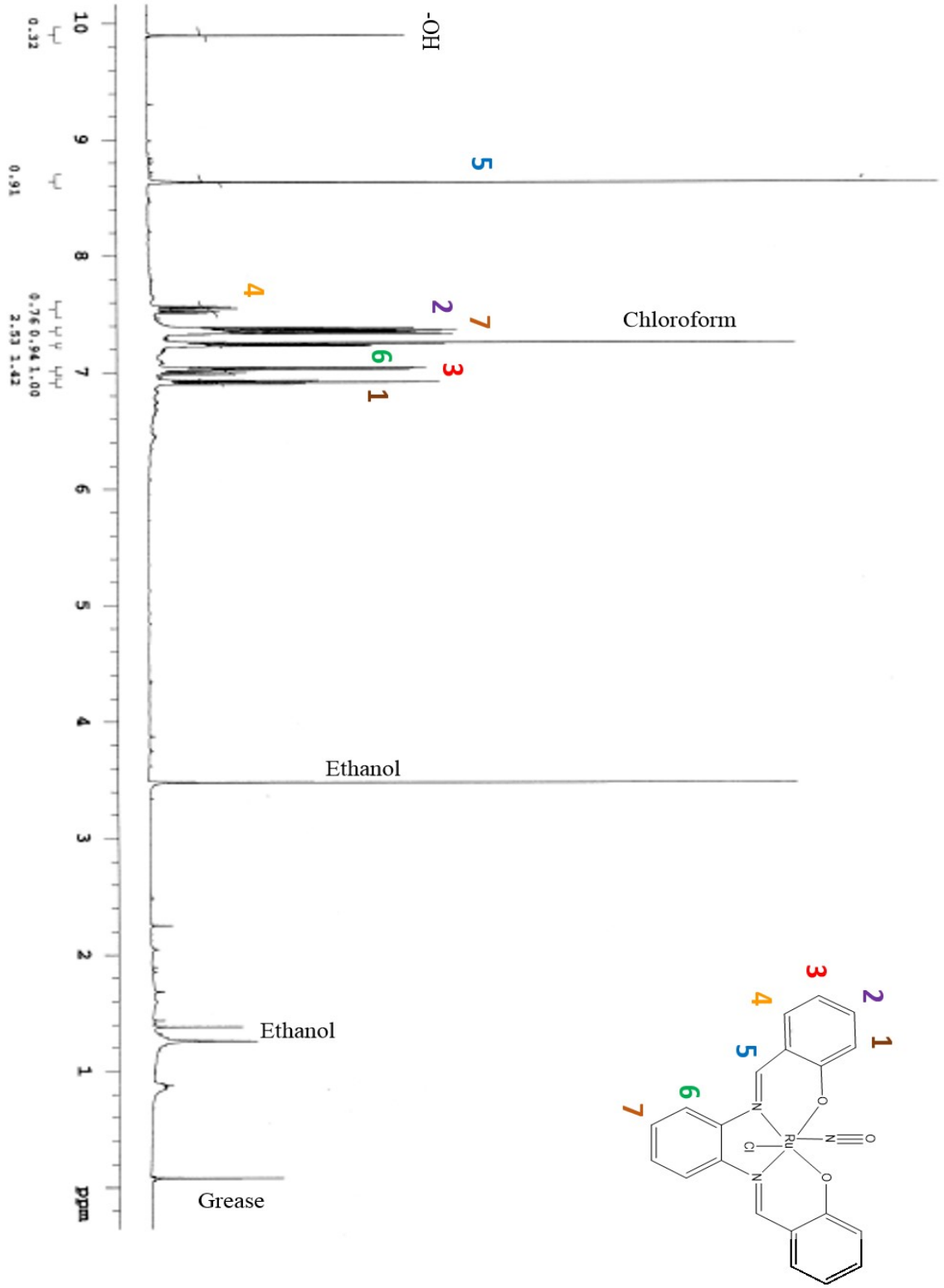

Figure 9. ^{1}H NMR spectra of the Ru(NO)(salophen)Cl in $CDCl_3$ at room temperature. Full spectra.

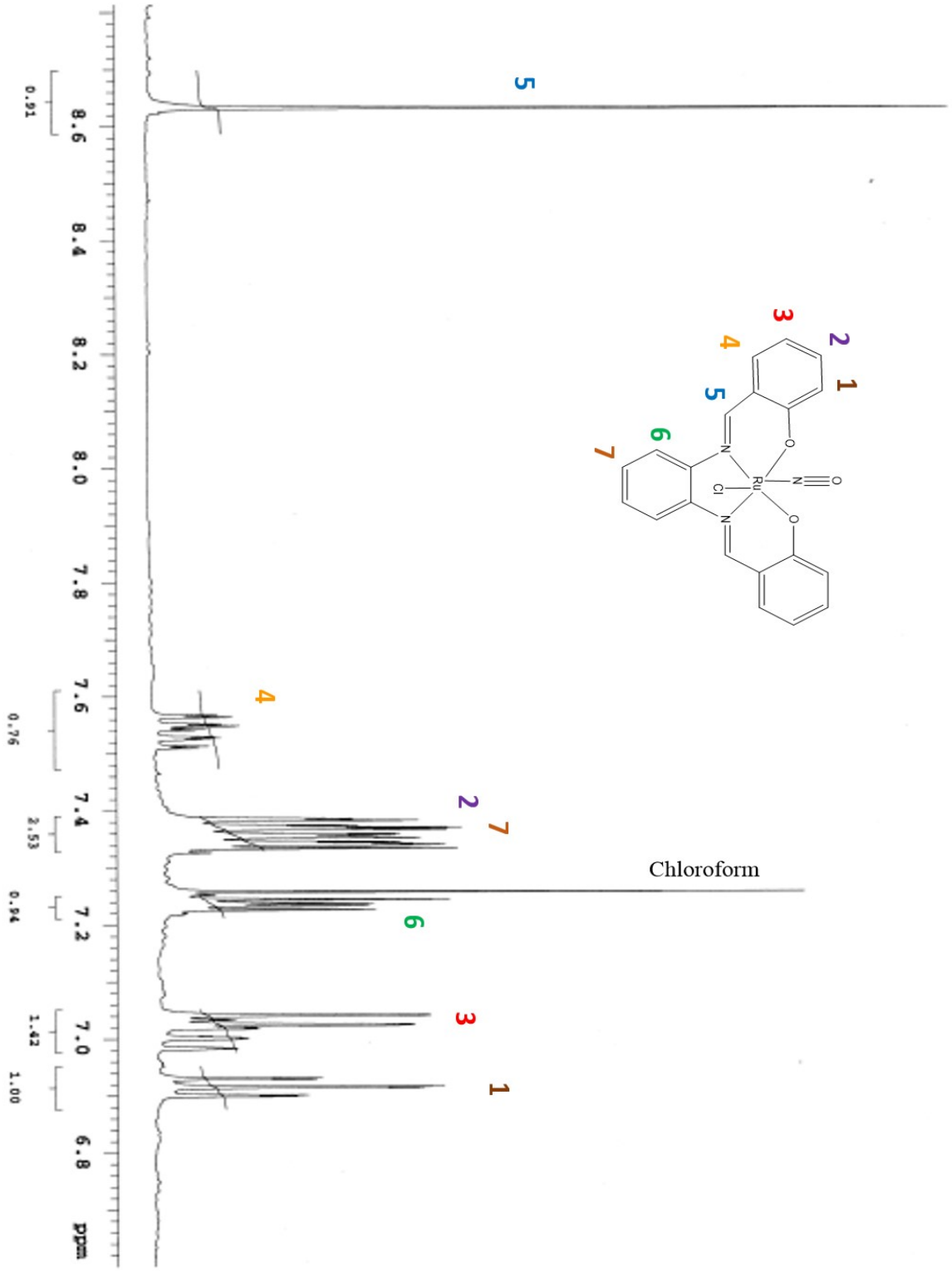

Figure 10. ^{1}H NMR spectra of the Ru(NO)(salophen)Cl in $CDCl_3$ at room temperature. Relevant peaks highlighted.

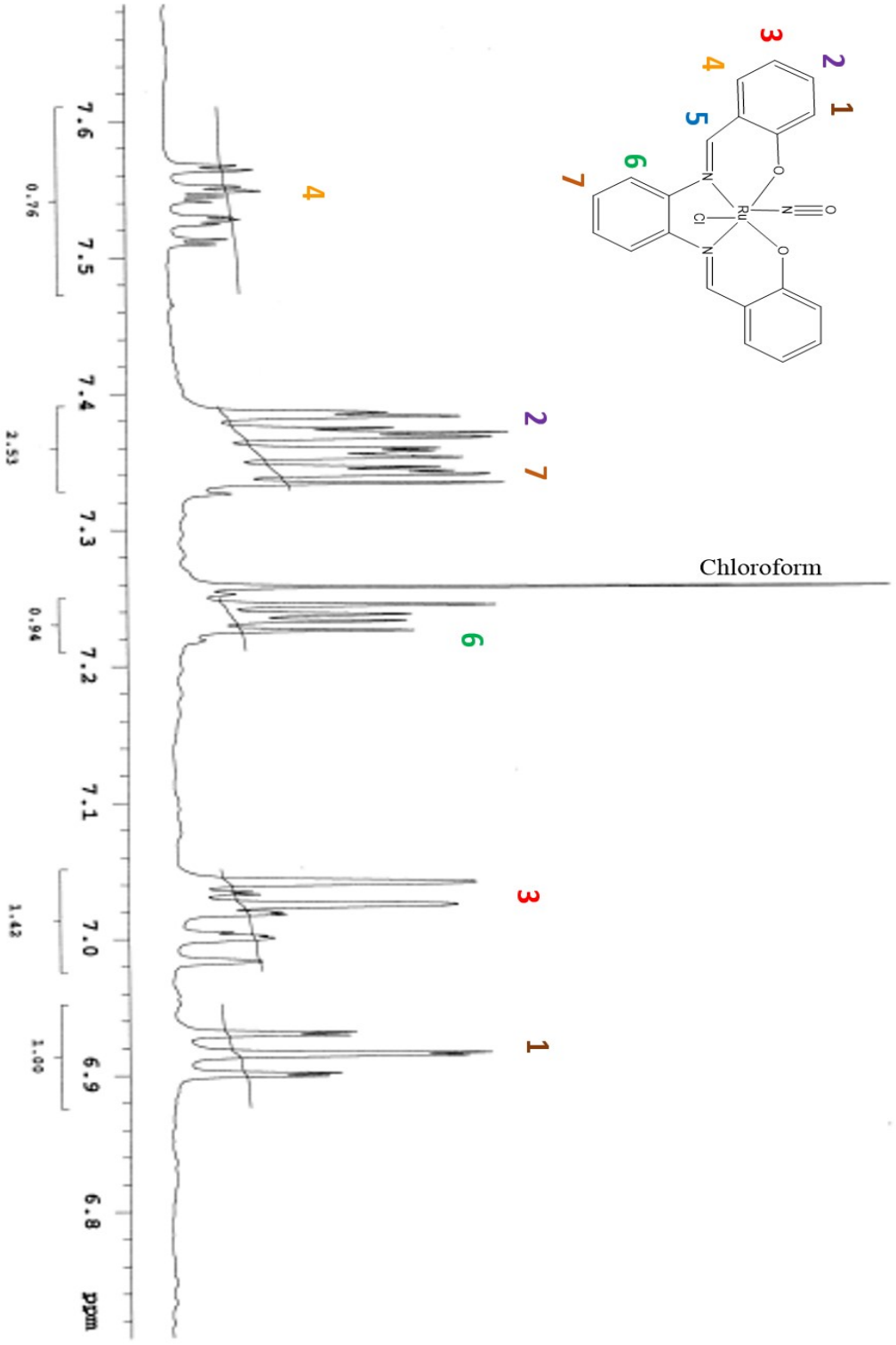

Figure 11. ^{1}H NMR spectra of the Ru(NO)(salophen)Cl in $CDCl_3$ at room temperature. Aromatic region highlighted.

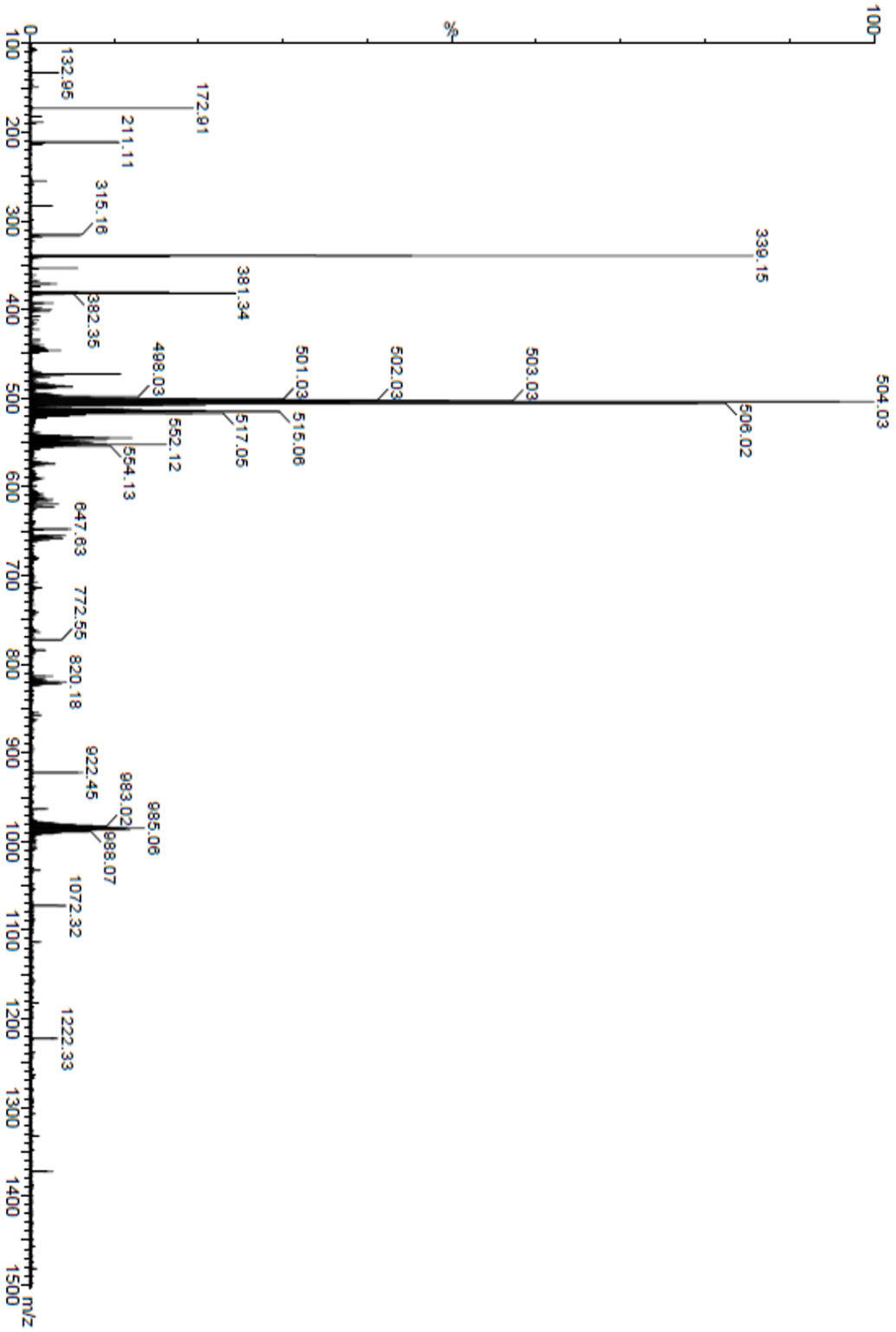

Figure 12. Mass spectra, ESI+ for Ru(NO)(salophen)Cl + Na^+ MW= 480.978 + 23

2.4 Quantum yield measurements

Quantum yields of NO release Φ_{NO} were measured using a GE model NOA 280i Sievers Nitric Oxide Analyzer (NOA), which quantitatively measures the NO present in a gas that has been entrained through the photolysis solution.[3] The carrier gas is either helium or medical grade breathing air. This was first passed through a glass chamber containing only the solvent solution prior to entering the reaction cell in order to prevent evaporative solvent loss and to maintain a constant volume in the reaction cell throughout the experiment. The solvent saturated carrier gas was then run through a four sided, quartz cuvette (Y-cell) containing the photolysis solution to actively purge any NO generated. This gas was then analyzed by the NOA for its NO content. Unless otherwise noted, experiments contained 3 mL of reaction solution. The peak area was calculated using the software "Liquid", and the moles of NO were calculated based on the calibration curve. Quantum yields were calculated by plotting the moles of NO released by the Einsteins of light absorbed during each exposure.

Quantum yield measurements at the pH values at 1.0, 4.5, 6.0, 7.4, 9.0, and 11.0 were conducted individually using a stock solution of compound **1**. The cuvette was filled with 3 mL of pH adjusted solutions of **1** and entrained with carrier gas for 5 minutes, in order to allow the NOA establish a stable baseline. The photolysis was conducted at λ_{irr} 365 nm with the light from a high pressure mercury lamp passed through a narrow band pass interference filter or at 470 nm with a blue LED from Luxeon. The intensity of the excitation at 365 nm was determined using ferrioxolate actinometry;[1] and intensity of the LED light was measured with a Newport power meter. Individual samples were irradiated for varied time intervals controlled by a Uniblitz shutter, and the photchemically released NO was recorded using the NOA software, Liquid. The plotted slope is Φ_{NO}, therefore a slope of y = 0.0036x + 4E-11 results in Φ_{NO} = 0.0036 or 0.36%.

2.4.1 Quantum Yield Calculations

The moles of photons of light absorbed by a reaction for quantum yield measurements requires the photons of light produced from the light source to be calculated. The photons absorbed by the sample are calculated by using the absorbance at the wavelength of irradiation. These are laid out in equations 1 and 2 where I_o is equal to the incident light (photon flux) of the light source and I is equal to the photons transmitted through the sample. The incident light (I_o) is subtracted by ten raised to the negative absorbance of the solution at the wavelength of irradiation. The light absorbed by the sample (I_a) therefore is equal to the moles of photons of light absorbed by the sample determined by subtracting transmitted light from incident light.

Equation 1. $$I = I_o - 10^{-Abs}$$

Equation 2. $$I_a = I_o - I$$

The moles of incident light are determined experimentally by either chemical actinometry or by a power meter measurements. Ferrioxolate actinometry has been the gold standard of actinometry for the wavelengths of 366, 405, 436, 468, 509, 546 nm,[1] for other wavelengths a power meter has been used in this work.

2.4.1.1 Calculations for Ferrioxolate Actinometry

The procedure for ferrioxolate actinometry is written in Calvert and Pitts[1]; the calculations are described below.[1] Potassium ferrioxolate has a well-defined quantum yield of photo reduction to Fe^{2+} in light when expose to 1,10-phenanthroline after photolysis. The

moles of Fe^{2+} are calculated in Eq. 3 from the spectral difference of the actinometry solution at 510 nm after photolysis compared to a non-irradiated sample. Following the procedure laid out in Calvert and Pitts, vol. FeOx irr = volume of the irradiated sample (0.003 L), vol. FeOx used = volume of the irradiated sample aliquot used (0.002 L), Δ *Abs* = the change in absorbance at 510 nm between the irradiated and blank samples. The incident light in photons per second (N_p) is calculated from the moles of Fe^{2+} (Eq. 4), using the known quantum yield at the irradiation wavelength (Φ_{irr}) of the reaction, the duration of irradiation (t) resulting in photons per second, and I_a which is calculated with the absorbance of the ferrioxolate solution at the irradiation wavelength ($I_a = 1 - 10^{-Abs}$). The final incident light is converted to moles of photons per second (known as Einsteins) by dividing N_p by Avogadro's number (Equation 5). Incident light (I_o) from Eq. 5 is used in equations 1 and 2 to calculate the quantum yield of an unknown compound.

Equation 3. $$\text{Moles Fe}^{2+} = \left(\frac{(6.022\text{E}23)(vol.\ FeOx\ irr)(vol.\ FeOx\ used)(\Delta\ Abs.)}{(vol.\ FeOx\ used)(b)(\varepsilon)} \right)$$

Equation 4. $$N_p = \left(\frac{moles\ Fe^{2+}}{(\Phi_{irr})(t)(I_a)} \right)$$

Equation 5. $$I_o = \left(\frac{N_{p/s}}{(6.022E23)} \right)$$

2.4.1.2 Calculations for Power Meter Measurements

A power meter was also used in these studies to find I_o for wavelengths not covered by ferrioxolate actinometry. Power meters such as the Newport power meter used in these experiments, give a power reading in units of Watts with a range from W to nW scale. To convert watts to moles of photons of light absorbed, the number of photons must first be

calculated. The number of photons (N_p, Eq. 6) is calculated from watts measured (E) and energy quanta of the wavelength of light (E_p). The energy quanta is calculated by multiplying Plancks constant (h = 6.63E-34 J•s) with the frequency (f), the frequency is the product of the speed of light (c = 2.988E-8 m/s^2) divided by the irradiation wavelength in meters (λ) (Eq. 7). To convert into photon flux, N_p is divided by Avogadro's number which results in the photon flux in Einsteins.

Equation 6. $$N_p = \left(\frac{E}{E_p}\right)$$

Equation 7. $$E_p = h \bullet f = \left(h \frac{c}{\lambda}\right)$$

Equation 8. $$I_o = \left(\frac{N_p}{(6.022E23)}\right)$$

2.5 pKa measurements

Shifts in UV-visible spectrum of **1** as the pH was changed are indicative of the functioning of several acid/base dependent equilibria for this compound. In order to determine these quantitatively, compound **1** was dissolved in slightly basic water and diluted to a concentration of 0.15 mM in 50 mM KCl solution. The pH was adjusted with slow addition of dilute hydrochloric acid and determined with a pH meter. The pH was allowed to stabilize each time before the UV-visible spectrum was recorded.

2.6 Cell viability studies

Murine melanoma B16F10 cells were grown (2×10^5 cells/well), incubated, and plated in 96-well plates according to published procedures[4]. Each well contained 200 μL of Roswell Park Memorial Institute 1640 medium (RPMI) enriched with 2% Fetal Bovine Serum (FBS). Stock solutions of **1** were prepared in concentrations of 20 mM, 10 mM, 2 mM, and 1 mM, and 2 μL aliquots of these solutions were added to individual wells to establish different concentrations. The final concentrations of **1** in the wells were 200 μM, 100 μM, 20 μM, 10 μM, and 0 μM (control). The cells were incubated with **1** in the dark for 4 h. After incubation the media containing **1** was removed and replaced with fresh media before exposure to light. Phenol red indicator was not used in the media during the photolysis to avoid light being absorbed by the indicator. Half of the cell plates were irradiated with 470 nm light for 4 min with a modified cell plate LED. All plates were then incubated for either 24 or 48 h.

Cell viability was determined by the MTT (3-(4,5-dimethylthiazol-2-yl)-2,5-ditetrazolium bromide) assay protocol.[4] After 24 or 48 h, the media was removed and 200 μL MTT solution (5mg/mL phosphate buffer) was added to each well. The plates were incubated with the MTT for 3 h before the solution was removed and replaced with 200 μL of DMSO. (MTT solution; 12 mM thiazolyl blue tetrazolium bromide in phosphate buffer was diluted in media to a final concentration of 1.2 mM.) The plates were left in the dark for 18 h, and their absorbance was recorded by a Thermo Plate leitora de microplaca TP-reader plate reader at 492 nm. The reported values are an average of two weeks of cell studies equating to 4 plates for each time point. Each plate had 8 samples of the same concentration under identical conditions. Viability was determined based on the results of the MTT assay. The data was

normalized to the control wells in each plate not containing compound 1. Data was compiled and processed using Prism 3.0 software.

2.7 Vascular dilation studies

Male rats (180-200 g) were sacrificed by decapitation under anesthesia. The thoracic aorta was quickly removed, and cut into rings (4-5 mm length). The endothelium was mechanically removed from one of the two rings by gently rolling the lumen of the vessel on a thin wire. Aortic rings with and without endothelium cells were studied concurrently. The aortic rings were placed between two stainless-steel stirrups and connected to an isometric force transducer (Letica Scientific Instruments, Barcelona–Spain) to measure tension in the vessels. The rings were placed in an organ chamber containing Krebs solution with the following composition (mM): NaCl (130.0), KCl (4.7), KH_2PO_4 (1.2), $MgSO_4$ (1.2), $NaHCO_3$ (14.9), glucose (5.5) and $CaCl_2$ (1.6). The solution was maintained at pH 7.4 and bubbled with a gas mixture of 95% O_2 and 5% CO_2 at 37 °C. The rings were initially stretched to a basal tension of 1.5 g and allowed to equilibrate for 60 min. The presence of endothelium was evaluated by the degree of relaxation induced by acetylcholine (1 μM) in the presence of contractile tone first induced by phenylephrine (PE, 0.1 μM). Endothelium-intact arteries were discarded if relaxation with acetylcholine was not greater than 80% while endothelium-denuded arteries were discarded if there was degree of relaxation for acetylcholine higher than 10%. The comparisons between groups were assessed by student *t*- test. The level of statistical significance was defined as $P<0.05$.

The rings were returned to the basal tension of 1.5 g with 10 μL of PE (0.1 μM) and allowed to stabilize for 10 minutes prior to the injection of **1** and two tests for induced

relaxation were conducted, the incremental increase of **1** and the time course relaxation with a high concentration of **1**.

Stock solutions of **1 at** concentrations from 0.1 μM - 5 mM were prepared and injected in sequence to the Krebs buffered organ chambers. The final concentrations ranged of 10^{-10} M up to 10^{-4} M. Tension levels were allowed to stabilize prior to the addition of a higher concentration of **1** (Figure 4). The time course for **1**-induced relaxation was monitored over the course of an hour following the single injection of 20 μL of 5 mM **1** for a finial concentration of 10^{-5} M. (Figure 5). Experiments were conducted in either the dark or in ambient light.

2.8 NOA Calibration

Calibration curves for the NOA were run once a month to ensure accuracy. Stock solutions of sodium nitrite in nanopure water were prepared in serial dilution ranging from 1 μM to 100 μM. The stock solution was injected in triplicate at 5 μL resulting in a calibration curve ranging from a total of 5 pmoles to 500 pmoles. A standard operating procedure (SOP) is listed in Appendix 1.

The NOA was calibrated per the manufacturer's specifications.[5] Briefly, the reaction cell was prepared by dissolving KI (50 mg) into 2 mL of nanopure water and 4 mL of glacial acetic acid. Helium was bubbled through the cell until a baseline below 10 mV was reached. Nitric oxide was generated in the cell by injecting 5 μL aliquots of increasing concentrations of $NaNO_2$ in nanopure water through a septum. The PMT response of the NOA was allowed to return to baseline before the next injection. The integrated signal was used to create a calibration curve.

2.9 UCNP experimental Synthesis of NaYF4: Yb30Gd20Tm0.2 @ NaYF4

UCNPs used in this experiment were synthesized at the Molecular Foundry in Berkeley, Ca. using the automated robotic system WANDA (Workstation for Automated Nanomaterial Discovery and Analysis). The highly precise reaction conditions that WANDA is able to control on individual reactors allows for high reproducibility in nanoparticle synthesis. Synthesis data described in the work of P. T. Burks, *et. al.*[6]

2.10 PLGA Nanoparticles

Poly(lactic-*co*-glycolic acid) (PLGA) nanoparticles with hydrophobic UCNPs and PhotoNORMs, $Yb_{30}Gd_{20}Tm_{0.2}$ @ $NaYF_4$ and Ru(NO)(salophen)Cl (**2**) were synthesized and characterized by Dr. Agustin Pierri and Po-Ju Huang.[7]

2.11 PDMS Polymer Disks

2.11.1 Synthesis of PDMS Polymer Disks

Polymer disks were prepared working with Dr. John Garcia according to manufacturer's specifications for SYLGARD 184. The polydimethylsiloxane (PDMS) liquid was mixed with the curing agent (Catalyst 87-RC) in a 10:1 ratio and thoroughly mixed. The mixture was put under reduced pressure for 30 minutes to remove oxygen and bubbles that had formed during mixing. A Teflon mold was then filled with the viscous polymer solution and was allowed to cure at room temperature for 36 hours until solid.

2.11.2 Loading Up-converting Nanoparticles into PDs

The PDMS disks with up-converting nano particles (UCNPs) were prepared in the same manner as the blank PDs. However, the molds were filled half way with the PDMS and

then 2 mg, 5 mg, or 8 mg of $Yb_{30}Gd_{20}Tm_{0.2}$ @ $NaYF_4$ UCNPs were added. The UCNPs were stirred into the viscous polymer and additional polymer was added to fill the mold. UCNP loaded PDs were left to cure at room temperature for 36 hours.

2.11.3 Infusing Ru(NO)(salophen)Cl into PDs

The hydrophobic complex Ru(NO)(salophen)Cl was infused into the PDMS polymers in the dark under ambient conditions. A concentrated solution of Ru(NO)(salophen)Cl was prepared in THF. One 1 cm diameter polymer disk was suspended in 2 mL of the stock solution for 5 minutes. The solvent was slowly removed over the course of 2 hours under negative pressure. The cycle was repeated three times for each polymer disk, suspending the polymer in an additional 2 mL of stock solution and allowing the sample to rest before the slow concentration of the solution and removal of the solvent.

The samples were washed with nanopure water until UV-visible spectra showed no ruthenium leeching from the polymer. The samples were stored under vacuum.

2.11.4 Efficiency of NO release experiments

The loaded polymer disks (PDs) were attached to a glass coverslip with clear, double side adhesive strips. The glass coverslip was loaded into the flow cell chamber (custom built for the related study by Burks *et. al.*[6]), which has an input valve and an output valve to flow carrier gas through the dry chamber and into the Sievers Nitric Oxide Analyzer for accurate NO release data. The samples were irradiated with a 980 nm multimodal diode laser and exposure time was controlled using a Uniblitz shutter.

2.12 References

[1]J. G. Calvert and J. N. Pitts, Jr., *Photochemistry*, p. 780-815, John Wiley, New York (1966)

[2] Béreau, V.; Jubéra, V.; Arnaud, P.; Kaiba, A.; Guionneau, P.; Sutter, J.-P.; "Modulation of the luminescence quantum efficiency for blue luminophor $\{Al(salophen0\}^+$ by ester-substituents" *Dalton Trans.*, 2010, **39**, 2070-2077.

[3] "Photochemical Studies on Cr(III) Cyclam Complexes. Photosensitization with Semiconductor Quantum Dots and Nitric Oxide Release. Alexis D. Ostrowski, Ph.D. Dissertation, UC Santa Barbara, July 2010

[4] Mosmann, T. "Rapid colorimetric assay for cellular growth and survival: application to proliferation and cytotoxicity assays", *Journal of Immunological Methods*, **65**, 55–63.

[5] "Photochemical Studies on Cr(III) Cyclam Complexes. Photosensitization with Semiconductor Quantum Dots and Nitric Oxide Release. Alexis D. Ostrowski, Ph.D. Dissertation, UC Santa Barbara, July 2010

[6] Peter T. Burks, John V. Garcia, Ricardo GonzalezIrias, Jason T. Tillman, Mutong Niu, Alexander A. Mikhailovsky, Jinping Zhang, Fan Zhang, and Peter C. Ford "Nitric Oxide Releasing Materials Triggered by Near-Infrared Excitation Through Tissue Filters" *Journal of the American Chemical Society* **2013**, *135* (48), 18145-18152

[7] Pierri, A. E.; Stanfill, J. G.; Garcia, J. V.; Wu, G.; Zheng, N.; Ford, P. C.; "A photoCORM nanocarrier for CO release using NIR light", *Submitted*.

Chapter 3. Physical and Spectral Properties of Ru(NO)(Salen-CO_2H)Cl

3.1 Introduction

Ruthenium salen species have been studies for the past several years for their ability to release NO when irradiated with light.[1] Previous studies with ruthenium salen derivatives have involved complexes that are photoactive when irradiated in the near-ultra violet spectral region but have poor water solubility. Described here is the synthesis of a carboxylated salen complex Ru(NO)(Salen-CO_2H)Cl (salen-CO_2H = 3,3'-((1E,1'E)-(ethane-1,2-diylbis(azanylylidene))bis(methanylylidene))bis(4-hydroxybenzoic acid)) that should have markedly improved water solubility, at least at pH values higher than the pKa of the pendant carboxylates. This compound was further studied to evaluate its solubility, photochemical reactivity, oxygen stability, and fluorescent properties. The synthetic procedure leading to this functionalized ruthenium salen nitrosyl complex Ru(salen-CO_2H)(NO)Cl (**1**) is outlined in Scheme 3.1. Details are presented in the Experimental section (sec 1.2 – 1.3.1).

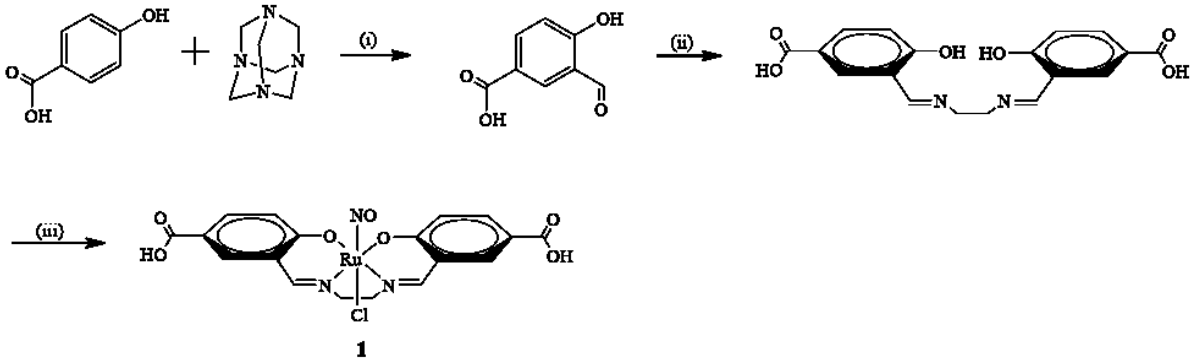

1

Scheme 3.1. Synthesis of Ru(salen-CO_2H)(NO)Cl: (i) triflouroacetic acid, 4 h reflux under argon; (ii) Ethylenediamine (0.5 equiv.), EtOH, reflux 1 h; (iii) NaH (2.3 equiv.), $Ru(NO)Cl_3 \cdot H_2O$ (1 equiv.), EtOH, 4 h reflux under argon.

3.2 pH Dependent Spectroscopic Properties

The optical absorption spectrum of compound **1** displays considerable pH dependence. For example, the band maxima (λ_{max}) for both the visible and UV peaks (Figure 3.1) vary with changing pH. These spectral shifts can be attributed to three acid/base dependent reactions: the nitrosyl (NO) to nitrite (NO_2) conversion and the deprotonation/protonation of both ligand carboxylates (**Scheme 3.2**). Ruthenium based nitrosyl to nitrite conversions have been studied by Tfouni and coworkers[2, 3] and others.[4]

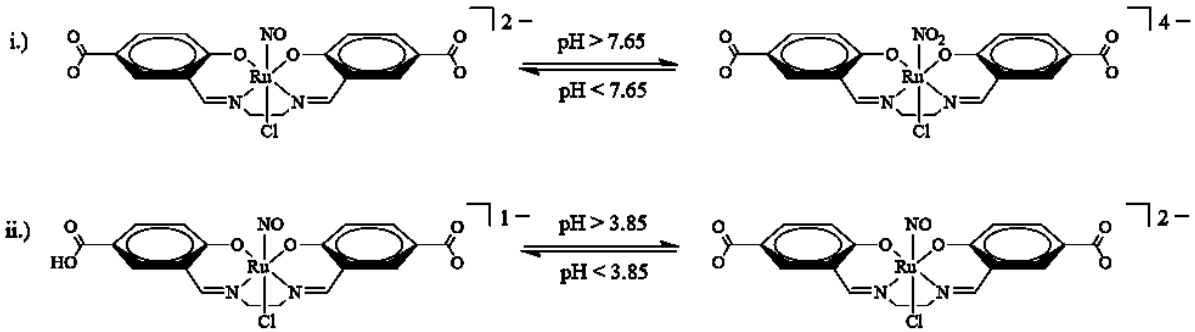

Scheme 3.2. pH dependence of compound 1: i.) nitrosyl to nitrite conversion at a pH greater than 7.65 and ii.) deprotonation of one carboxylic acid

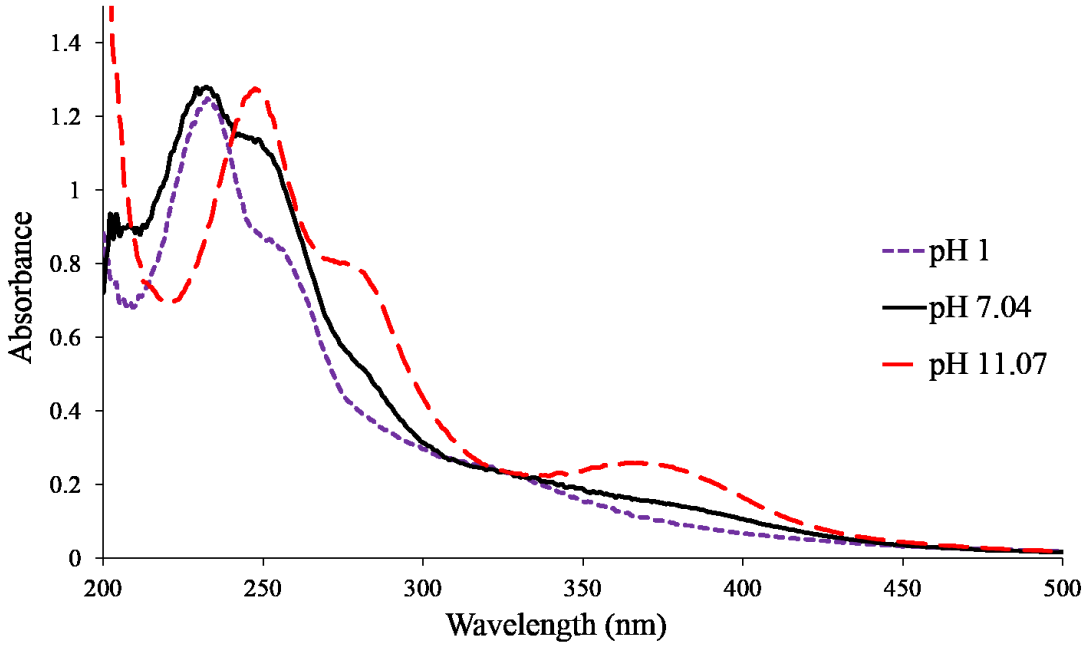

Figure 3.1. pH dependent spectra of Ru(salen-CO_2H)(NO)Cl (**1**) in 50 mM phosphate solution titrated to a pH of 1.0, 7.04, and 11.07. At pH 7.4, absorbance maxima are at 248 nm ($\varepsilon = 3.8 \times 10^4\ M^{-1}\ s^{-1}$) and 359 nm ($\varepsilon = 6.6 \times 10^3\ M^{-1}\ s^{-1}$).

3.2.1 pK_a characterization

A 0.3 mM solution of **1** was prepared in nanopure water containing 10 mM sodium chloride. The solution was adjusted to a pH of 11.5 with NaOH and allowed to equilibrate for 1 minute to establish a stable solution pH prior to titration. At this pH both carboxylate groups should be deprotonated (example: terephthalic acid $pK_a1 = 3.52$, $pK_a2 = 4.46$[5]) and the nitrite species should be prevalent over the nitrosyl species.[6, 7] The solution was then titrated slowly with HCl and the UV-visible spectra was recorded at each interval to identify the spectroscopic shift due to pH. Over the pH range from 11.5 to 0.5, 100 separate pH dependent spectral data points were collected. The dilution of the samples were normalized based on isosbestic points at 323 nm and 438 nm were identified by preparing phosphate buffered solutions at different pH values from a stock solution of 30 μM of **1**.

The separate pK_a values can be identified by specific decreases in absorbance at 371 nm, 323 nm, and 247 nm. The pK_a of the nitrosyl/nitrite reduction was identified by plotting the ratio of the absorbance at 371 nm to that at 323 nm (Abs_{371}/Abs_{323}) over the pH range 3.5 to 11.5 (Figure 3.2). The observed inflection point at pH 7.65 is consistent with known pK_a values of the nitrosyl/nitrite conversion (Scheme 3.2, eq. i). The nitrosyl ligand undergoes nucleophilic attack by hydroxide resulting in a ruthenium coordinated N-nitrito complex as observed in research by Tfouni and co-workers.[6, 7, 8] The pH dependent NO^+ to NO_2^- conversion is further supported by observed spectral changes in the IR spectra where the 1865 cm^{-1} nitrosyl peak disappears and nitrosyl peaks appear at 1427 and 878 cm^{-1} when dissolved in a sodium hydroxide solution. Upon the addition of hydrochloric acid, the nitrite peaks are no longer present and the nitrosyl peak returns at 1865 cm^{-1}.

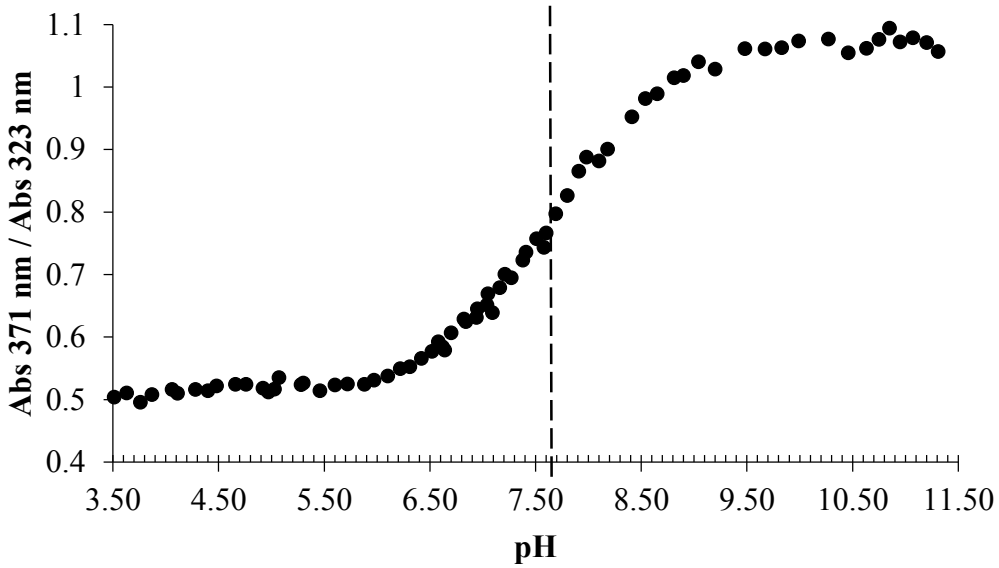

Figure 3.2. Ratio of the absorbance at 371 nm to the absorbance at 323 nm with varying pH. The inflection point (dashed line) represents the pKa of the nitrite to nitrosyl conversion at pH 7.65.

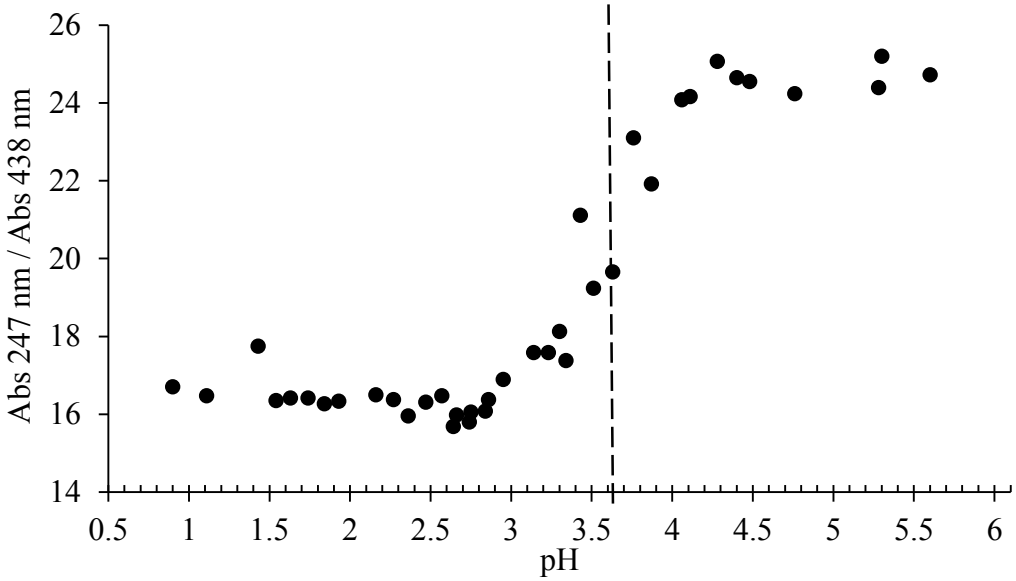

Figure 3.3. Ratio of the absorbance at 247 nm to the absorbance at 438 nm with varying pH. The inflection point (dashed line) represents the pKa of one (or both) of the carboxylate groups at pH 3.65.

Although pK_a values were expected for each of the carboxylic acid/ carboxylate protonation at lower pH, only one was identified. The expected second pK_a of the carboxylic acid was not spectrally observed in the pH titration, very likely because once the compound has reached the second pK_a the compound will be neutral and lose its solubility in water. This

was observed once the pH of solution dropped below 1 and the compound would precipitate from solution. The pK_a of the carboxylate/ carboxylic acid was determined by charting the appearance of a band at 247 nm with decreasing pH. To adjust for dilution, the ratio of absorbance change for 247 nm versus 428 nm was plotted against pH change where 428 nm is an isosbestic point. The Abs_{277}/Abs_{428} ratio was plotted versus a pH from 0.5 to 6. A single inflection point was apparent at a pH of 3.65 which was attributed to the pK_a of one or both carboxylic acid groups (Figure 3.3).

All pH dependent spectral changes were recovered when the solution was back titrated from acidic pH to a basic solution. The spectral reversibility suggests that the compound is stable at a wide range of pH values (pH 0.5-11) and does not decompose. The clear isosbestic points are also indicative of the nitrite compound converting to the nitrosyl followed by the protonation of the carboxylate. The compound is highly stable with reversible carboxylic acid and nitrosyl/ nitrite equilibria that are pH dependent (Scheme 3.2).

3.3 Quantum yields

The quantum yield of nitric oxide release from **1** (Φ_{NO}) was determined under a variety of conditions. These included changing the pH of solution, the presence or absence of oxygen, and the wavelength of the irradiation light.

3.3.1 Quantum yields at pH 7.4, 6.0, and 4.5

Quantum yields are the measure of moles of product divided by the number of photons of light absorbed by the compound undergoing photolysis. The generation of nitric oxide in these experiments was determined using a Sievers Nitric Oxide Analyzer (NOA) to directly measure the moles of NO produced under a specific set of conditions. The quantum yields

will be depicted as Φ_{NO} to designate the quantum yield of NO production upon photolysis of a photoNORM. In graphs used to display Φ_{NO}, the production of NO release is plotted on the y-axis versus the light absorbed in Einsteins on the x-axis, providing a slope equal to the Φ_{NO}.

Experiments to determine the quantum yield of NO release were conducted in 50 mM buffered solutions at several pH values to examine effects of the dramatic shift in the absorbance spectra due to pH changes and establish any possible pH dependence on the ruthenium nitrosyl bond photolysis. Phosphate buffers were used at pH 11.0, 7.4, 6.0, and 4.5 while an HCl/KCl buffer was used for pH 1.0. Tris(hydroxymethyl)aminomethane ("Tris") was used to prepare buffer at pH 9.0. Buffered samples within the biologically relevant pH range of 7.4 – 4.5 are of particular interest as hypoxic tumors and cancerous tissue can have an internal pH ranging from 6.8 – 4.5 whereas healthy tissue generally maintains a pH of 7.4.[9] Quantum yields in phosphate buffer with helium carrier gas exhibits a pH dependent Φ_{NO} with quantum yields of 0.0026 ± 0.0003, 0.0048 ± 0.0003 and 0.0052 ± 0.0002 for the respective pH values 7.4, 6.0 and 4.5 when irradiated at 365 nm (Figure 3.4, 3.5, 3.6, respectively). Under oxygenated conditions, with medical grade breathing air carrier gas, Φ_{NO} values of 0.0020 ± 0.0001, 0.0022 ± 0.0001 and 0.0033 ± 0.0001 were obtained for the same sequence of pH values (Figure 3.7, 3.8, 3.9). Changing the excitation to 470 nm provides quantum yields with the same pH dependence, increasing NO release with decreasing pH. The Φ_{NO} values for pH 7.4, 6.0, and 4.5 at this longer wavelength excitation are 0.00020 ± 0.00002, 0.00024 ± 0.00001, and 0.00026 ± 0.00001 (Figure 3.10, 3.11, 3.12, respectfully).

3.3.1.1 Quantum Yield Charts with pH and oxygen dependence

The charts below are collected data from triplicate runs to determine Φ_{NO} at varying pH values, under inert carrier gas (helium) or in aerated conditions, and with irradiation wavelengths at 365 nm or 470 nm. As the pH decreases and more of the nitrite is converted to nitrosyl, there is an increase in Φ_{NO}. The plots show the moles of NO produced as determined by the NOA verses the amount of light absorbed in Einsteins (I_a*t). (I_a is the intensity of the light absorbed in Einsteins per second, t is in seconds.)

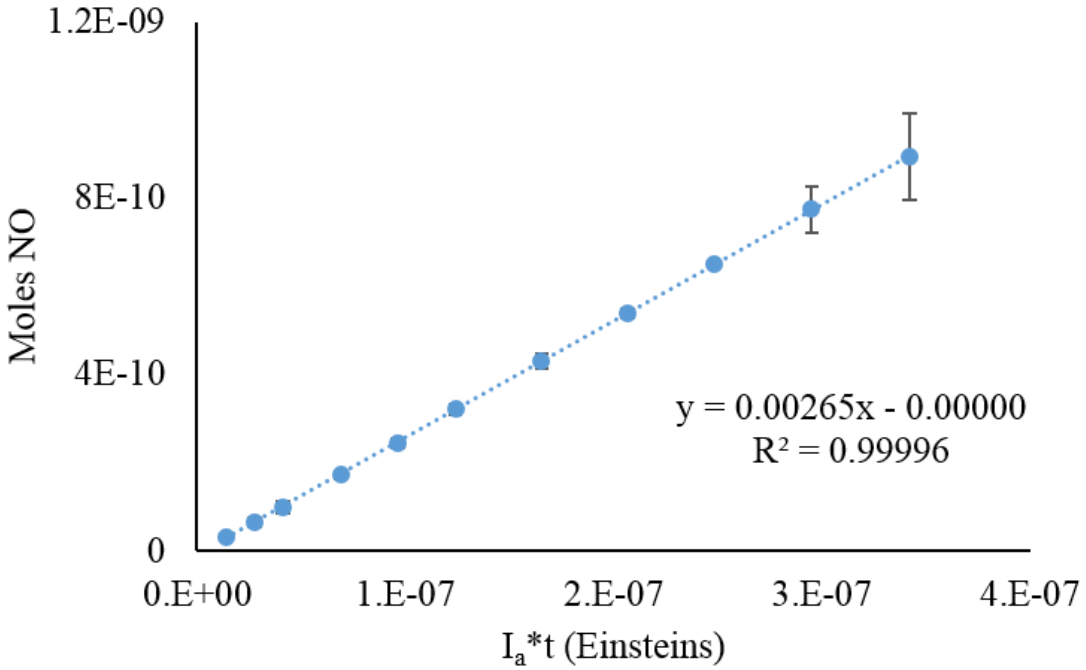

Figure 3.4. Quantum Yield of NO release from Ru(salenCO2H)(NO)Cl at pH 7.4 in phosphate buffer. Irradiated at 365 nm under helium carrier gas.

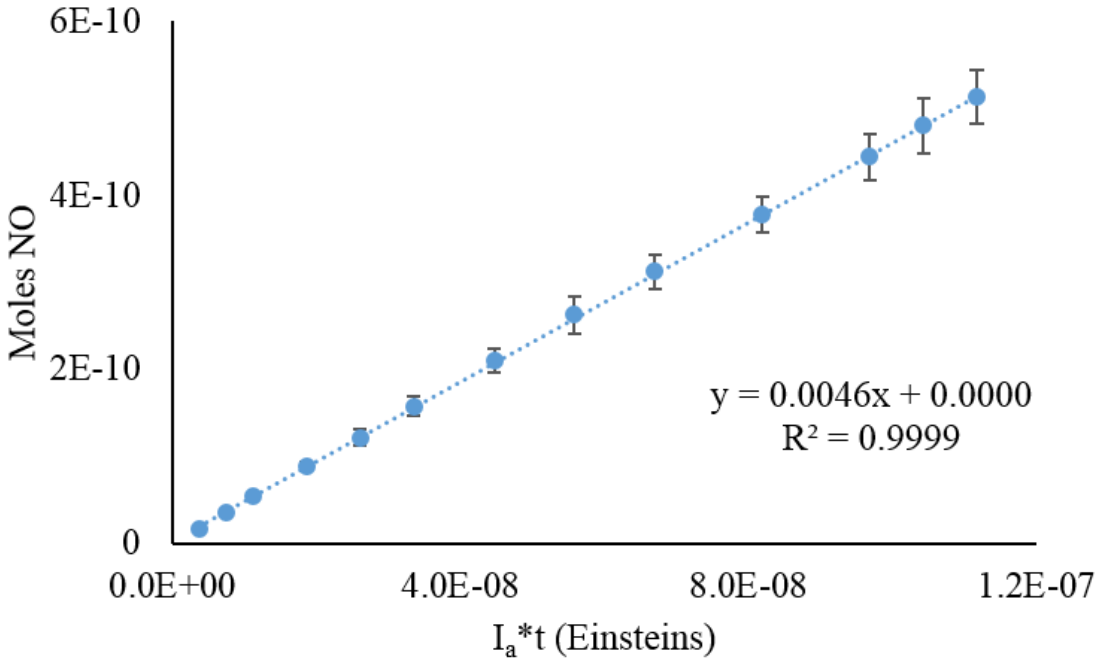

Figure 3.5. Quantum Yield of NO release from Ru(salenCO2H)(NO)Cl at pH 6.0 in phosphate buffer. Irradiated at 365 nm under helium carrier gas

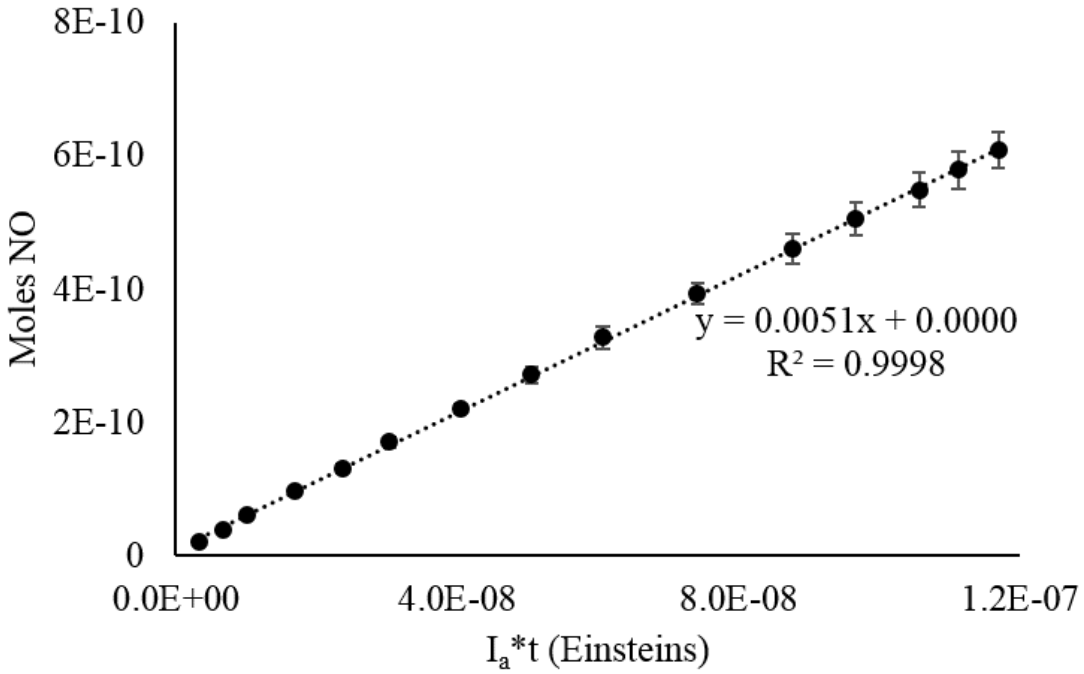

Figure 3.6. Quantum Yield of NO release from Ru(salenCO2H)(NO)Cl at pH 4.5 in phosphate buffer. Irradiated at 365 nm under helium carrier gas.

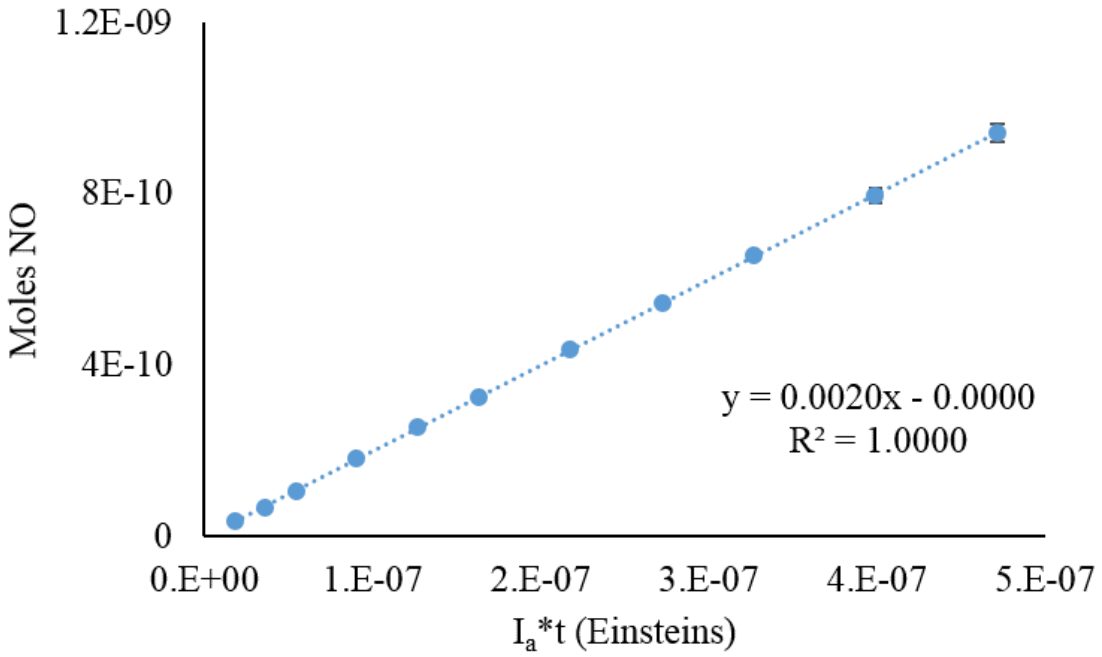

Figure 3.7. Quantum Yield of NO release from Ru(salenCO2H)(NO)Cl at pH 7.4 in phosphate buffer. Irradiated at 365 nm under medical grade air carrier gas.

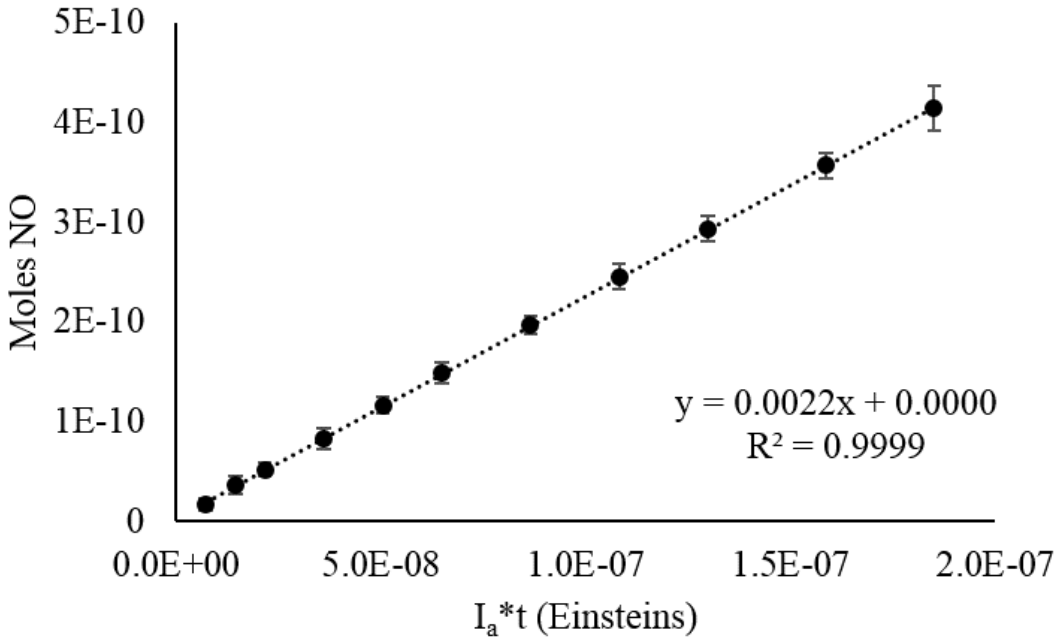

Figure 3.8. Quantum Yield of NO release from Ru(salenCO2H)(NO)Cl at pH 6.0 in phosphate buffer. Irradiated at 365 nm under medical grade air carrier gas.

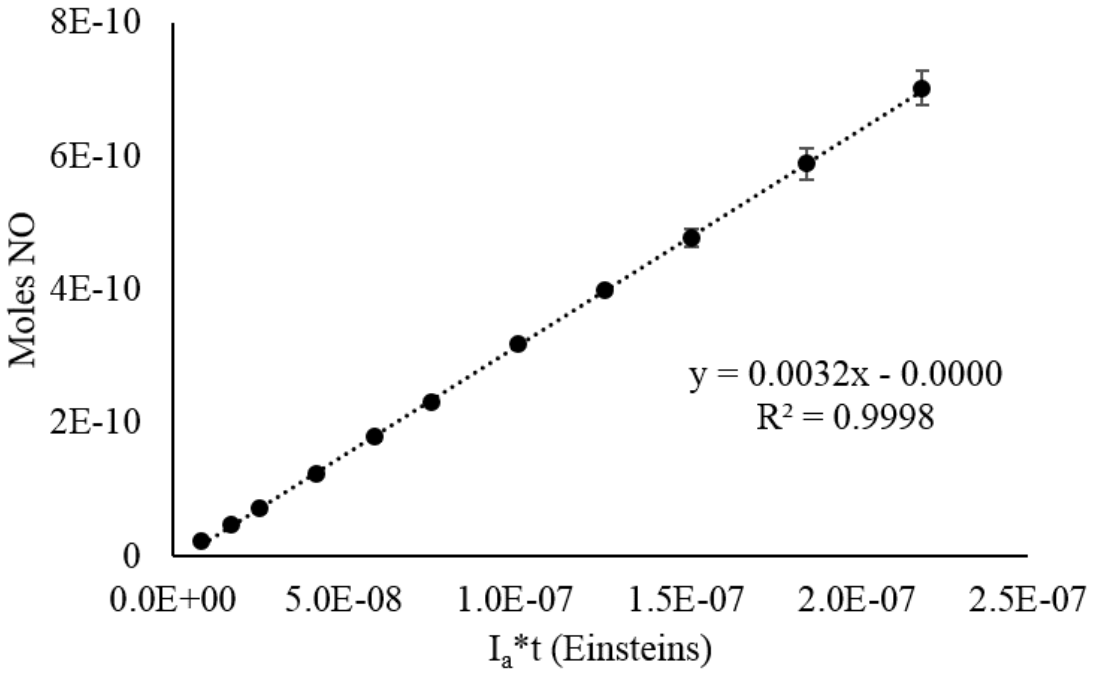

Figure 3.9. Quantum Yield of NO release from Ru(salenCO2H)(NO)Cl at pH 4.5 in phosphate buffer. Irradiated at 365 nm under medical grade air carrier gas.

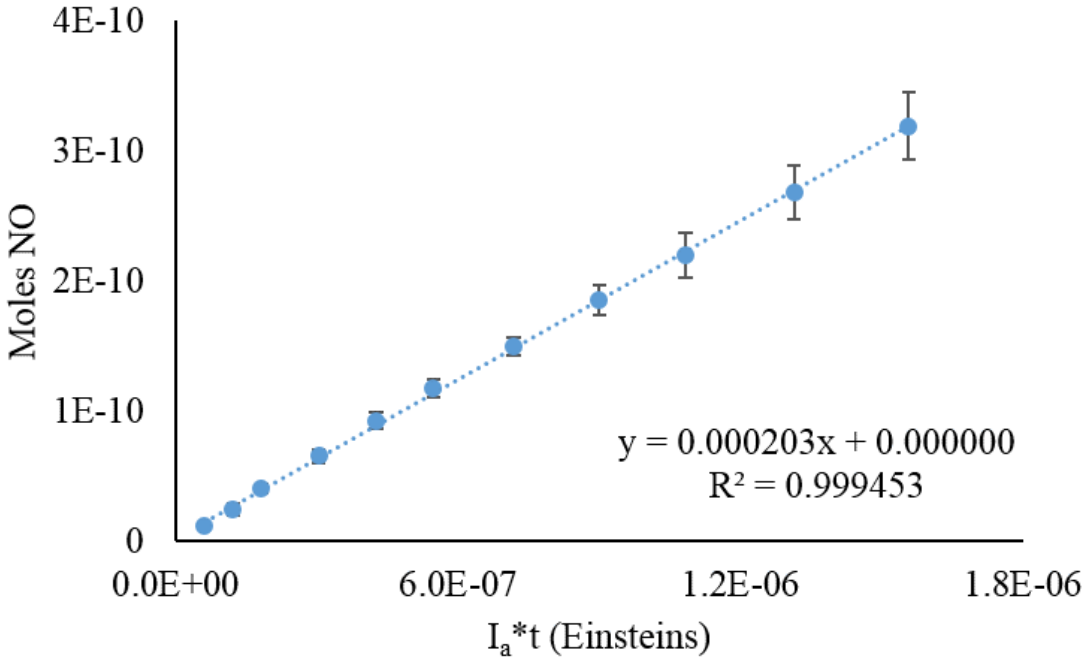

Figure 3.10. Quantum Yield of NO release from Ru(salenCO2H)(NO)Cl at pH 7.4 in phosphate buffer. Irradiated at 470 nm under medical grade air carrier gas.

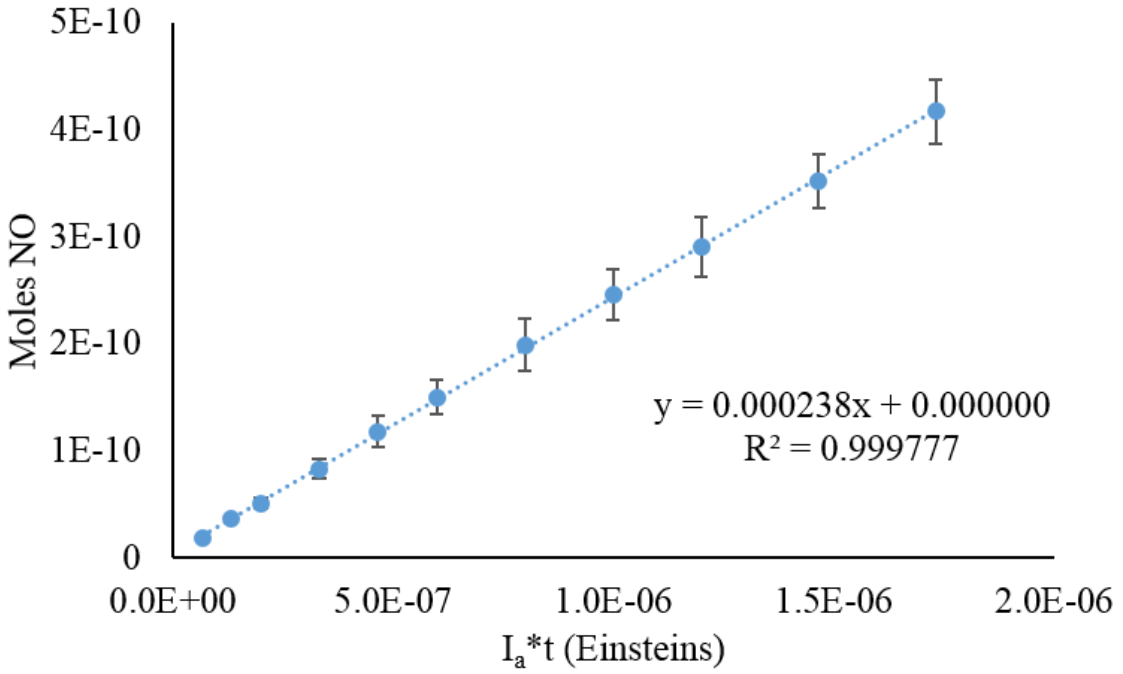

Figure 3.11. Quantum Yield of NO release from Ru(salenCO2H)(NO)Cl at pH 6.0 in phosphate buffer. Irradiated at 470 nm under medical grade air carrier gas.

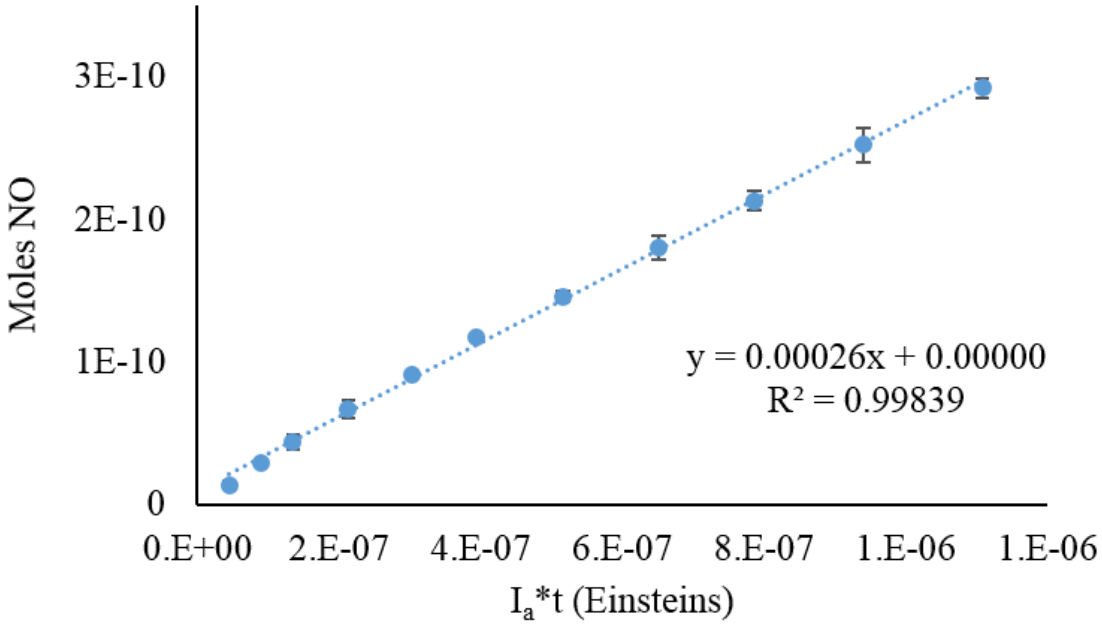

Figure 3.12. Quantum Yield of NO release from Ru(salenCO2H)(NO)Cl at pH 4.5 in phosphate buffer. Irradiated at 470 nm under medical grade air carrier gas.

Table 3.1. Percent abundance of **1** with an axial Nitrite versus Nitrosyl and carboxylate versus carboxylic acid at experimental pH values.

pH	Nitrite Population	Nitrosyl Population	Carboxylate Population	Carboxylic acid Population
11.0	99.99956%	.00044%		
9.0	95.7%	4.3%		
7.4	35.97%	64.03%	99.982%	.018%
6.0	2.2%	97.8%	99.56%	0.45%
4.5	0.07%	99.93%	87.63%	12.37%
1.0	.00002%	99.99998%	0.22%	99.78%

Values established using the Henderson-Hasselbalch Equation [pH = pKa + log10 ([A-]/[HA])].

3.3.2 Quantum yield Discussion

The increase in Φ_{NO} at lower pH can be correlated to the pH dependent population of the axial nitrosyl group versus an axial nitrite group. The ratio of nitrite: nitrosyl at pH 7.4 is approximately 36:64 while the population of the nitrosyl sharply increases as the pH decreases to values below the nitrite/ nitrosyl pK_a (Scheme 3.2 eq. i). At pH 6.0 the ratio has shifted to a ratio of 2:98 and at 4.5 almost all of the axial ligand has converted to the nitrosyl. There is a corresponding increase in Φ_{NO} supporting the view that the nitrosyl form is considerably more photoactive than is the corresponding nitrito complex. This equilibrium is shown in Scheme 3.2 and presented in table 3.1 along with the population of protonated and deprotonated carboxylic acid. Therefore, as the pH drops from 7.4 to 6.0 the percentage of the nitrosyl has increased from 64% to 98% while the Φ_{NO} increased more than 80% (from 0.0026 ± 0.0003 to 0.0048 ± 0.0003, helium carrier gas, λ_{irr} = 365 nm). As the pH decreases and the population of the nitrosyl increases, the release of NO becomes more favorable and the quantum yields increase.

The introduction of oxygen into the system induces a sharp decrease in the NO quantum yield, which is exaggerated as the pH drops from 7.4 down to 4.5. The Φ_{NO} at 7.4

decreased by 25% compared to the oxygen free photolysis conditions while the Φ_{NO} decreased by 55% for samples at a pH of 6.0 and a drop in Φ_{NO} of 65% was observed at pH 4.5. The trend of increasing Φ_{NO} with decreasing pH is maintained even when oxygen is introduced. The Φ_{NO} values here are consistent with reported data for the Φ based on the formation of the photoproduct for the [Ru(salen)(H_2O)(NO)]Cl when photolysed at 365 nm in water resulting with a Φ_{NO} of 0.005 ± .001.[10]

3.3.3 Quantum Yields at Extreme pH values

Extreme pH values were also studied to ascertain their effect on the production of NO. At pH 11.0 and 9.0 the nitrite: **1** is almost entirely in the nitrite form resulting in a low Φ_{NO} of 0.0009 ± 0.0002 and 0.0005 ± 0.0001 when irradiated at 365 nm in aerated conditions (Figures 3.13 and 3.14). Similarly when considering the impact of acidic pH on nitrosyl/nitrite equilibrium, the high population of nitrosyl at pH 1 results in a Φ_{NO} of 0.0024 ± 0.0002 (Figure 3.15). As reported above, the Φ_{NO} at pH 4.5 in oxygen saturated solutions has a quantum yield of NO release of 0.0033 while at pH 1 the Φ_{NO} drops to 0.0024 (Scheme 3.2, eq. 2).

The large difference between Φ_{NO} at pH 11.0 and 9.0 versus that at pH values below the nitrite/nitrosyl pK_a (7.65) shows the unfavorable photogeneration of NO from nitrite and increased production of NO once the ratio of axial nitrosyl has increased. In contrast to the strong dependence of Φ_{NO} on the nitrosyl pK_a the acidification of the carboxylates functions (pK_a 3.65) appears to have little effect.

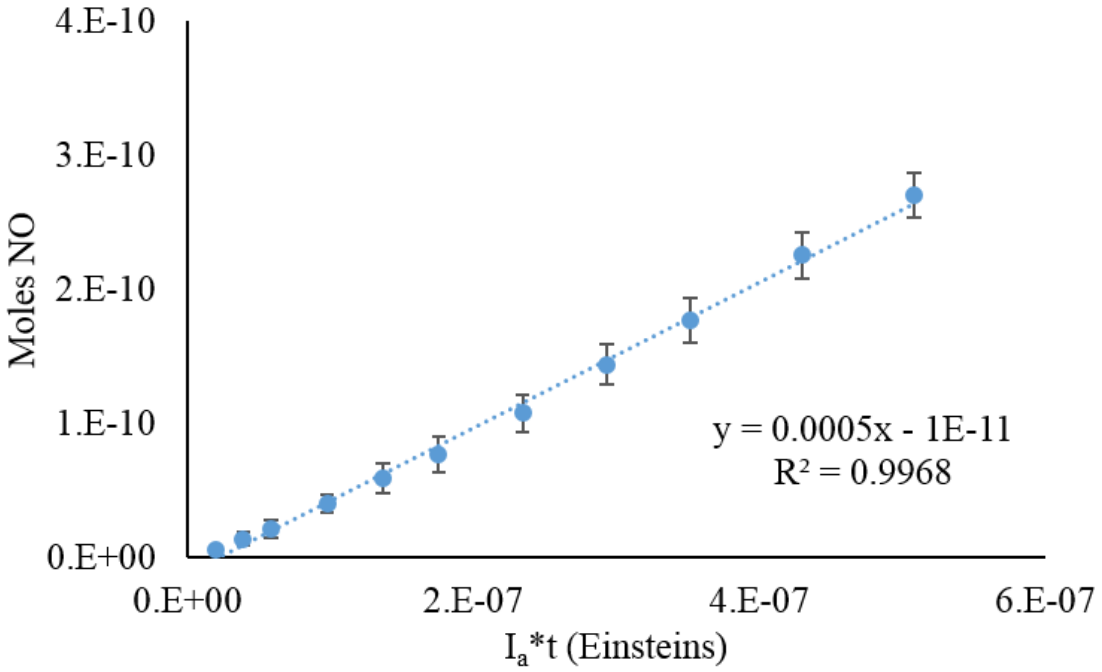

Figure 3.13. Quantum Yield of NO release from Ru(salenCO2H)(NO)Cl at pH 11.0 in phosphate buffer. Irradiated at 365 nm under medical grade air carrier gas.

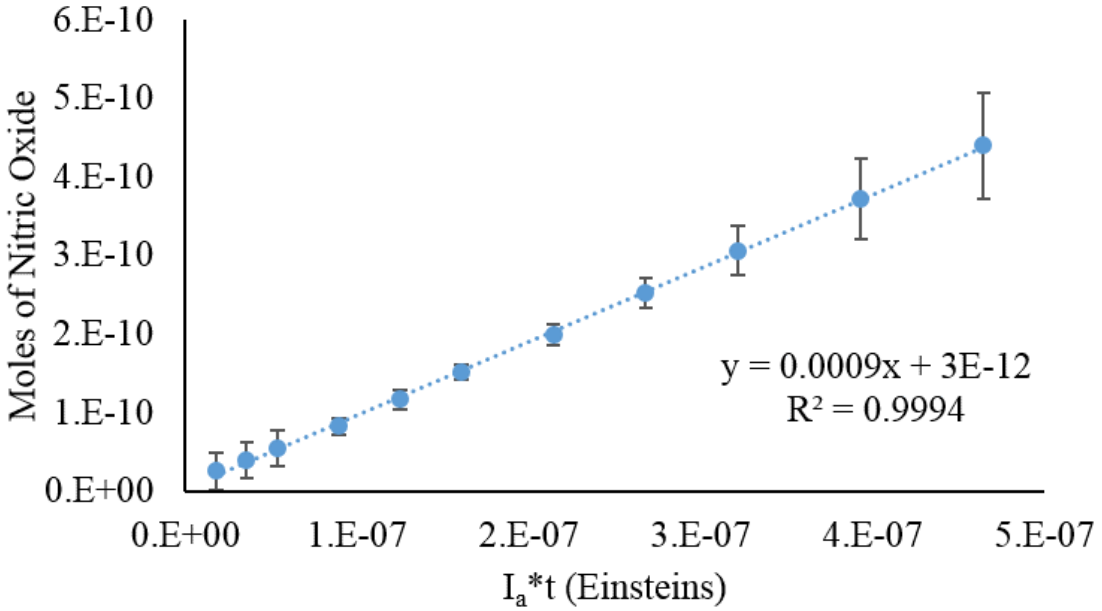

Figure 3.14. Quantum Yield of NO release from Ru(salenCO_2H)(NO)Cl at pH 9.0 in Tris buffer. Irradiated at 365 nm under medical grade air carrier gas.

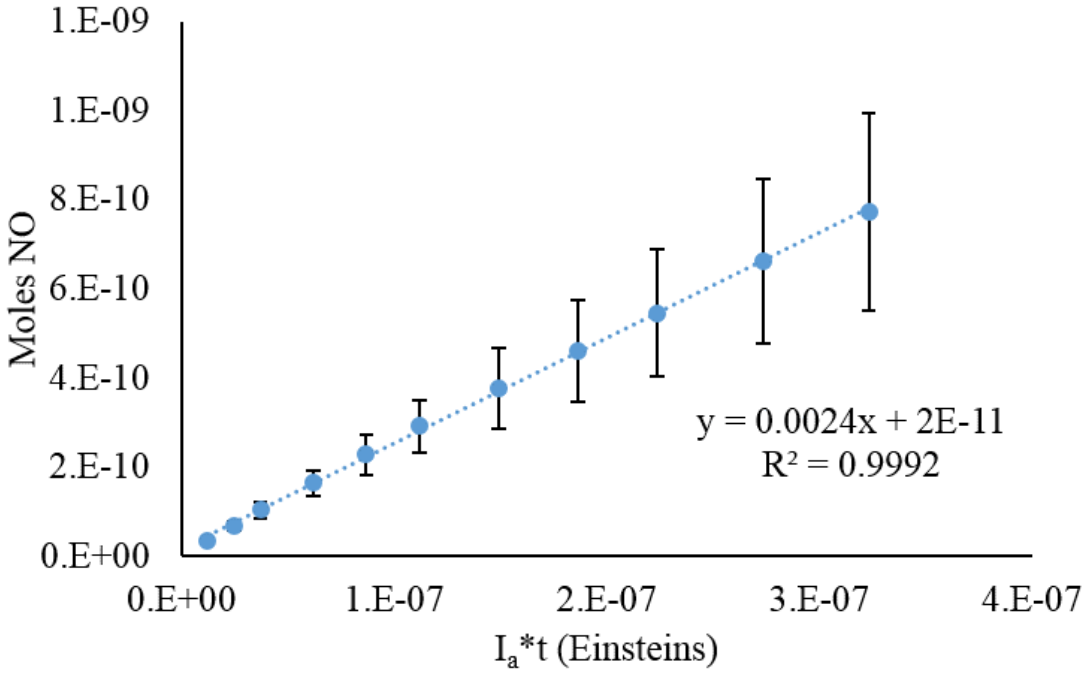

Figure 3.15. Quantum Yield of NO release from Ru(salenCO_2H)(NO)Cl at pH 1.0 in HCl/ KCl buffer. Irradiated at 365 nm under medical grade air carrier gas.

3.4 Fluorescence Properties of Compound 1

While extensive NO release experiments were performed, the low quantum yields of NO release indicated alternative relaxation pathways for the excited compound. Therefore, the fluorescence properties were also examined and are described below.

3.4.1 Fluorescence Experimental Design

Emission and excitation samples were prepared from the same stock solution of Ru(NO)(salen-CO_2H)Cl (45.5 mM in nanopure water with NaOH). Each of the 6 samples were prepared by adding 40 μL of stock solution and separate buffers were added to bring the samples up to volume in 10 mL volumetric flasks. Phosphate buffers were prepared for pH values 11.0, 7.4, 6.0, and 4.5 while an HCl/KCl buffer was used for pH 1.0 and tris(hydroxymethyl)aminomethane was used to prepare the pH 9.0 buffer.

3.4.2 Experimental Fluorescence Properties

A stock solution of **1** (45.5 mM) was diluted into a total volume of 10 mL at each buffered pH value tested resulting in a final concentration of 182 μM of compound **1** at each of the pH values listed above. Samples were excited with 355 nm light and the emission maximum was observed at 505 nm regardless of pH, with the brightest emission specifically observed at pH 7.4 (Figure 3.16). Emission was adjusted for I_o to account for the change in absorbance due to differences in pH. The emission at pH 11.0 decreases 30% from the pH 7.4 sample, while pH values 9.0 and 6.0 show 50% less emission than that of the pH 7.4 sample. Excitation of compound **1** at pH 4.5 displayed only limited fluorescence emission while the most acidic solution (pH 1) displaying essentially no emission. Therefore, the fluorescence emission spectra as well as the Φ_{NO} are both highly pH sensitive, with differences owing to the pK_a values and the overall charge of the compound in varying pH environments.

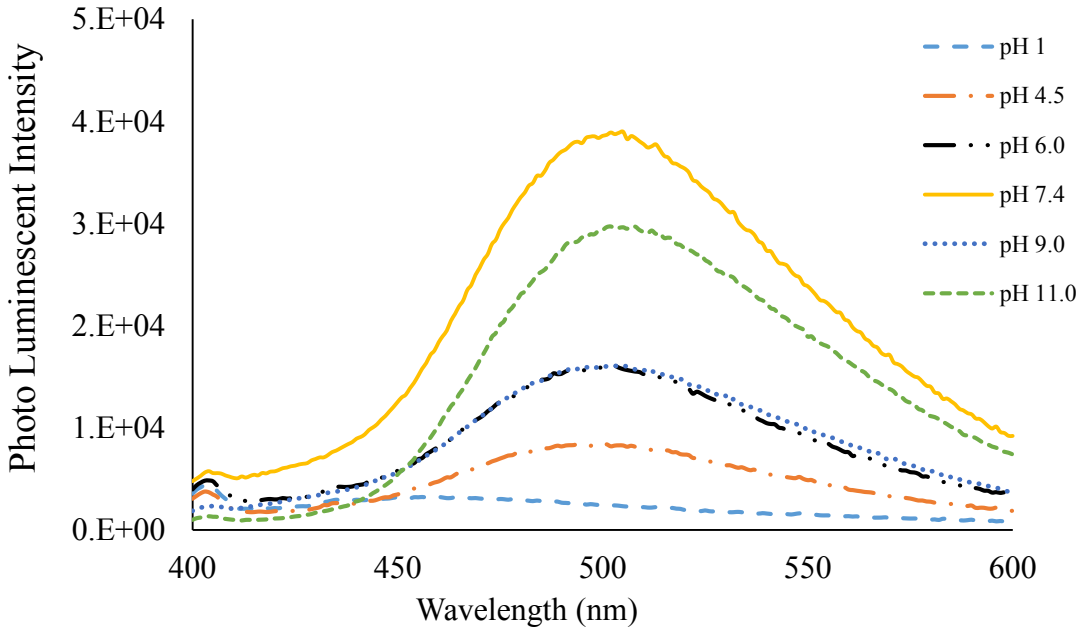

Figure 3.16. Fluorescence emission of compound 1 with a λ_{em} at 505 nm. Concentration 182 μM of 1 in 50 mM buffered solutions at each indicated pH.

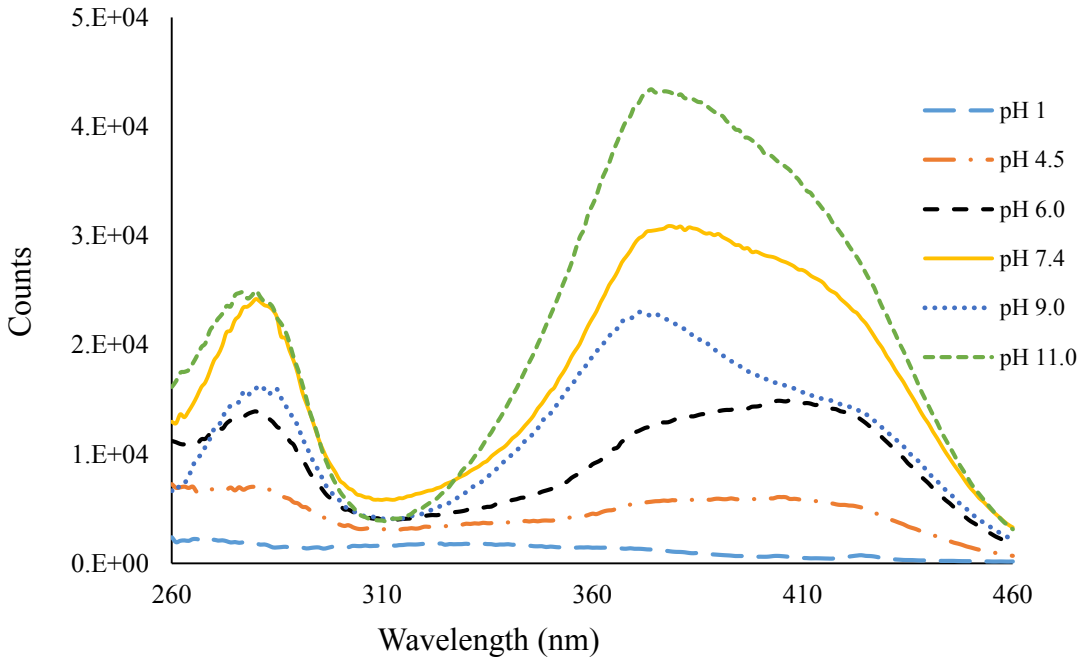

Figure 3.17. Excitation spectra monitoring at 495 nm emission while scanning from 260 nm to 460 nm. Starting from top to bottom, λ_{max} = 277nm at pH 11.0, shifting to 280 nm at lower pH. The second band beginning at λ_{max} = 375 nm with the plateau ending at 425 nm.

As evident by the excitation spectra (Figure 3.17), excitation at 280 nm and at 375 nm result in strong emission at 495 nm. This emission is stronger at higher pH values and greatly decreases with the protonation of the carboxyl groups and are heavily influenced by the nitrite/nitrosyl conversion. Therefore, at the lowest pH solutions (4.5 and 1.0) are less emissive at 495 nm. From pH 9 to pH 7.4 the nitrosyl: nitrite ratio changes from 100% nitrite to 56:44, NO: NO_2 (ratio calculated from the Henderson-Hasselbalch equation). A second excitation wavelength is allowed once the pH drops below the nitrosyl pKa causing a spike in the excitation and broadening the excitation band. The excitation spectra therefore shows the highest emission at 495 nm when at pH 11.0. A 25% decrease in emission at a pH of 7.4, followed by 9.0 and 6.0. As the pH continues to decrease the aromatic carboxyl groups begin to heavily influence the fluorescence quantum yield. [11] At a pH of 4.5 the ratio of deprotonated

to protonated carboxylate ratio has decreased to 88:12 resulting in lower emission while at pH of 1.0 where the ratio is 0.2:99.8, no emission is observed when excited.

Parallels can be drawn between this compound and fluorescein. Fluorescein has multiple pK_a values which translate into absorbance and emission spectrums being highly pH dependent. When the pH drops below the pK_a for the phenol group the quantum yield of emission dramatically decreases.[12] Fluorescein's emission decreases as it moves from the dianionic to anionic to neutral and regains a portion of the emission once in the cationic state (xanthylium species).

3.5 Conclusion

Here we have synthesized and characterized a novel water soluble photoNORM. Several pK_a values were identified for the nitrosyl to nitrite conversion at 7.65 consistent with research on similar compounds, and a single carboxylic acid pK_a at 3.65, while protonation of the second carboxylate is thought to occur at a pH that is not evident in aqueous solutions employed, possibly due to a loss of solubility.[13] The defined pK_as proved to be of great importance and impact both the quantum yields as well as emission and excitation of the species. The pH dependent Φ_{NO} proves that the NO is released from a nitrosyl ligand and not from the nitrite. As the pH decreases, the alternative modes of energy release through fluorescence decrease and improve the release of NO, therefore Φ_{NO} increases.

The Φ_{NO} is also highly dependent on the presence of oxygen. Changing the carrier gas for the quantum yield experiments from helium to medical grade air, causes the production of NO to drop. At pH 4.5, the Φ_{NO} drops from 0.0052 to 0.0030 when oxygen is used to purge the reaction cell (λ_{irr} = 365 nm). The drop in NO release can be due to the production of a small amount of NO_x species such as NO_2 once oxygen is present,[14,15] since the NOA does

not identify NO_x species, the production of these species cannot be included in the quantum yield. The oxygenated experiments however, still exhibit the same trend of an increased quantum yield with decreased pH resulting from the increased population of the ruthenium nitrosyl.

3.6 References

[1] Works, C. F.; Jocjer, C. J.; Bart, G. D.; Bu, X.; Ford, P. C.; "Photochemical Nitric Oxide Precursors: Synthesis, photochemistry, and ligand substitution kinetics of ruthenium salen nitrosyl and ruthenium salophen nitrosyl complexes", *Inorg. Chem.*, **2002**, 41, 3728-3739.

[2]Doro, F. G.; Rodrigues-Filho, U. P.; Tfouni, E.; "A regenerable ruthenium tetraammine nitrosyl complex immobilized on a modified silica gel surface: Preparation and studies of nitric oxide release and nitrite-to-NO conversion", *Journal of Colloid and Interface Science*, **2007**, 307 (2), 405-417.

[3]Caramori, G. F.; Kunitz, A. G.; Andriani, K. F.; Doro, F. G.; Frenking, G.; Tfouni, E.; "The Nature of Ru-NO bonds in ruthenium tertraazamacrocycle nitrosyl compleses- a computational Study", *Dalton Trans.*, **2012**, 41, 7327-7339.

[4]Codesido, N. O.; Weyhermüller, T.; Olabe, J. A.; Slep, L. D.; "Nitrosyl-Centered Redox and Acid-Base Interconversions in $[Ru(Me_3[9]aneN_3)(bpy)(NO)]^{3,2,1+}$. The pK_a of HNO for its Nitroxyl Derivative in Aqueous Solution", *Inorg. Chem.*, **2014**, 53 (2), 981-997.

[5] Brown, H. C.; Baude, E. A.; Nachod, F. C.; "Determination of Organic Structures by Physical Methods", *Academic Press*, NY, **1955**.

[6]Tfouni, E.; Krieger, M.' McGarvey, B. R.; Franco, D. W; "Structure, chemical and photochemical reactivity and biological activity of some ruthenium amine nitrosyl complexes", *Coord. Chem. Rev.*, **2003**, 236, 57-69.

[7]Roncaroli, F.; Ruggiero, M. E.; Franco, D. W.; Estiú, G. L.; Olabe, J. A.; "Kinetic, mechanistic, and DFT study of electrophilic reactions of nitrosyl complexes with hydroxide", *Inorg. Chem.*, **41** (**2002)**, 5760.

[8]Bottomley, F.; P.S. Braterman (Ed.), Reactions of Coordinated Ligands, vol. 2, Plenum Press, New York, **1989**.

[9]C. W. Song, R. Griffin, and Heon Joo Park, "Influence of Tumor pH on Therapeutic Response", *Cancer Drug Discovery and Development: Cancer Drug Resistance*, p. 21- 42, ed. B. Teicher Humana Press Inc., Totowa, NJ (2006)

[10] Works, C. F.; Jocjer, C. J.; Bart, G. D.; Bu, X.; Ford, P. C.; "Photochemical Nitric Oxide Precursors: Synthesis, photochemistry, and ligand substitution kinetics of ruthenium salen nitrosyl and ruthenium salophen nitrosyl complexes", *Inorg. Chem.*, **2002**, 41, 3728-3739.

[11] Watkins, A. R.; "Protination of aromatic carboxylic acids in the first excited singlet state", *J. Chem. Soc., Faraday Trans. 1*, 1972, **68**, 28-36.

[12] Sjöback, R.; Nygren, J.; Kubista, M.; "Absorption and fluorescence properties of fluorescein", *Spectrochimica Acta Part A*, **51** (1995) L7-L21

[13] Ingram, A. J.; Dunlap, A, G.; DiPietro, R.; Muller, G.; "Speciation, Luminescence, and Alkaline Fluorescence Quenching of 4-(2-Methylbutyl)aminodipicolinic acid (H2MEBADPA)", *J. Phys. Chem. A.*, **2011**, 115(27): 7912–7920.

[14] Ashmore, P. G.; Burnett, M. G.; Tyler, B. J.; "Reaction of Nitric Oxide and Oxygen", *Trans. Faraday Soc.*, 1962, **58**, 685-691.

[15]Lewis, R. S.; Deen, W. M.; "Kinetics of the Reaction of Nitric Oxide with Oxygen in Aqueous Solutions", Chem. Res. Toxicol., **1994**, 7, 568–574.

Chapter 4. Biological Studies of Ru(NO)(salen-CO2H)Cl

4.1 Introduction

Compound **1** has potential pharmaceutical applications due to its ability to release NO within cells upon photoexcitation. With valuable properties compatible with biological systems, such as high water solubility, photoactive release of NO, and pH dependent quantum yield, compound **1** will release NO only in cellular regions that have been irradiated with the necessary wavelength of light. The compound was therefore tested for toxicity in a murine melanoma cell line and for its ability to induce vasodilation in murine (rat) arteries. The majority of the work in this chapter was completed at the Univerdidade de São Palo, Ribeirão Preto in Brazil in the labs of Dr. Roberto Santana da Silva and Dr. Lusiane M. Bendhack.

4.2 Cell Viability

Toxicity studies were completed using murine melanoma B16F10 cells. Melanoma B16F10 cell lines were grown to a concentration of 2×10^5 cells/ mL and 200 μL of such suspensions were aliquoted into each well of 96-well plates with RPMI growth media. The cells were incubated within the 96-well plate for 24 h, allowing the cells to affix to the surface of the 96-well plate.

Stock solutions of compound **1** in RBMI media were prepared at concentrations of 20 mM, 10 mM, 2 mM, and 1 mM. Each well contained 200 μL of media and a 2 μL aliquot of the stock solutions with varying concentration was added to each well. The final concentration of **1** was 200 μM, 100 μM, 20 μM, 10 μM, and 0 μM as a control. Cells were incubated in the dark for 4 h followed by exposure for 4 min to 470 nm light or shielded from light and then incubated traditionally, in the dark for an additional 24 or 48 h. Experiments that were exposed

to light were done so on a custom plate mount with individual 470 nm LEDs in each well of the 96-well plate and calibrated to a power of 13.69 mW. The reported values are an average of triplicate samples in three different experiments.

Cell viability was determined using the well-established MTT (3-(4,5-dimethylthiazol-2-yl)-2,5-ditetrazolium bromide) assay to determine the population of living cells via NAD(P)-H enzymatic activity.[1] For the MTT assay, after completion of incubation time the media is replaced with MTT solution (12 mM thiazolyl blue tetrazolium bromide in phosphate buffer was diluted in media to a final concentration of 1.2 mM). The MMT is absorbed through the plasma membrane of living cells and processed by the mitochondria to produce a formazan dye that absorbs strongly at 570 nm. The absorbance spectra is recorded and a higher absorbance in a sample indicates a higher concentration of living cells. Wells incubated without exposure to **1** were used as control.

After 24 h, cells incubated with a concentration of 10 μM of **1** showed no statistical difference from the control as determined by Tukey's post-hoc test with cell viability at 94% and 97% for dark and light exposed samples. As the concentration of **1** was incrementally increased to 200 μM, cell survival decreased moderately to about 60% after 24 h. There was little statistical difference between the photolyzed (light exposed) and unphotolyzed (dark) cell samples until the concentration of **1** was increased to 200 μM. At this concentration, the cells exposed to light have statistically less cell death, with cell viabilities of 68% compared to 60% for cells not exposed to 470 nm light ($P < 0.0001$) (Figure 1). However, this difference is quite modest.

With an increased incubation time of cells with **1** (to 48 h), there was a similar slight increase in viability for those solution that had 4 minutes exposure to light. At a concentration

of 100 μM **1**, the photolyzed cells display a cell viability of 64%, while incubation in the dark without any light exposure results in 58% viability, while at 200 μM of **1** the difference is 51% dark: 59% light. ($P < 0.01$ and $P < 0.0001$, respectfully, Figure 2). Thus, after 48 h incubation and at the maximum concentration of 200 μM, cell survival remains above 50% for both irradiated and non-irradiated samples. Therefore **1** is only moderately toxic towards B16F10 cells up to 100 μM. NO is cytoprotective at low concentrations,[2] therefore the increased cell viability in the photolyzed samples is possibly due to a small production of NO or that the photoproduct is less cytotoxic that **1**. Statistical analyses were completed on the cell viability of the light and dark samples by student *t*- test and resulted in $P < 0.05$, confirming statistical significance. Due to solubility limitations at a maximum concentration of 200 μM, an LD_{50} could not be determined.

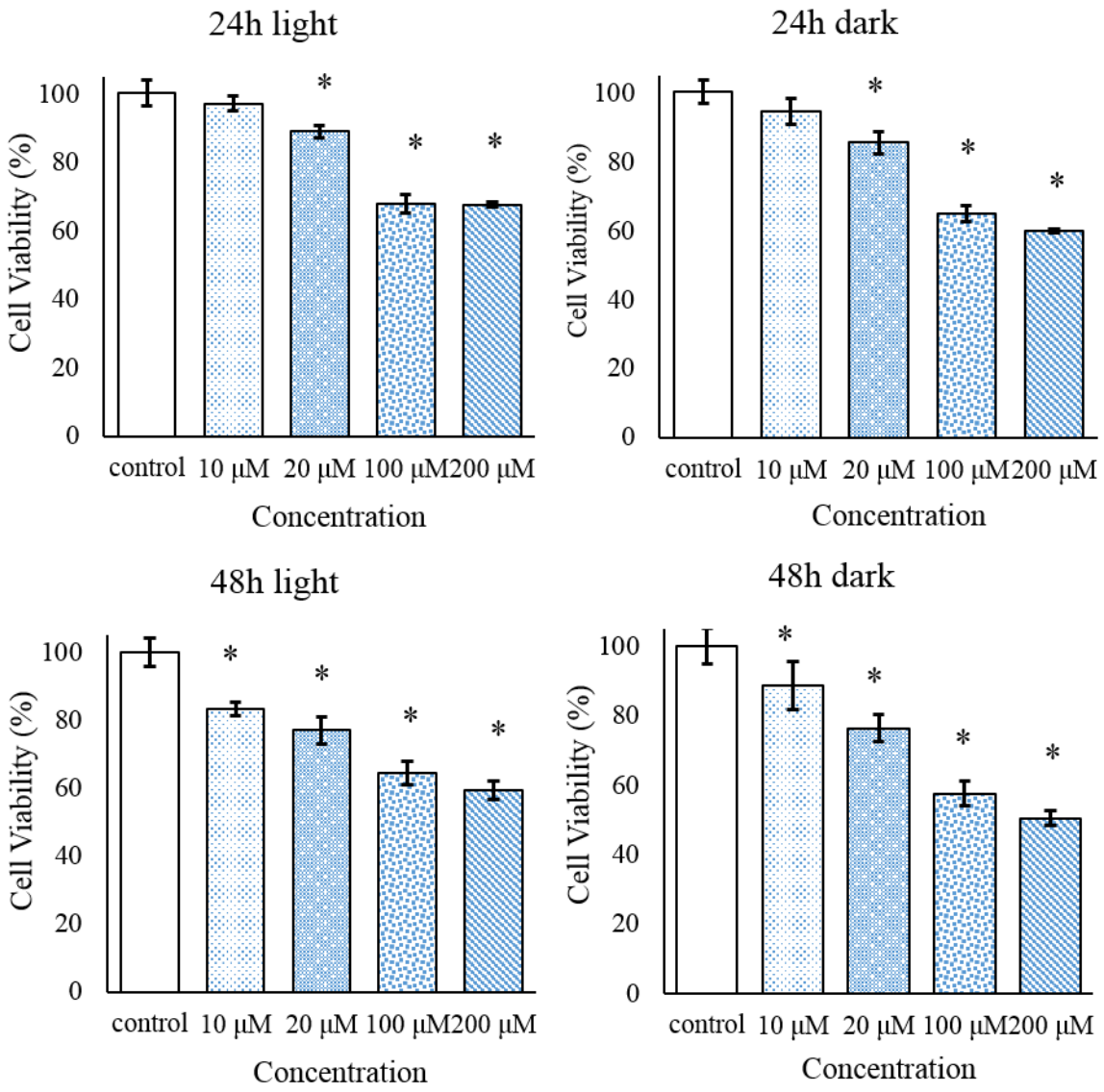

Figure 4.1. Cell viability plots with exposure to increasing concentrations and duration of compound **1**. The plates under light were irradiated for 4 min at 470nm (4 J/cm^2) while plates under dark were not exposed to light. Cell viability was assessed by the MTT assay and results expressed as a percentage relative to the control (absence of compound **1**). The values are the mean ± SEM. * $p < 0.05$ in comparison to others treatments and the control obtained by ANOVA analyses using Tukey's post-hoc test.

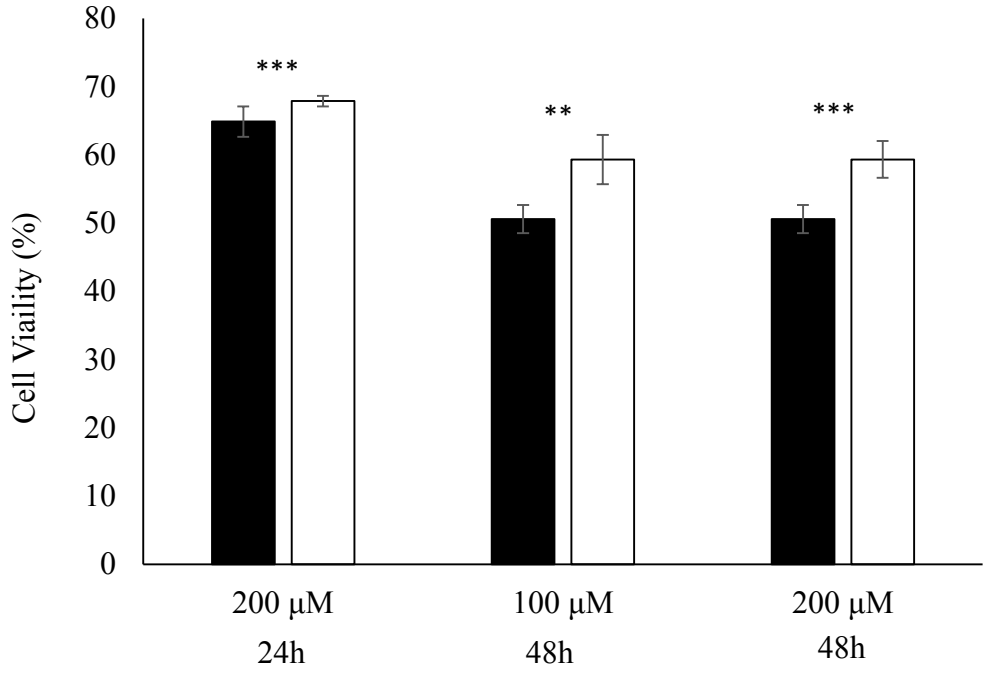

Figure 4.2. Cell viability of cells incubated in the dark (black) or after irradiated at 470 nm for 4 min (white). Cells incubated with either 100 μM or 200 μM of 1 followed by an incubation of 24 or 48 h as listed. $P < .01$ (**), $P < .001$ (***).

4.3 Myography Studies

As a signaling molecule, NO plays a large role in the dilation of veins and arteries to help control blood pressure.[2] Myography or vasodilation can therefore be used to identify the production of NO in a biologically relevant environment. The present studies were completed using Krebs buffer solution with bubbling oxygen and carbon dioxide (with or without light as specified). Therefore the relaxation of the aortic rings in this study would show irradiation of the compound **1** can generate biologically relevant concentration of NO.

4.3.1 Vascular reactivity

Myography studies were completed to test the release of NO from **1** inducing the relaxation of rat aortic rings. The experiment was performed in a pH 7.4 Krebs buffer solution (composition in mM: NaCl (130.0), KCl (4.7), KH_2PO_4 (1.2), $MgSO_4$ (1.2), $NaHCO_3$ (14.9),

glucose (5.5) and $CaCl_2$ (1.6), adjusted to pH 7.4) and the concentration of **1** was slowly increased by sequentially adding aliquots of a stock solution of **1** over time. At the initial concentration of 10^{-10} M, there was no obvious effect on the aortic relaxation (Figure 3) in the dark or under ambient light. As the concentration of **1** was increased stepwise the effects shown in Figure 3 were evident. Under ambient light, a 10^{-6} M concentration of compound **1**, was sufficient enough to induce vasodilation. Complete relaxation was established at 10^{-5} M. Alternatively, when the assay was performed in the dark with ambient light excluded, vasodilation was not observed even when the concentration of **1** was increased to 10^{-4} M.

Upon the addition of **1** at a concentration of 10^{-5} M directly into the experimental setup containing a fully contracted aortic ring, relaxation was slow in ambient light and required approximately 50 min to attain full relaxation (Figure 4). The amount of vasodilation induced by **1** over the course of 60 minutes is plotted as the area under the curve (AUC) for the system exposed to ambient light and the system kept entirely in the dark. It is evident that **1** induced vasorelaxation in ambient light while having little relaxation in the dark (Figure 4, inset). No discernable difference in response was seen between aortic arteries with or without endothelium cells. These results confirm that NO was produced from **1** in combination with ambient light and not by residual NO within the experimental setup.

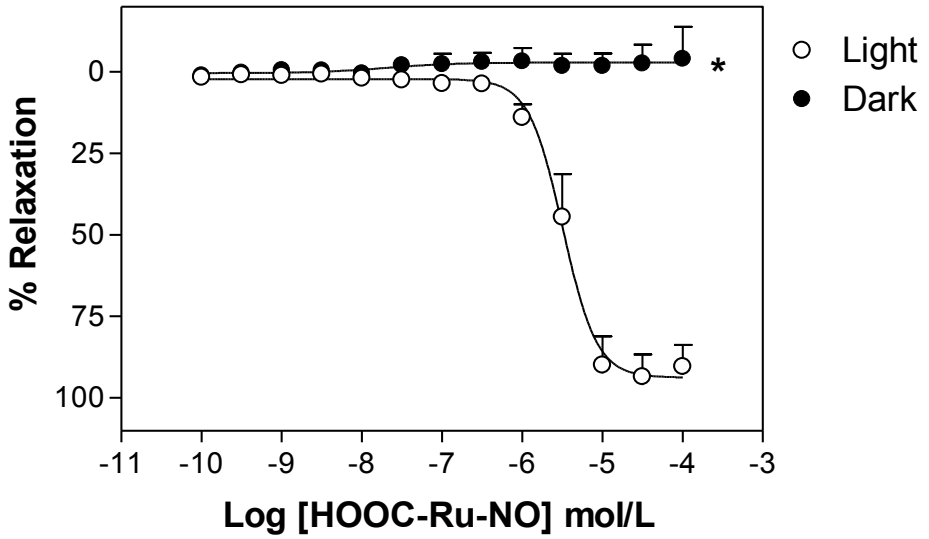

Figure 4.3. Vascular relaxation induced by Ru(NO)(salen-CO_2H)Cl in denuded rat aortic rings in ambient light or dark. Data are mean ± SEM (n=6).

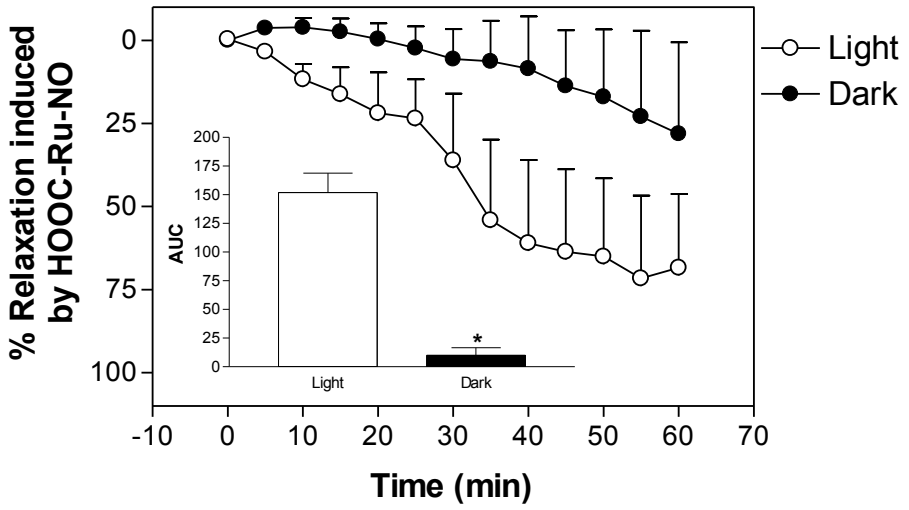

Figure 4.4. Time-course for Ru(NO)(salen-CO_2H)Cl -induced relaxation. Denuded thoracic aortic rings were pre-contracted with 0.1 μmol/L phenylephrine and 0.1 μmol/L Ru(NO)(salen-CO_2H)Cl was added. Area under curve (AUC) was used to express to total relaxation induced by compound 1 in ambient light or dark over 60 min. Data are means ± SEM of n = 3-6 experiments performed on preparations obtained from different animals.

4.4 Chemical and electrochemical release of Nitric Oxide

Nitric oxide has been shown to be released through several mechanisms, such as thermal, chemical, and photo activated release.[3, 4] Although this work has focused on the release of

NO through photolysis, other methods to cleave the ruthenium nitrosyl bond were also explored. The two methods employed were electrochemical (through voltammetric studies) and chemical release through the use of ascorbic acid. The results of these two studies are discussed below.

4.4.1 Voltammetric experiments

Differential pulse voltammograms of **1** were used to identify the reduction peak of {Ru-NO}$^{3+/2}$. Experimentally, a charging potential at -0.5 V was required to induce NO release electrochemically from compound **1**. The charging potential was maintained for a specific duration ranging from 0 – 300 seconds (Figure 5a). The oxidation peak at -0.3 V *vs* Ag/AgCl is attributed to the {Ru-NO}$^{3+/2+}$ reduction centering on the nitrosyl ligand, as seen in similar compounds.[5] As the charging potential was maintained, the peak intensity at -0.3 V decreased corresponding to the loss or labilization of the nitrosyl ligand and formation of a solvent species (Scheme 1). Additionally, there is a peak growth at 0.1 V *vs* Ag/AgCl during the anodic run attributed to the formation of the solvent species {Ru-H_2O}$^{2+/3+}$ after the reduction process, and this new peak is not observed during the cathodic run where the charging potential is set at +0.5 V (Figure 5b). The isosbestic point within the anodic run further confirms the release of NO and conversion from one species to the solvent species.

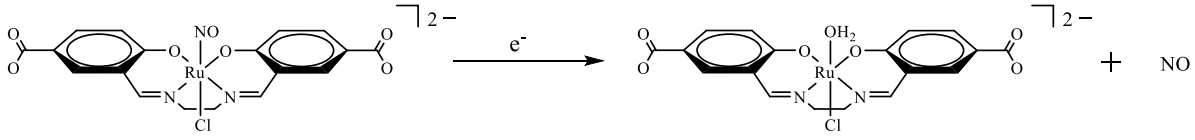

Scheme 4.1. Photochemical release of nitric oxide and solvent coordination to ruthenium center.

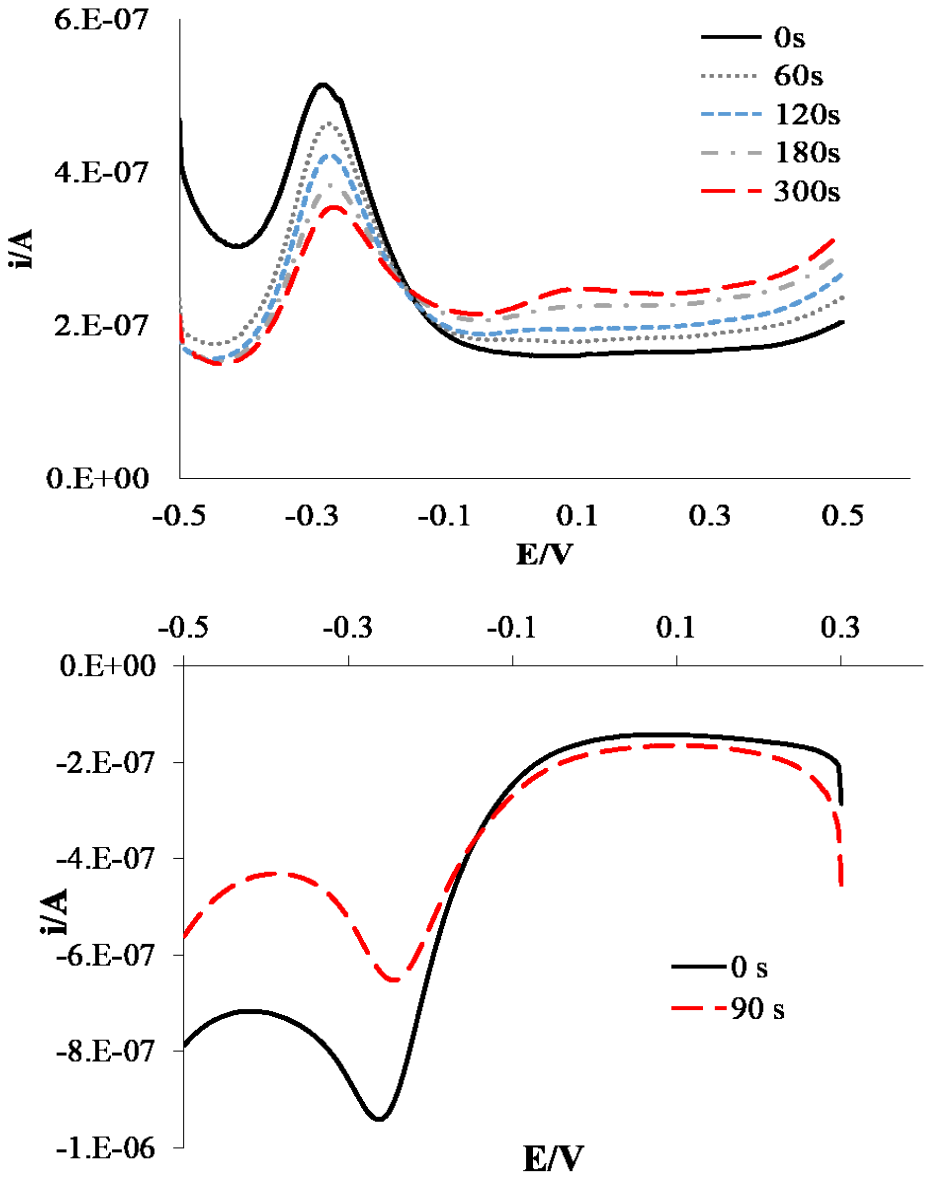

Figure 4.5. Differential pulse voltammetric scans with carbon glass electrode with silver chloride reference electrode. Scans recorded after specified timed charging with conditioning potential of -0.5 V and run between (top) -0.5 – 0.5 V and (bottom) 0.3 – -0.5 V.

4.4.2 Ascorbic Acid Studies

Ascorbic acid was selected as an oxidant to examine chemical interaction of **1** with a representative redox capable molecule (especially one that is common in biological systems), due to the charge potential observed in the voltammetric experiments above. Literature values show that a 0.01 M ascorbic acid solution has a potential of 0.06 V at pH 7.4.[6] The reduction

potential necessary for NO generation at 0.3 V can be achieved by the addition of 0.14 M ascorbic acid to induce NO release from a solution containing 28 μM of **1**. The procedure was performed following a protocol described previously.[7] The NO electrode and a 3.0 mL solution of **1** were kept under argon atmosphere, magnetic stirring and protected from light. The release of NO was monitored by UV-visible spectral changes and the generation of NO by utilizing a NO specific electrode (inNO Nitric Oxide measuring system by Innovactive Instruments Inc.) in pH 7.4 phosphate buffer solution. After the baseline had been established, 0.5 mL of 1 M ascorbic acid (final concentration 0.14 M) was injected by an airtight syringe at 100 seconds, resulting in generation of NO observed by an increase in the measured current (Figure 6). The release of NO resulted in a UV-visible spectral change indicating the chemical release of NO (Figure 7).

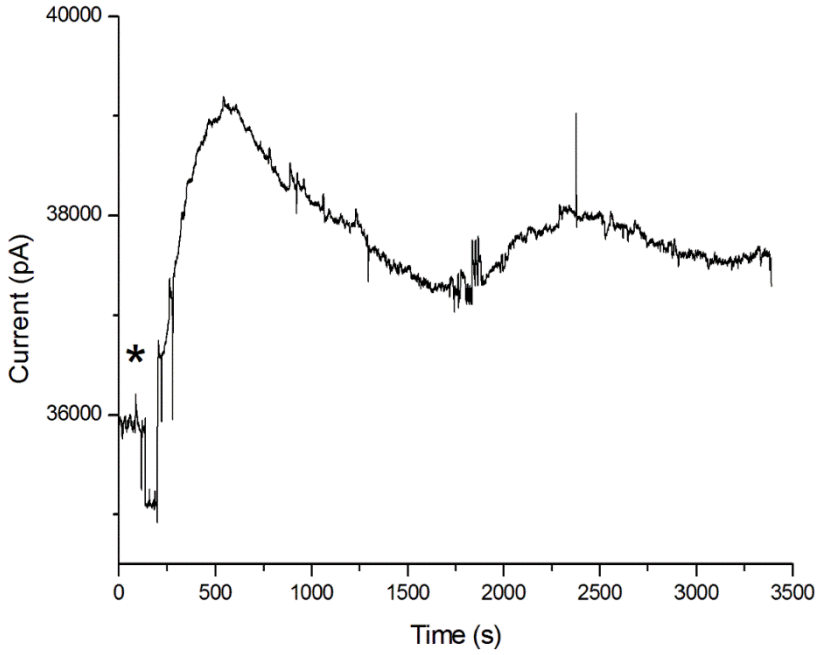

Figure 4.6. Release of NO upon addition of ascorbic acid to a solution of 1. Current measured using an NO specific electrode. * indicates the addition of 0.14 M ascorbic acid solution to evaluate the NO release upon redox reaction.

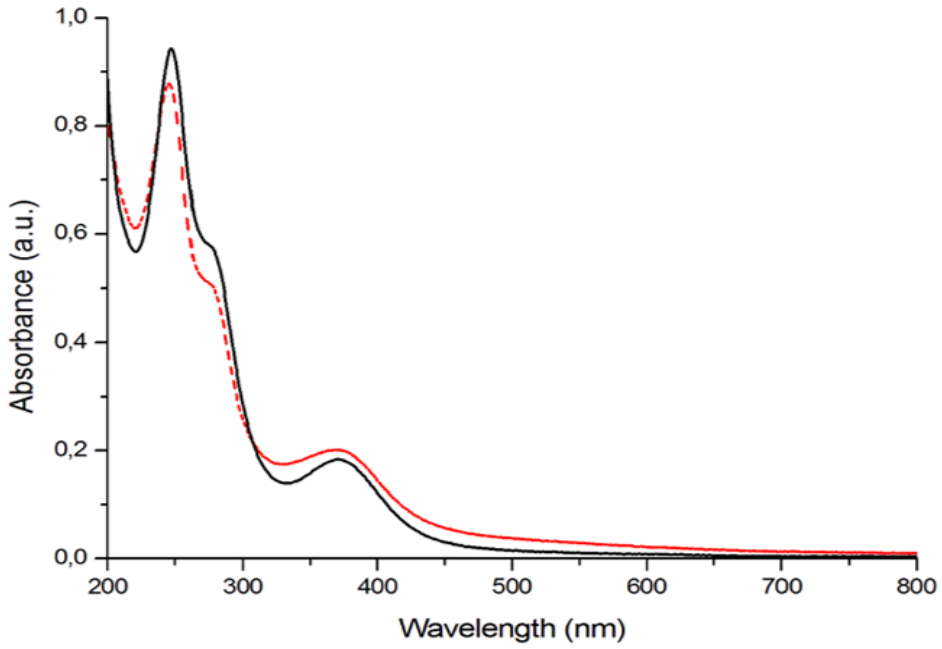

Figure 4.7. UV-visible spectra of 1 before and after the addition of [0.14 M] ascorbic acid to a pH 7.4 phosphate buffered solution. The change in spectra is due to the loss of NO as shown in photochemical studies. Black: absorbance spectra prior to ascorbic acid addition. Red: absorbance spectra after ascorbic acid induced release of NO. The absorbance spectra after ascorbic acid addition has been corrected for the change in volume.

4.5 Conclusion

Compound **1** possesses low cytotoxicity up to 100 μM and shows slight improvement of cell viability when irradiated with a low intensity 470 nm light source generating a small amount of NO. Experiments performed in aortic rings also confirm the ability of **1** to induce vasodilation at low concentrations (as low as 1 μM) with only ambient light illumination, whereas incubation in the dark does not result in any vasodilation even at a concentration of 100 μM. The aortic relaxation in ambient light resulted in the slow production of NO and complete vasodilation required 50 minutes. The long time scale provides beneficial regulation as the slow relaxation reduced the risk of a dramatic drop in blood pressure after drug administration. The release of NO has also been observed in several alternative processes,

particularly through electrochemical incubation and chemical processes resulting from the addition of ascorbic acid monitored by spectral changes and a NO specific electrode.

As described in chapter 3, there is a strong pH dependence to the quantum yield of NO release. Previous research has identified that human tumors are highly hypoxic which results in a drop of pH to 5.7 – 7.8[8] while the lysosomes have a pH range of 4.5 – 5.0.[9] Such low pH environments can result in higher quantum yields within hypoxic cells and the generation of more NO at lower wavelengths of light or shorter irradiation timescales. Therefore, the NO concentration and subsequent radical concentration would be higher in hypoxic cells where radiation therapy is least effective, possibly improving radiation treatment to localized regions. Future research should be performed in hypoxic tissue to study both the release of NO and any possible therapeutic applications, as the higher concentrations likely to result from reduced pH in hypoxic tissue may no longer be beneficial to cell growth but rather result in inhibition and, ideally, reduction in cell viability of cancerous tissue.

4.6 References

[1] Mosmann, T. "Rapid colorimetric assay for cellular growth and survival: application to proliferation and cytotoxicity assays", *Journal of Immunological Methods*, **65**, 55–63.

[2] Feldman, P. L.; Griffith, O. W.; Hong, H.; Stuehr, D. J.; "Irreversible inactivation of macrophage and brain nitric oxide synthase by L-NG-methylarginine requires NADPH-dependent hydroxylation", *J. Med. Chem.*, **1993**, 36 (4), 491-496.

[3] Roussin, M. L. "Recherches sur les nitrosulfures doubles de fer (nouvelle classe de sels)", Ann. Chim. Phys. **52**, (1858), 285–303.

[4] Bourassa, J.; Lee, B.; Bernard, S.; Schoonover, J.; Ford, P. C.; "Flash Photolysis Studies of Roussin's Black Salt Anion: $Fe_4S_3(NO)_7^-$" *Inorg. Chem.* **1999**, 38, 2947-2952

[5] Lang, D. R.; Davis, J. A.; Lopes, L. G. F.; Ferro, A. A.; Vasconcellos, L. C. G.; Franco, D. W.; Tfouni, E.; Wieraszko, A.; Clarke, M. J.; "A Controlled NO-Releasing Compound: Synthesis, Molecular Structure, Spectroscopy, Electrochemistry, and Chemical Reactivity of R,R,S,S-trans-[RuCl(NO)(cyclam)]2+(1,4,8,11-tetraazacyclotetradecane)", *Inorg. Chem.*, **2000**, 39, 2294

[6] Borsook, H.; Keighley, G.; "Oxidation-reduction potential of ascorbic acid (Vitamin C)", *PNAS*, **1933**, 19, 875-878.

[7] Carnerio, Z, A.; Biazzoto, J. C.; Alexiou, A. D.P.; Nikolaou, S.; "Nitric oxide photorelease from a trinulear ruthenium nitrosyl complex and its in vitro cytotoxicity against melanoma cells", *J. Inorg. Biochem.*, **2014**, 134, 36-38.

[8] Vaupel, P.; "Tumor Microenvironmental Physiology and its Implications for Radiation Oncology", *Semin. Radiat. Oncol.* **2004**, 14, 198-206

[9] Bruye`re, H.; Westwell, A. D.; Jones, A. T. "Tuning the pH Sensitivities of Orthoester Based Compounds for Drug Delivery Applications by Simple Chemical Modification" *Bioorg. Med. Chem.* **2010**, 20, 2200–2203

Chapter 5. Ru(NO)(Salophen)Cl and Encapsulation in Secondary Structures

5.1 Introduction

Ru(NO)(salophen)Cl (**2**) was synthesized for two important reasons: its hydrophobic nature and red-shifted spectral properties. The hydrophobic character of **2** allows it to be incorporated into the lipophilic polymers PLGA *(*poly(lactic-co-glycolic acid)) and PDMS (Polydimethylsiloxane) and makes it less likely to leach into a surrounding aqueous environment, thus providing a valuable drug delivery option. The same polymer can also incorporate light harvesting antenna, such as nano particles, allowing for energy transfer processes to induce NO release upon long wavelength light excitation of the polymer-salophen complex.

The use of an antenna as a light harvesting technique for drug release has been studied extensively within the Ford group[1] and others.[2, 3] In previous studies, $Cr(cyclam)(ONO)_2^+$ (Figure 5.1) was suspended in a solution with negatively charged quantum dot, CdSe/ZnS core/shell nanoparticles that would associate with the positively charged species via ion pairing.[1] This nonspecific interaction of the added nanoparticles increased the release of NO tenfold versus simple photolysis the $Cr(cyclam)(ONO)_2^+$ in solution without nanoparticles.[1]

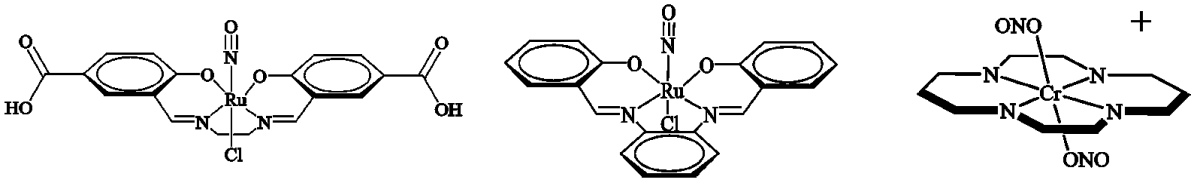

Figure 5.1. PhotoNORMs Ru(NO)(salen-CO2H)Cl (compound 1) discussed in chapters 3 and 4, Ru(NO)(salophen)Cl (compound **2**) and $Cr(cyclam)(ONO)^{2+}$.

This work indicated that energy transfer from nanoparticles to a photoNORM could enhance

NO release, even with only nonspecific ionic interaction. For biological applications, which possess many positively and negatively charged species, an approach with improved specificity is needed to release NO without concern of nonspecific ion pairing or diffusion limited processes for nanoparticle-photoNORM association. Encapsulating the light harvesting antenna and photoNORM into a biologically stable polymer could allow for the close association needed for energy transfer and release of NO while limiting concerns of background biological interactions.

5.2 PhotoNORM Encapsulation

Two separate biocompatible polymers were used in testing the encapsulation of photoNORMs. Biocompatible silicone polymers are used as coatings in many medical implants and for a variety of surgical procedures such as coatings for pacemaker leads and breast implants[4] while PLGA (Poly(lactic-co-glycolic acid)is a biodegradable polymer that can be synthesized to have time dependent degradation varying from hours to years according to the monomer ratios within the polymer.[5] PLGA particles have been loaded with drugs and used in cancer treatments, vaccinations, and used in the treatment of inflammatory diseases.[3] The biological inertness of these polymers allows their use for a drug delivery scaffold, as concerns for background interactions are already minimized with FDA approval in a variety of applications. However, discovery of the optimal system for utilization of silicone polymers for drug discovery purposes is difficult, as controlled release of the drug molecule can be complicated.[2, 3] Including a photoactive drug in the polymer would allow for a more controlled drug release and the ability to modulate drug release depending on the condition of the patient. Unfortunately, many photo active drugs absorb in the near UV, a wavelength region that has poor penetration through tissue.[6] The efficient release of cargo from the photoactive drug by

using more penetrating longer wavelength near-infrared (NIR) light can be aided by the addition of a two-photon absorbing compound, which then releases a single photon of higher energy light. By closely associating a two-photon NIR absorbing molecule to a photoactive species with absorbance overlapping the two-photon emission, photo-uncaging can occur and the drug can be released.

This chapter focuses on the two-photon up-converting nanoparticle (UCNP) $NaYF_4$: $Yb_{30}Gd_{20}Tm_{0.2}$ @ $NaYF_4$, which absorbs at 980 nm and emits at 365 nm, 450 nm, 475 nm, and 645 nm. The polymer PLGA was selected due to its varied uses throughout the field[3] while PDMS (Polydimethylsiloxane) was selected due to its optical clarity, hydrophobicity, large pore size, insensitivity to NO, and ability to encapsulate UCNPs into the polymer structure and retain structural integrity.[7] Both PLGA and PDMS has also been FDA approved for use in medical procedures including contacts, catheters, and implants.[8] This chapter will include the preparation of the photoNORM and UCNP incorporated PLGA microparticles and into PDMS polymer, photolysis experiments, and NO release upon polymer excitation under a variety of conditions. The best performing NO releasing platform was studied further by irradiating through porcine tissue to determine the ability of the photoNORM/ UCNP system to produce NO with scattered and diffused light due to a tissue analog.

5.3 Results and Discussion

The Ru-salophen photoNORM studied in this chapter was synthesized by procedures described in the Experimental (sec. 2.3.2). It product was purified by column chromatography and stored under vacuum at room temperature in the dark.

5.3.1 UV-visible Spectral changes

The salophen ligand provided a considerable 125 nm red-shift in the absorbance spectra versus the ruthenium salen structure **1** [Ru(NO)(salen)Cl], shifting the MLCT band from 315 nm to 440 nm in acetonitrile (Figure 5.2). The second peak at 253 nm was also red-shifted by 62 nm to 315 nm, a bathochromic shift directly related to the additional conjugated ring in the ligand. The Ru(NO)(salophen)Cl complex was observed to maintain thermal, oxygen, and water stability similar to the Ru(NO)(salen) compound with the advantage of photoactive NO release upon irradiation at lower energy light.

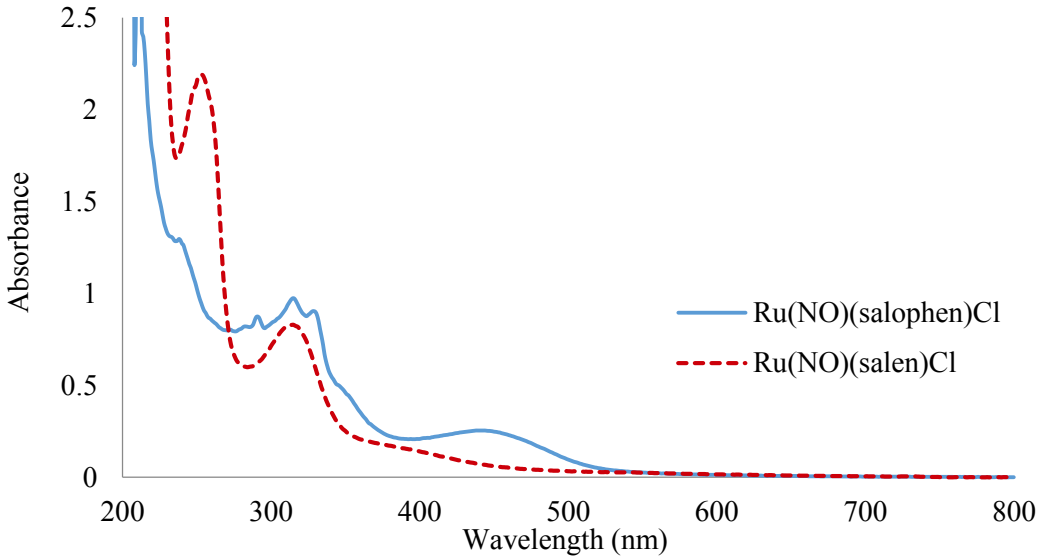

Figure 5.2. Spectroscopic shift in absorbance from 1 (red dash) to 2 (solid blue) in acetonitrile at equal concentration. Absorbance peaks of 1 at 253 nm and 315 nm shift out to 315 nm and 440 nm for compound **2**.

5.3.2 Quantum Yield studies

A stock solution of 60 μM concentration of **2** was created in isopropyl acetate and aliquot into 3 mL portions for each individual experiment. The sample was photolyzed in a 4-sided, Y-shaped cuvette which allows the carrier gas (medical grade air, bubbled through 5 mL isopropyl acetate prior to entering the photolysis cell) to flow through the cell and purge the experiment as NO is generated (Appendix ii). Photolysis timing was controlled with a

uniblitz optical shutter, ranging from 0.25 seconds up to 1 second in quarter second increments. After each photolysis, the Nitric Oxide Analyzer (NOA) was allowed to return to baseline for a minimum of 1 minute prior to the next irradiation time point. (A complete description of the Sievers 1080i NOA is described in Appendix i.)

Isopropyl acetate was selected for quantum yield (QY) experiments due to functional group similarities to the PLGA polymer and because the high boiling point and vapor pressure of the solvent is required for NOA experiments to avoid evaporation into the instrument. These experiments were aimed at mimicking the dielectric properties of nitric oxide release within the polymer microparticles. The absorbance spectra (Figure 5.2) shows a λ_{max} at 331nm, 451 nm with molar absorptivities at 17,000 and 4,600 respectfully. The ruthenium salophen in isopropyl acetate with medical grade purging air gave a QY_{NO} of 0.0312 or 3.12 % when irradiated with a 470 nm focused LED.

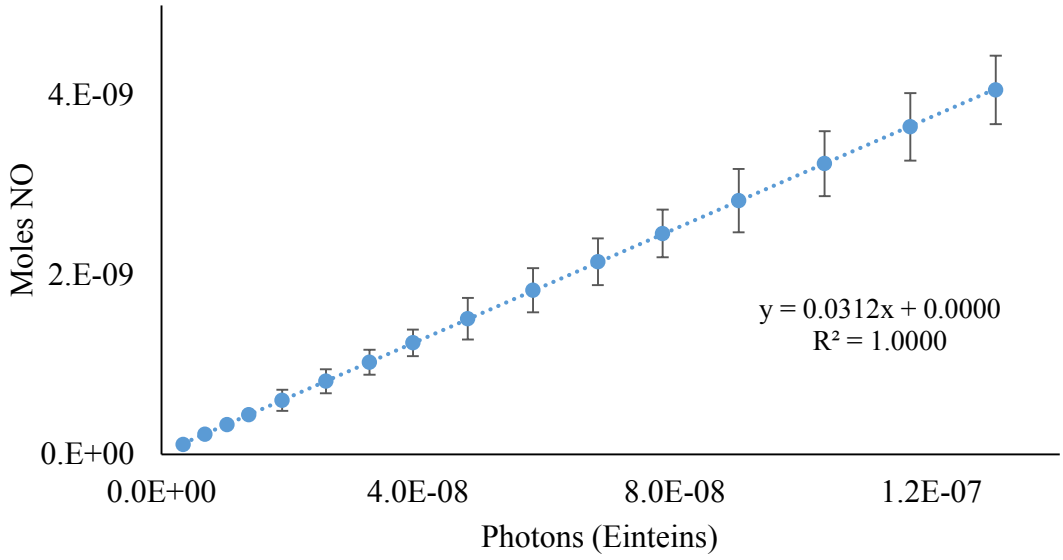

Figure 5.3. QY calculations of **2** in isopropyl acetate when irradiated at 470 nm under oxygenated conditions.

5.3.3 Up-Converting Nanoparticles (UCNPs)

Up-conversion of light is a process in which multiple photons of light are absorbed simultaneously or successively to promote an electron into higher excited states.[9] The emission of light is then of higher energy (lower wavelength) than either of the initially absorbed photons of light. In lanthanide doped UCNPs, the rare earth emitters have forbidden relaxation pathways, and this property leads to long lived excited states and can up-conversion due to sequential absorptions of photons.[10] The thulium doped nanoparticles used in this study are $NaYF_4$: $Yb_{30}Gd_{20}Tm_{0.2}$ @ $NaYF_4$. The yttrium 3^+ species absorbs 980 nm light to give the excited state $^2F_{5/2}$, which can undergo inter-system crossing (ISC) to the thulium excited state $^3H_5$.[11] Sequential photons are then absorbed by the yttrium $^2F_{5/2}$ excited state, transferring the excited photon to populate the $^1D_2$, $^1G_4$, and $^3H_4$ excited states on Tm which can relax to either $^3H_6$ or $^3F_4$. These relaxations result in a spectra with 5 sharp emission lines at 365, 451, 481, 646, and 800 nm corresponding to the relaxations $^1D_2 \rightarrow {}^3H_6$, $^1D_2 \rightarrow {}^3F_4$, $^1G_4 \rightarrow {}^3H_6$, $^1G_4 \rightarrow {}^3F_4$, and $^3H_4 \rightarrow {}^3H_6$.[12]

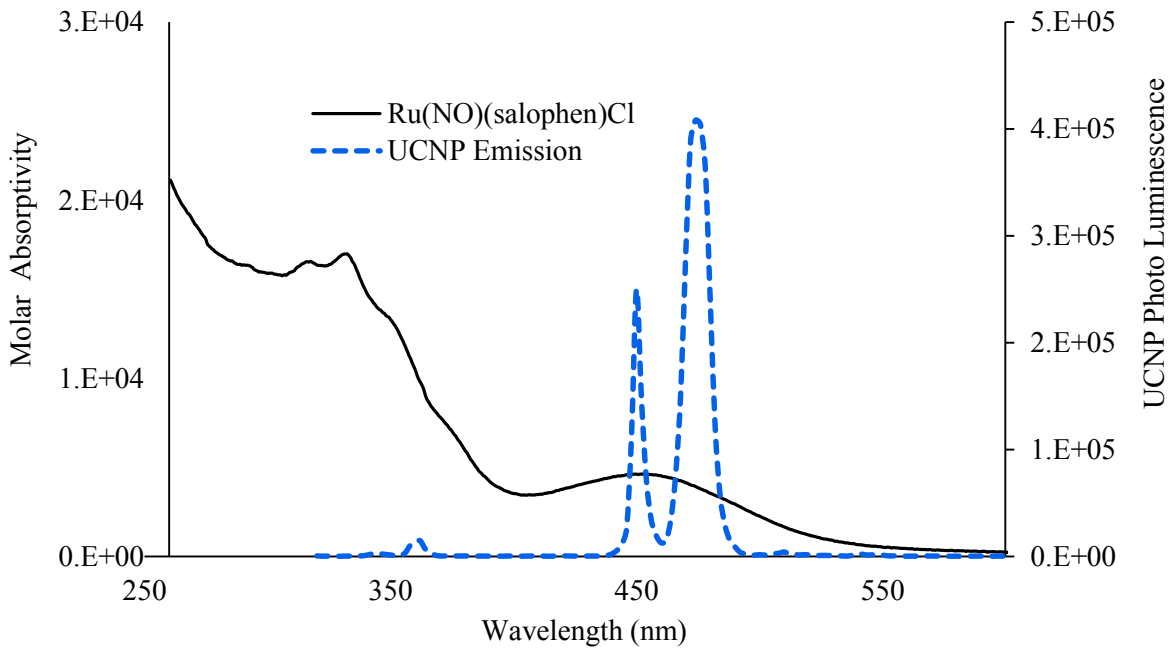

Figure 5.4. Absorbance spectra of 2 (solid black line) overlaid with the emission of $NaYF_4$: $Yb_{30}Gd_{20}Tm_{0.2}$ @ $NaYF_4$ when irradiated at 980 nm (dashed blue line).

5.3.4 FRET

Förster resonance energy transfer (FRET) can be employed to convert the emission of the UCNP to the ruthenium nitrosyl in order to break the ruthenium-nitrosyl bond and release NO. FRET is an energy transfer mechanism that relies on the proximity of emitter to acceptor and the spectral overlap between two chromophores through dipole-dipole coupling. These two parameters are displayed in the FRET equation with the distance (r) inversely related to FRET efficiency and the spectral overlap of the two chromophores (J) is directly related to the efficiency of energy conversion. The mechanism also relies on the dipole-dipole orientation, k, which is assigned as 2/3 for two randomly oriented dipoles, the photo-luminescent quantum yield Φ_{PL}, and the lifetime of the photoluminescence in the absence of an acceptor chromophore $\tau_{D(0)}$. The UCNP and **2** were selected because of their strong overlap of emitter/ acceptor while the distance is controlled by encapsulating the two chromophores within the polymer disk.

$$k_{EN}\,(r) = \frac{C\Phi_{PL}k^2}{\tau_{D(0)}r^6n^4}J(\lambda)$$

5.4 PLGA micro particles

5.4.1 Control

A 32 nM solution of compound **2** in isopropyl acetate was purged by medical grade air for 5 minutes on the NOA. The sample was irradiated with 980 nm light for 4 minutes time with no change in the background noise on the NOA. As no particles are present that can absorb 980 nm light and transfer to higher energy, no release of NO was expected and none was observed. Therefore, the production of NO in all other experiments is due to the absorbance of light by the UCNPs and the subsequent emission and absorbance of the higher energy light to the photoNORM resulting in NO production.

5.4.2 Preparation of PLGA nano particles containing UCNPs and 2

UCNPs and **2** were suspended in acetonitrile along with a dilute mixture of PLGA. The solution was added drop-wise through a 0.4 mm polypropylene tube into a beaker with 1% aqueous polyvinyl alcohol solution into a beaker of water with a submersed sonicating wand, the addition speed was carefully controlled by a syringe pump at a rate of 10 mL/hour. As the acetonitrile evaporated, small micelles formed, encapsulating the hydrophobic PLGA with the hydrophobic UCNP and ruthenium species. The microparticles were collected by centrifugation and washed with water. This method resulted in spherical particles with a diameter of approximately 100 nm ± 50 nm.

5.4.3 QY measurements

A 3 mL solution of 100 nm PLGA nanoparticles loaded with UCNPs and compound **2** was purged with medical grade air for 5 minutes prior to NOA experimentation. A 980 nm laser was used to excite the agitated solution with increasing exposure time and laser power to induce photolysis of the Ru-NO bond. Additionally, QY measurements were completed at 470 nm irradiation to compare the QY of NO release to verify the photoactivity of **2** within the PLGA particles.

5.4.4 QY Discussion

Experiments of PLGA nano particles loaded with UCNPs and the photoNORM, compound **2** gave very little NO release upon excitation at 980 nm in water (this wavelength that does not cause NO release from the ruthenium compound alone and requires up-conversion from the UCNPs). In order to test the efficient release of NO through the PLGA matrix, the loaded PLGA micro particles were additionally photolyzed at 470 nm and suspended in water.

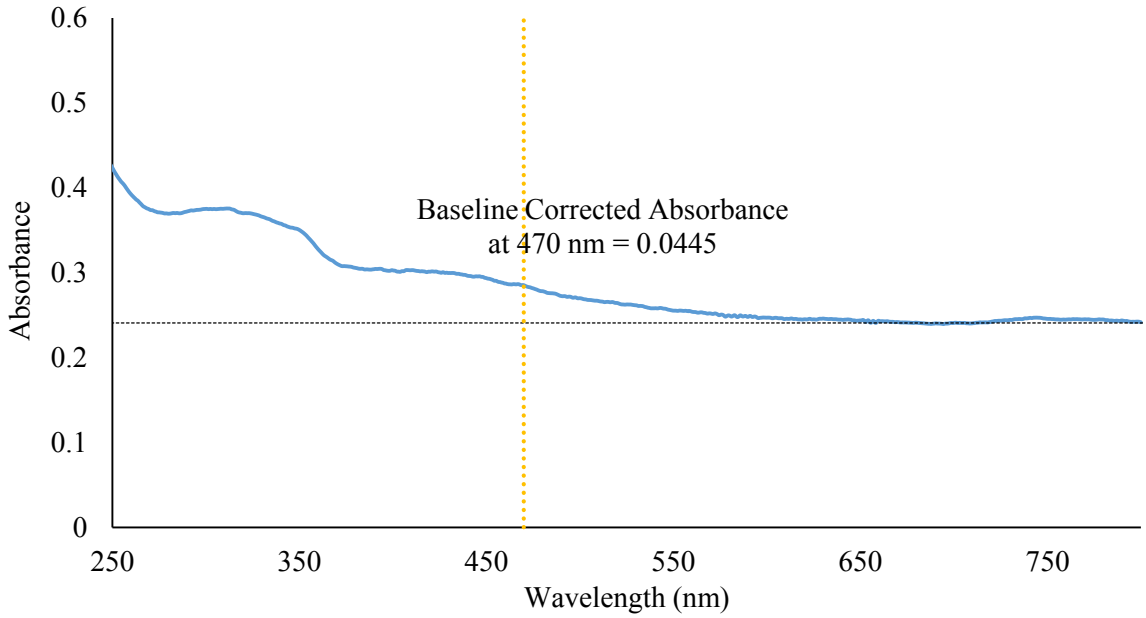

Figure 5.5. PLGA nanoparticles loaded with UCNP and 2 suspended in water. Absorbance was adjusted to the baseline at 700 nm for QY measurements (horizontal dashed black line). The absorbance was corrected at the wavelength of irradiation, 470 nm (vertical dashed yellow line).

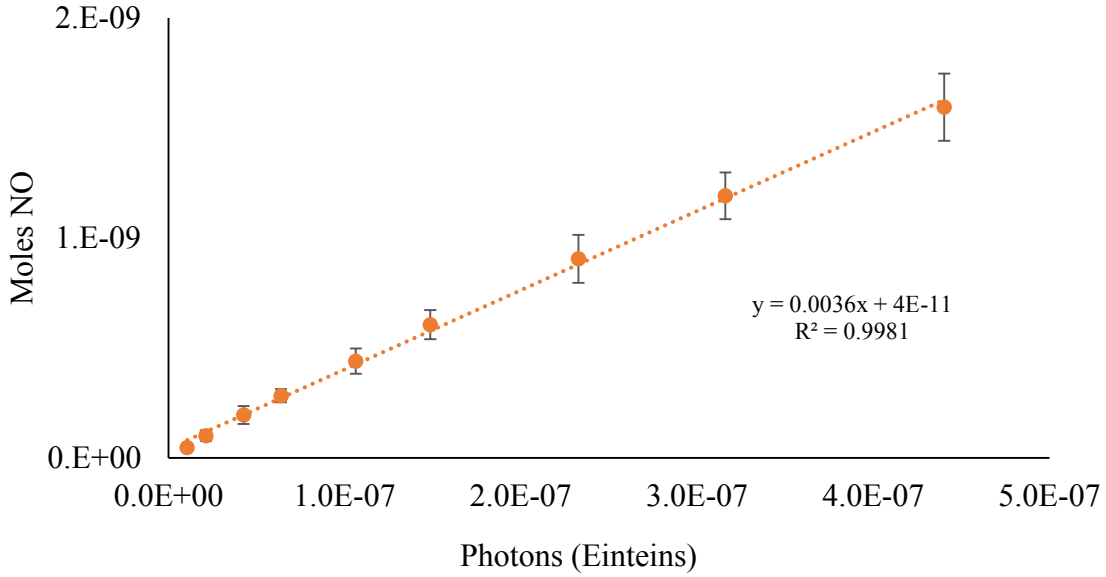

Figure 5.6. Cumulative QY of NO release from PLGA micro particles loaded with UCNPs and 2, suspended in water. QY is equal to the slope of the line, 0.0036 when irradiated at 470 nm.

Quantum yields of NO release in the PLGA matrix were adjusted for absorbance due to the large amount of scatter the PLGA particles caused in solution. Absorbed light for QY

calculations were based on the absorbance at 470 nm minus the average absorbance between 700nm and 800nm, where the ruthenium compound has no absorbance. This is depicted visually in Figure 5.5 where the black line shows the adjusted baseline due to scattering and the dashed yellow line identifies the irradiation wavelength.

Experimental calculations show the QY_{NO} drops from an average of $\Phi_{NO} = 0.0312$ when in solution of isopropyl acetate to $\Phi_{NO} = 0.0036$ when photolyzed with the UCNPs in the PLGA particle with 470 nm light (Figure 5.6). This drop can be associated with further light scattering within the particle that was unaccounted for. There may also be a process where the nitrosyl is stabilized on the ruthenium, effectively lowering the QY of NO release. NO may even react with the PLGA polymer before the NO is purged by the carrier gas, therefore only large quantities of NO will show any response on the NOA. Due to the low yield release of NO through microparticle photolysis with PLGA particles, other polymer manifolds were tested for their ability to release NO.

5.5 PDMS Polymer Disk Experimental

PDMS Polymer disks (PDs) were prepared by mixing the PDMS and curing agent in a 10 to 1 ratio by weight and vigorously stirred for 5 minutes (according to the manufacturer procedure, Sylgard® 184 elastomer kit Dow Corning). Air introduced by mixing of the two prepolymer solutions was removed by placing the liquid polymer under vacuum for 30 minutes. UCNPs were added to the liquid polymer after it had partially set (approximately 1 hour). The PDMS disks containing UCNPs were loaded with 2, 5, or 8 mg of $NaYF_4$: $Yb_{30}Gd_{20}Tm_{0.2}$ @ $NaYF_4$ UCNPs. They were then annealed at room temperature for 48 hours in a Teflon mold to prepare 5 mm sized polymer disks. PDs with and without UCNPs were stored at room temperature on the bench top until use.

5.5.1 Incorporation of ruthenium salophen nitrosyl into the PD

Polymer disks (PD) were impregnated with the hydrophobic ruthenium nitrosyl salophen complex, **2**, by submerging the PD in a concentrated THF solution of the ruthenium compound in the dark. The PD was left in the concentrated solution for 10 minutes followed by the slow evaporation of the THF under vacuum. This process was repeated three times to ensure a high loading of **2** into the PD. To eliminate variability, the PD was allowed to fully dry between cycles.

To remove excess **2** from the exterior surface of the loaded PDs, the disks were washed with a small volume of THF and placed under vacuum until fully dry. The excess ruthenium was then removed by several washing steps with nanopure water until the UV-Vis spectra of the water solution contained no evidence of ruthenium salophen absorbance after 1 hour. The final PDs were stored under vacuum to prevent water from settling on the surface which proved to be detrimental in previous studies.[7]

5.5.2 Oscillating 980 nm laser

The size disparity between the pin laser width (0.7 mm) and the PD diameter (5 mm) forces the results to depend on the loading of a small fraction of the PD. Therefore to ensure consistency of NIR excitation across the entire surface of the PD, an oscillating 980 nm laser was used for photolysis experiments. The oscillating system allowed the 980 nm laser beam to scan across a broader portion of the PDs during a single run. This was achieved by mounting the angling mirrors to a vibrating mount controlled by a frequency generator. A Techtonic AFG320 digital generator was used to maintain a constant vibrational frequency for the mounted mirrors, ensuring a consistent photolysis path between samples. By adjusting the frequency of each mirror, the size of the scanned area was defined with each mirror controlling

the scanning width in one direction (horizontal or vertical control). The experiments were run with frequencies for the two mirrors at 78.93 Hz and 48.93 Hz respectfully, to give a vibrating mirror system which scanned the majority of the 5 mm PD.

5.5.3 Loading the sample

The PD was suspended in the specially designed NOA photolysis chamber on a glass coverslip and attached with a double-sided adhesive strip. The glass coverslip was inserted into a Teflon mount that fit into the base of the photolysis chamber. The crew cap lid was equipped with glass mounts that could suspend fat and tissue samples in front of the PD for photolysis studies through tissue, providing experimental insight into photo initiated NO release through real biological barriers. The vibrating laser was aligned to the mounted PD at low power to ensure accuracy of the moving laser before each experiment. Swagelock to glass attachments were used to connect the purge gas from the tank, through the reaction chamber and into the NOA for continuous NO monitoring.

5.5.4 Control of Quantum Yield of Ru(NO)(salophen)Cl loaded PD at 980 nm

PDs loaded with **2** only were loaded into the photolysis chamber and allowed to purge with medical grade air for 5 minutes with continuous analysis by the NOA. After the baseline was established, the PD with compound **2** was exposed to the 980 nm oscillating laser with variable power and duration of exposure. No release of NO was observed even when these disks were exposed to 4 W of power for 60 seconds, which is twice the power and duration of any other NO releasing experiments completed in this study.

Compound **2** has no absorbance at 980 nm, is thermally stable, and does not decompose in oxygen. Therefore, no release of NO was expected upon exposure to 980 nm

light. Additionally, **2** is stable in the PDMS polymer under the applied experimental conditions (save for obvious photolysis). This experiment proves that any further study where NO is seen to be produced upon photolysis is not caused by the direct absorbance of 980 nm light to the PhotoNORM **2**, even at high laser power where heating of the polymer may occur.[7]

5.5.5 Control of Quantum Yield of Ru(NO)(salophen)Cl loaded PD at 470 nm

Quantum yield measurements for loaded Ru(NO)(salophen)Cl in a PDMS PD were completed at λ = 470 nm (control experiment in isopropyl acetate is described in 5.3.2). The sample was loaded in the NOA photolysis chamber and the chamber was purged with medical grade are carrier gas. The LED beam was focused to the full diameter of the PD *(therefore, the oscillating system was not used)*. The exposure time was controlled by a uniblitz shutter and the release of NO was monitored on the NOA.

The average of the triplicate samples are plotted with moles of NO versus the photons of light absorbed (Figure 5.7). Therefore, at 470 nm irradiation in a PD in solid state, Φ_{NO} = 0.00329. The decrease in Φ in the solid state versus in solution has been seen in several other processes due to scatter and rotational restriction in solid state. DFT calculations on similar ruthenium nitrosyls show that upon excitation into the metal to ligand charge transfer band (MLCT) the Ru-NO bond angle bends and the bond length changes as the compound relaxes back to ground state.[13] The decrease in Φ can be associated with the loss of vibrational and rotational modes and the absence of a solvent to stabilize the photo product.

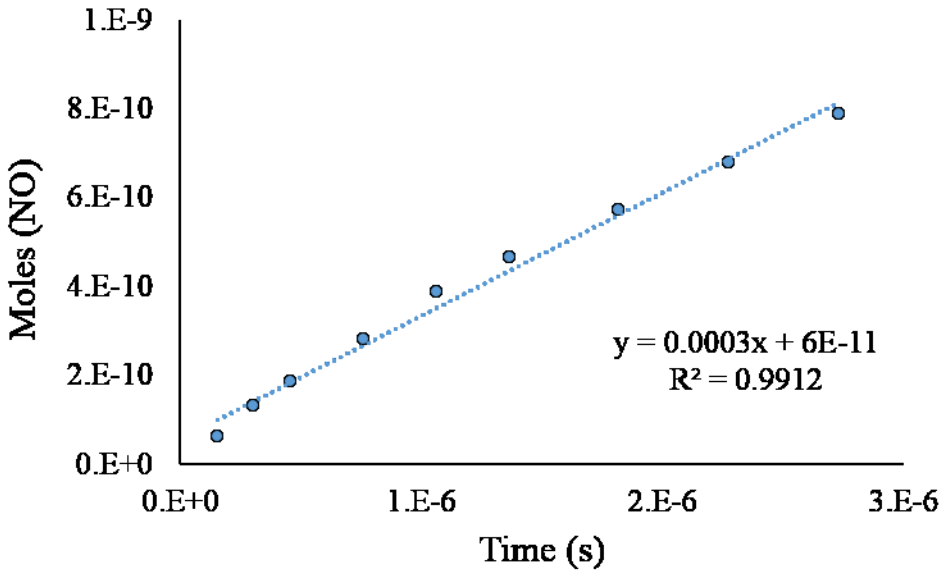

Figure 5.7. Quantum Yield of Ru(NO)(salophen)Cl at λ = 470 nm while suspended in a PDMS polymer disk with medical grade air carrier gas. Φ = 0.00329.

5.5.6 Running samples

Three sets of UCNP samples loaded with **2** were irradiated with the 980 nm oscillating laser system and data collected in real time for NO release on the NOA. Power settings began at 0.5 W and were increased in 0.5 W increments to 2 watts or until consistent signal was observed. The exposure time ranged from 2 to 30 seconds. Higher power and longer exposure times introduced the risk of burning the PD due to UCNP heating of the polymer, although this was not seen at the lower power and time regimes used, but had been observed in previous studies.[7]

5.5.7 Results

Each PDs contained a defined mass of UCNPs within the polymer prior to the infusion of **2**. PDs were either synthesized with 2 mg, 5 mg, or 8 mg of $NaYF_4$: $Yb_{30}Gd_{20}Tm_{0.2}$ @ $NaYF_4$ UCNPs. The NO release was monitored using a Sieverson 1080i Nitric Oxide Analyzer (NOA). Individual data is described for each experimental parameter.

5.5.8 PDs with UCNP loading

PDs loaded with 2 mg, 5 mg, or 8 mg of $NaYF_4$: $Yb_{30}Gd_{20}Tm_{0.2}$ @ $NaYF_4$ UCNPs were infused with **2** and fully dried as described in the experimental section. While working with multiphoton UCNPs, power and scan rate of the laser have a large effect on the generation of excited states.[7] The scan rate is defined as the speed in which it takes the laser to cross the sample while power is measured in watts allowing more excited states to be generated on a UCNP. To test the relationship of power and time within these experiments, scan rate was held constant. Upon irradiation, NO was generated by the absorbance of 980 nm light by the UCNP followed by emission and subsequent absorbance by **2** resulting in NO production (Figure 5.4). The moles of NO generated were divided by the Einsteins of light (I_o = Einsteins per second) from the 980 nm laser and plotted against time in Figures 5.7 – 5.9. The plotted data will be referred to as the efficiency of NO release instead of QY ($\frac{moles\ NO}{photons\ absorbed}$) because of the two step process of absorbance by the UCNP, emission, and subsequent absorbance by **2** to induce NO production. Since the efficiency term incorporates the photons of light, the change in power on the plots show a corrected value of NO production and show a definite increase in NO production dependent on the power of the light source and time.

Figure 5.7 – 5.9 shows the moles of NO/ I_a plotted against time of irradiation with the amount of NO being produced relative to the laser power clearly being a non-linear function. Lower production of NO at reduced power is consistent with previously reported studies showing that the multi- photon absorbers have a non-linear response for emission when irradiated by higher power light due to a charging effect on the UCNPs.[7]

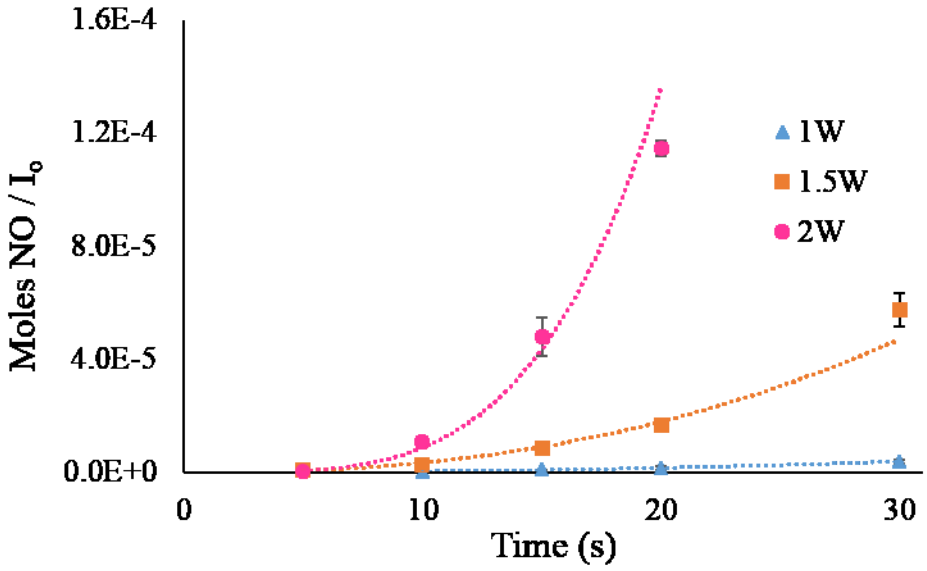

Figure 5.8. Efficiency of NO release loaded with 2 mg UCNP. Moles of NO produced per photon plotted against irradiation time. The separate lines indicating the power of the irradiation source. The curves show are based on the assumption of an exponential function.

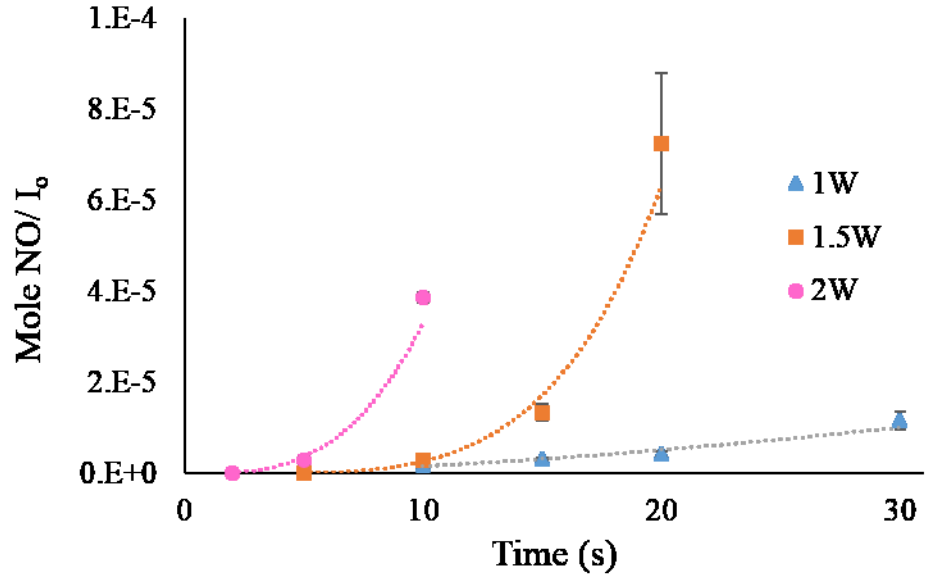

Figure 5.9. Efficiency of NO release loaded with 5 mg UCNP. Moles of NO produced per irradiation time. The separate lines indicating the power of the irradiation source.

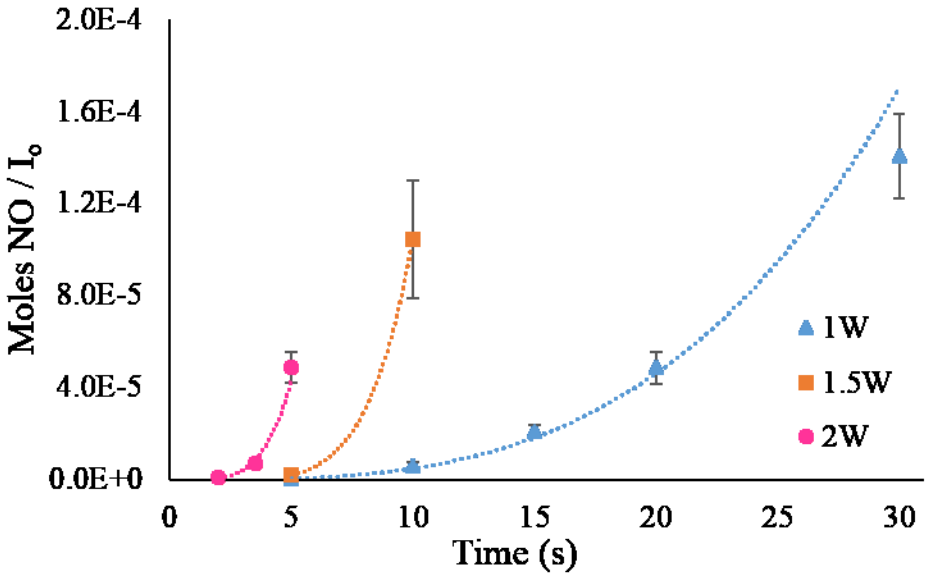

Figure 5.10. Efficiency of NO release loaded with 8 mg UCNP. Moles of NO produced per irradiation time. The separate lines indicating the power of the irradiation source with a non-linear response.

2 mg	1W	1.5W	2W
5s	--	8.3E-7 ± 9E-8	5.1E-7 ± 8E-8
10s	3.6E-7 ± 2E-57	2.5E-6 ± 7E-7	1.1E-5 ± 6E-7
15s	9.7E-7 ± 1E-7	8.6E-6 ± 1E-6	4.8E-5 ± 7 E-6
20s	1.6E-6 ± 8E-7	1.7E-5 ± 2E-6	1.2E-4 ± 3E-6
30s	3.8E-6 ± 6E-7	5.8E-5 ± 6E-6	--

Table 5.1. QY of PD loaded with 2mg UCNP and 2. QYs vary dependent on time and power.

5 mg	0.5W	1W	1.5W	2W
2s	--	--	--	2.4E-7 ± 9E-9
5s	--	--	--	2.8E-6 ± 9E-7
10s	--	1.8E-6 ± 6E-7	3.1E-6 ± 4E-7	3.9E-5 ± 1E-6
15s	--	3.1E-6 ± 3E-7	1.4E-5 ± 2E-6	--
20s	--	4.3E-6 ± 6E-7	7.3E-5 ± 2E-5	--
30s	4.1E-6 ± 1E-6	1.2E-5 ± 2E-6	--	--

Table 5.2. QY of PD loaded with 5mg UCNP and 2. QYs vary dependent on time and power.

8 mg	0.5W	1W	1.5W	2W
2s	--	--	--	7.1E-7 ± 4E-7
3.5s	--	--	--	6.9E-6 ± 3E-7
5s	--	4.5E-7 ± 2E-7	2.1E-6 ± 4E-7	4.9E-5 ± 7E-6
10s	2.5E-6 ± 8E-7	5.8E-6 ± 2E-6	1.0E-4 ± 3E-5	--
15s	2.1E-6 ± 8E-7	2.1E-5 ± 3E-6	--	--
20s	5.8E-6 ± 2E-6	4.9E-5 ± 7E-6	--	--
30s	7.7E-6 ± 9E-7	1.4E-4 ± 2E-5	--	--

Table 5.3. QY of PD loaded with 8mg UCNP and 2. QYs vary dependent on time and power.

5.5.9 Time comparison of UCNP loading

The loading of UCNPs also has a large impact in the efficiency of NO released. At low laser power (0.5 W) NO release was only observed in PDs with higher UCNP loading therefore and higher power photolysis was required to generate repeatable NO release throughout all UCNP loadings. The same non-linear trend is observed within the same irradiation time as power is increased from 1 W to 2 W. Figure 5.10 shows the increase of NO production after continuous laser excitation for 10 seconds with increasing laser power and increasing concentration of UCNPs (2 mg to 8 mg). The data in Figure 5.10 shows the moles of NO divided by the photons of light absorbed which is directly related to power. Therefore, more NO is produced at higher power independent of the number of photons absorbed. The exponential relationship to power is exaggerated when time remains constant, showing proof of a charging effect on the UCNPs that results in greater production of NO (consistent with Burks *et. al.*[7]). The highest loading of UCNPs also shows a strong influence on the production of NO and was selected for further experiments with tissue.

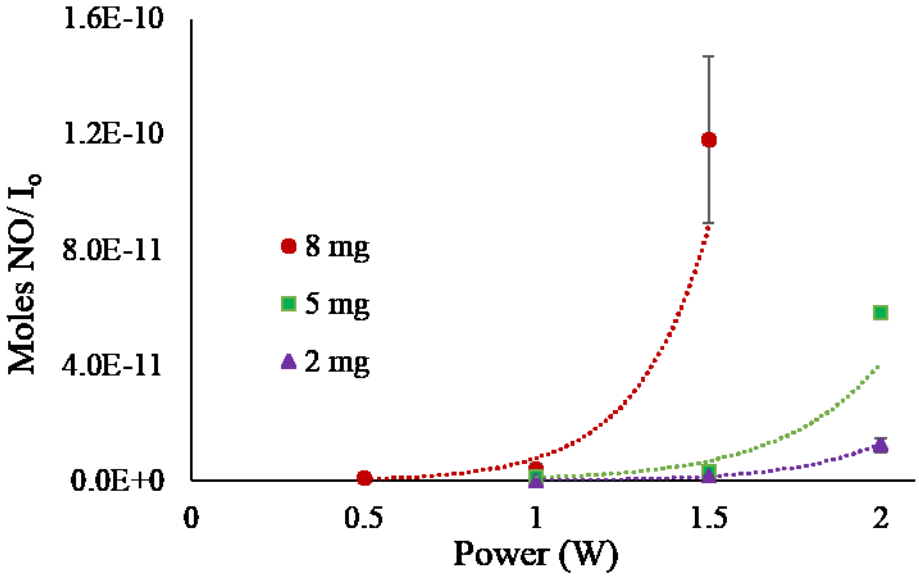

Figure 5.11. Efficiency of NO release when photolyzed for 10 s. Variable changes relating to the increased number of photons produced are adjusted for on the x-axis. The change of loading of UCNPs are plotted separately and indicated by the 8 mg (red), 5 mg (green), and 2mg (purple) designation.

5.5.10 Tissue samples

The PD with the highest efficiency of NO release with 8 mg UCNP loading was selected for studies using porcine muscular tissue at 2.5 mm thickness as filters. The tissue was suspended in front of the PD in the path of the 980 nm laser. The carrier gas of medical grade air was bubbled through nanopure water prior to entering the photolysis chamber, so that the flowing air did not dry the tissue sample throughout the experiment. The PD was irradiated for varying amounts of time (from 10 s to 40 s) through the tissue at 2 W, resulting in the non-linear production of NO in respect to increased time (Figure 5.11, blue circles). Furthermore, the PD can be re-used as shown in Figure 5.11 (orange triangles) to have equivalent NO production at 20 and 30 seconds. The PD is therefore not exhausted of NO releasing capabilities after 5 minutes of photolysis at 2 Watts. Additionally, there was no change in the appearance or thickness of the tissue at this power and time scale.

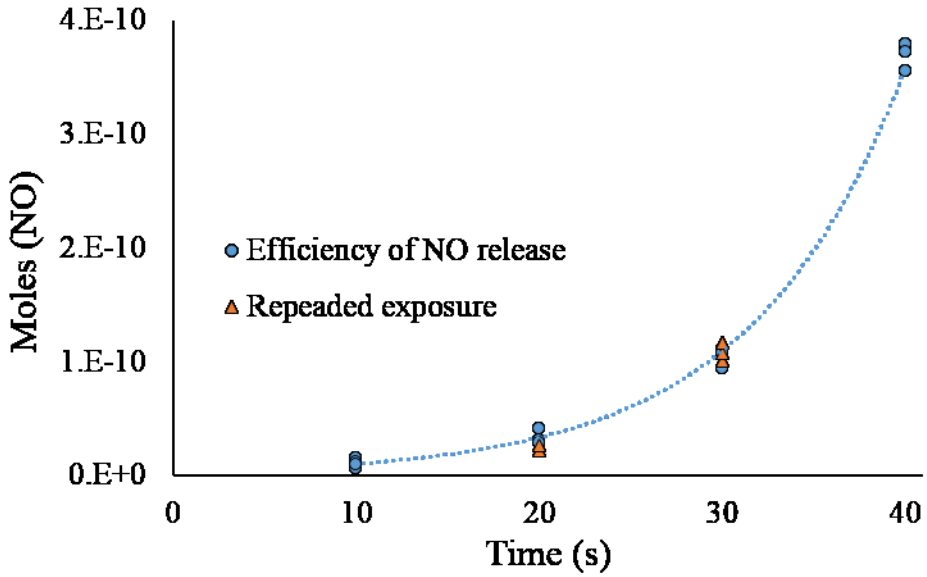

Figure 5.12. Release of NO after the light is passed through 2.5 mm of porcine tissue and hits the 8mg UCNP and **2** loaded PD. The moles of NO generated were measured against time (blue circles) and show an exponential response versus time. After efficiency measurements, the same sample was photolyzed at 20s and 30s to show repeatability between experimental runs with the same PD (orange triangles).

To account for the photons of light transmitted to the system, the moles of NO were divided by the photons of light produced by the 2 W 980 nm laser. This amounts to an I_o of 1.51E-5 Einstein's/ second. The efficiency of NO release is plotted in Figure 5.12 with respect to time as seen in the experiments without tissue. Without tissue present, an 8 mg UCNP loaded PD when irradiated at 2 W will have a QY of NO release 4.9E-5 ± 7E-6 at 5 second irradiation (Table 5.3). While tissue is present the efficiency decreases as light is absorbed and scattered by the tissue resulting in a lower QY of 7.2E-7 ± 2E-7 at twice the time, 10 second irradiation (Table 5.4). Despite the dramatic drop in the rate of NO production when tissue is filtering laser excitation, the QY of the individual PD is still sufficiently high to withstand moderate scatter and does not require a high power laser to induce photoactived release.

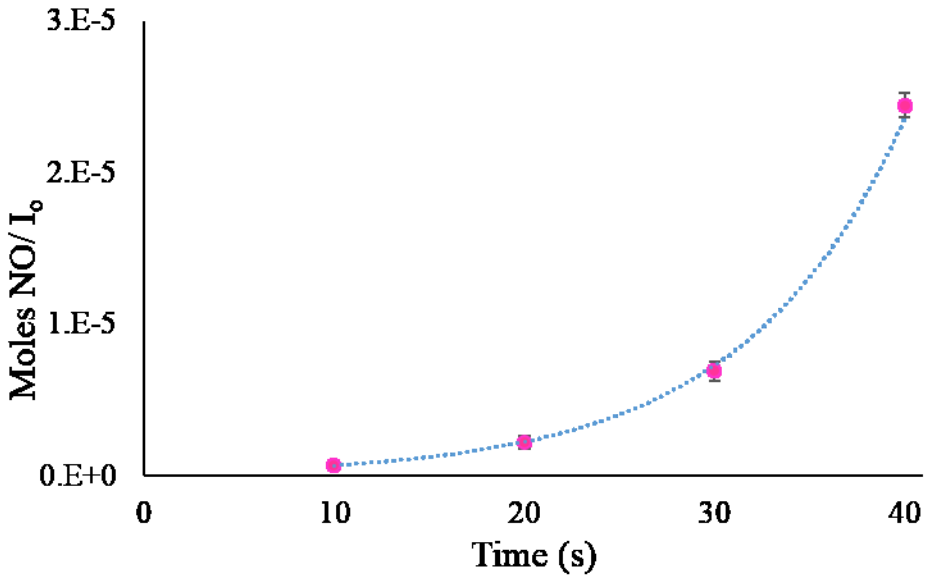

Figure 5.13. Efficiency of NO release from an 8 mg loaded UCNP after the light has passed through 2.5 mm of porcine tissue. Moles of NO produced per irradiation time while power remains constant at 2 W.

Irradiation Time	Quantum Yield 2W (no tissue)
2s	7.1E-7 ± 4E-7
3.5s	6.9E-6 ± 3E-7
5s	4.9E-5 ± 7E-6

Irradiation Time	Quantum Yield 2W with Tissue
10s	7.2E-7 ± 2E-7
20s	2.3E-6 ± 4E-7
30s	6.9E-6 ± 6E-7
40s	2.4E-5 ± 2E-7

Table 5.4. QY of NO release of PD loaded with 8mg UCNP and **2** irradiated at 980 nm with no tissue (left) or after irradiation through 2.5 mm porcine tissue (right). QYs vary dependent on time and power.

5.6 Conclusion

Biologically compatible microcarriers and implants are of great interest in the biomedical field as a method to deliver a drug to site specific locations. This chapter has focused on the release of NO using PLGA microparticles or PDMS polymer disks. The PLGA proved problematic in the generation of NO and reduced the efficiency of NO release, possibly stabilizing the bound ruthenium nitrosyl bond or reacting with free NO. However, the PDMS polymer disks loaded with UCNPs showed strong release of NO when irradiated at 980 nm light, even through tissue.

The loaded PD with 8 mg UCNP and **2** provided the highest production of NO through excitation at 980 nm. The generation of NO is dependent on both the intensity of incident light and the duration of excitation on the PD. However, the light used can transmit through tissue and cause NO production through the excitation of the thulium doped UCNP, emission and subsequent absorbance by **2**. This system could be used for coatings in surgical implants where the generation of a site specific drug would be beneficial to the healing process or reduce the risk of implant rejection. Use of small fiber optic LEDs could then be used to maneuver through a patient rather than using a high powered lasers to allow for deeper penetration and better control over site specific drug release.

5.7 References

[1] Neuman, D.; Ostrowski, A. D,; Mikhailovsky, A. A.; Absalonson, R. O.; Strouse, G. S.; Ford, P. C.; "Quantum Dot Fluorescence Quenching Pathways with Cr(III) Complexes. Photosensitized NO Production from*trans*-Cr(cyclam)$(ONO)_2^+$", *J. Am. Chem. Soc.*, **2008**, *130*, 168–175

[2] Liao, L.; Liu, J.; Dreaden, E. C.; Morton, S. W.; Shopsowitz, K. E.; Hammond, P. T.; Johnson, J. A.; "A Convergent Synthetic Platform for Single-Nanoparticle Combination Cancer Therapy: Ratiometric Loading and Controlled Release of Cisplatin, Doxorubicin, and Camptothecin", *J. Am. Chem. Soc.*, 2014, **136**, 5896−5899.

[3] Mackowiak, S. A.; Schmidt, A.; Weiss, V.; Argyo, C.; von Schirnding, C.; Bein, T.; Brauchle. C.; "Targeted Drug Delivery in Cancer Cells with Red-Light Photoactivated Mesoporous Silica Nanoparticles", *Nano Lett.*, 2013, **13**, 2576−2583.

[4] Baru, J. S.; Bloom, D. A.; Muraszko, K.; Koop, C. E. "John Holter's shunt", *J. Am. Coll. Surgeons*, **2001**, 192, 79. b.) Aschoff, A.; Kremer, P.; Hashemi, B.; Kunze, S.; "The scientific history of hydrocephalus and its treatment." *Neurosurg. Rev.*, **1999**, 22, 67.

[5] Danhier, F.; Ansorena, E.; Silva, J. M.; Coco, R.; Le Breton, A.; Préat, V.; "PLGA-based nanoparticles: An overview of biomedical applications", *J. Controlled Release*, **161** (2012) 505–522

[6] König, K.; "Multiphoton microscopy in life sciences", *J. Microscopy*, 2000, **200**, 83-104.

[7]Burks, P. T.; Garcia, J. V.; Gonzalez-Irias, R.; Tillman, J. T.; Niu, M.; Mikhailovsky, A. A.; Zhang, J.; Zhang, F.; Ford, P. C.; "Nitric Oxide Releasing Materials Triggered by Near-Infrared Excitation Through Tissue Filters", *J. Am. Chem. Soc.*, **2013**, *135* (48), 18145-18152.

[8] Curtis, J.; Colas, A.; Medical Applications of Silicones, *Biomaterials Science: An Introduction to Materials in medicine, 2nd ed.*, B.R. Ratner, A.S. Hoffman, F.J. Schoen, J.E. Lemons, Ed., Elseiver Academic press, 2004, 697

[9]Chen, G.; Qiu,H.; Prasad, P. N.; Chen, X.; "Upconversion Nanoparticles: Design, Nanochemistry, and Applications in Theranostics", *Chem. Rev.*, **2014**, 114, 5161−5214

[10] Ghosh, P.; Lorbeer, C.; Mudring, A. –V.; "Nanofluorides for Environmentally Benign Lighting and Energy Conversion in Solar Cells" *Fluorine-Related Nanoscience with Energy Applications,* Chapter 6, **2011,**pp 87-99 *ACS Symposium Series*, Volume 1064

[11] Zhang, F.; Wan, Y.; Yu, T.; Zhang, F.;Shi, Y.; Xie, S.;Li, Y.; Xu, L.; Tu, B.; Zhao, Z.; "Uniform Nanostructured Arrays of Sodium Rare-Earth Fluorides for Highly Efficient Multicolor Upconversion Luminescence", *Angew. Chem. Int. Ed.*, **46**, 7976–7979.

[12] Liu, Q.; Feng, W.; Yang, T.; Yi, T.; Li, F.: "Upconversion luminescence imaging of cells and small animals", *Nature Protocols,* **2013**, 8, 2033–2044.

[13] Freitag, L.; Gonzàlez, L.; "Theoretical spectroscopy and photodynamics of a ruthenium nitrosyl complex", *Inorg. Chem.*, **2014**, 50, 6415-6426.

Appendix i. Sievers NOA 1080i

Ai.1 Example Calibration Curve

(*Range 5 pmol – 500 pmol*)

*Note, Sodium Nitrite ($NaNO_2$) is hydroscopic. Completely dry the crystals under vacuum before making standards to ensure accuracy.

Stock Solution 1.00 mM $NaNO_2$ solution:

MW = 68.9953 g/mol. Weigh out 69 mg $NaNO_2$ and bring the total volume up to 1 L in a volumetric flask with nanopure water.

Dilution factors:

Samples were prepared with serial dilution

Sample	Conc. [NO]	Vol. H_2O	Vol. [NO_2^-] added	Moles injected in 5 μL injection
1	100 μM	900 μL	100 μL of stock solution	500 pmol
2	50 μM	200 μL	200 μL of solution 1	250 pmol
3	10 μM	900 μL	100 μL of solution 1	50 pmol
4	5 μM	200 μL	100 μL of solution 3	25 pmol
5	1 μM	900 μL	200 μL of solution 3	5 pmol

Example:

For sample 1. In a clean test tube or vial, add 100 μL of the stock solution (1.00 mM) and dilute it with 900 μL of nanopure water to bring the total volume to 1,000 μL with a concentration of 100 μM. Mix well.

For sample 2: In a clean test tube or vial, add 200 μL of the solution prepared in sample 1 (100 μM) and dilute it with 200 μL of nanopure water to bring the total volume to 400 μL with a concentration of 50 μM. Mix well.

For sample 3: In a clean test tube or vial, add 100 μL of the solution prepared in sample 1 (100 μM) and dilute it with 900 μL of nanopure water to bring the total volume to 1,000 μL with a concentration of 10 μM. Mix well.

Preparing the NOA:

Turn on NOA as described in the SOP "Start up". Prepare potassium iodine/ glacial acetic acid solution for the injection into the purge vessel and allow the vessel to purge for 10-15 minutes.

Injections:

Begin experiment on the NOA. Note the cell pressure in your lab notebook. Different cell pressures with require different calibration curves. Ideal cell pressure is 6.2 torr, however experiments can be completed with cell pressures as low at 4.2 torr. Changing the cell pressure for experiments will require a calibration curve at the new cell pressure within 0.1 torr.

Allow the background to collect for 5 minutes to ensure the NOA has a stable baseline before you begin. Using a 10 μL airtight syringe, inject 5 μL of your prepared sample (starting with the most dilute) into the purge vessel and inject in a single smooth motion. Once baseline is returned, wait 1 minute and repeat injection. The syringe should be washed a minimum of 3 times between injections with nanopure water and twice with the solution you will inject, discarding the solution as waste after each wash. Each concentration should be injected a minimum of 3 times.

Click “Mark Injection” to give a name to each peak. “Mark Injection” can be selected before or after an injection and the cursor moved. Name each injection with the concentration injected. E.g. 5 μM

The location of the cursor will not influence where the start or stop point for integration occurs.

Integrating Peaks:

Once the run is completed select **“STOP”** at the top center of your screen. (You will DELETE your entire run if you select “ABORT”.)

Adjust your threshold to be equal with the center of the baseline- such that the average of the noise would give you zero. Adjust the peak width to only include the injections you have made.

If your peaks are not identifiable, select “Integrate Manually”, set cursor at the beginning of your first peak and select “Start”. A new cursor will appear, move this to where the peak has returned to baseline, select “Stop”. The start cursor will turn green, the sop cursor will turn red – you can move these after the fact. Continue this until you have identified all peaks.

Identify each peak with the peak name. Select “Next” or add a peak names at this point. On the right of the plot, un-select the “use intercept” and select “Create Calibration”. Save the calibration curve.

Calculating Calibration:

The calibration curve must be completed in a separate program. The NOA will give calibration curves in units of concentration not moles. Input data of Area and Moles of NO

injected into Excel and plot. Plot the moles of NO versus the Area and add a linear trend line. Use the slope and intercept for measurement calculations.

Example Calibration Curve:

Injected concentration	Moles injected	Area
1 μM	5E-12	62.8
1 μM	5E-12	74.6
1 μM	5E-12	60.8
5 μM	2.5E-11	207.1
5 μM	2.5E-11	192.7
5 μM	2.5E-11	171.2
10 μM	5E-11	316.4
10 μM	5E-11	341.1
10 μM	5E-11	339.5
50 μM	2.5E-10	1589.4
50 μM	2.5E-10	1629.7
50 μM	2.5E-10	1592.2
100 μM	5E-10	3200.5
100 μM	5E-10	3242.3
100 μM	5E-10	3283.3

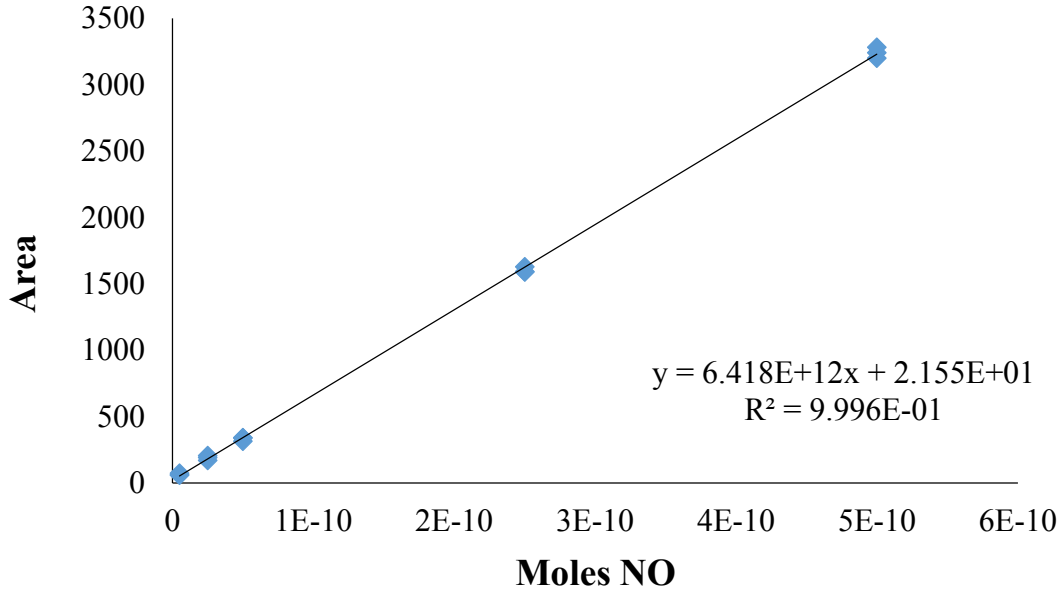

Figure 1. Example plotted calibration curve on the NOA. Data compiled and plotted in Excel.

Ai.2 Solution phase NOA experiments

Solution phase NOA experiments are conducted in the same manner. To maintain the solvent level in the cuvette, the carrier gas is initially bubbled through the NOA purge vessel prior to flowing into the cuvette. A 3 mL sample is photolyzed in a custom 4-sided, Y-shaped quartz cuvette which allows the carrier gas to flow through the cell and purge the experiment as NO is generated.

Photolysis timing is controlled with a uniblitz optical shutter, LED or laser is focused on the sample through manipulation of optical lenses. Following each photolysis, the Nitric Oxide Analyzer (NOA) must return to baseline prior to the next irradiation time point.

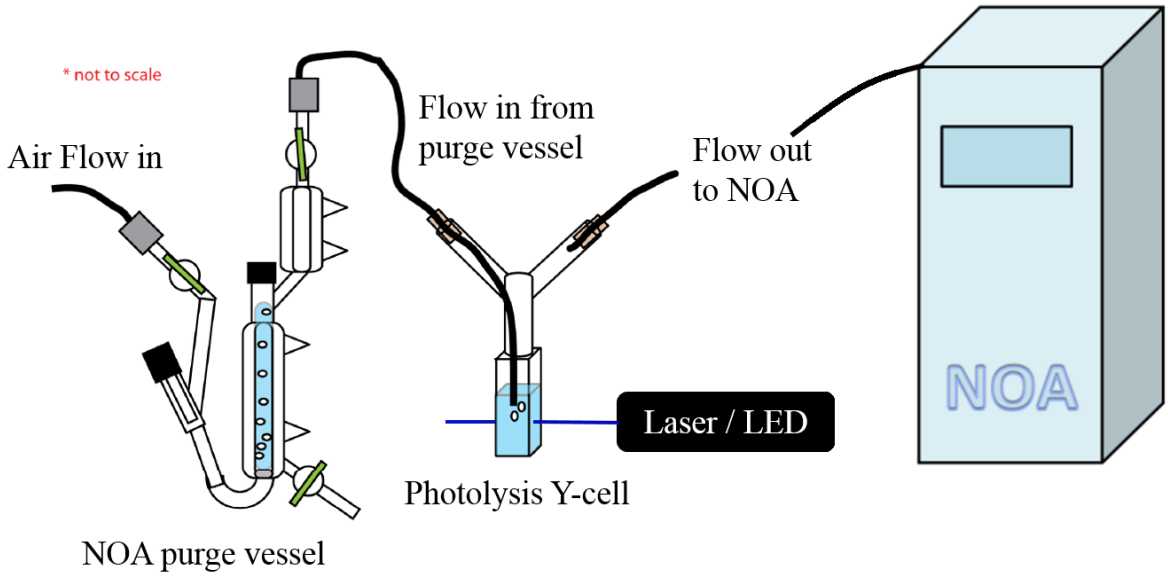

Figure i.1. Visual depiction of the solution phase NOA quantum yield system.

Ai.3 Solid phase NOA experiments

The solid phase NOA chamber is depicted in Figure i.2. The custom glass chamber is comprised of swage lock attachments to the carrier gas line and the NOA, a removable Teflon mount that holds a glass slide with the polymer disk sample (adhered with double sided tape). The cap of the solid state NOA cell has a glass fixture that can suspend tissue samples. When

tissue or skin is used in the NO release experiments, it is customary to attach the NOA purge vessel (Figure i.1) and bubble the carrier gas through water prior to entering the solid state chamber to avoid drying of the tissue over the course of the experiment.

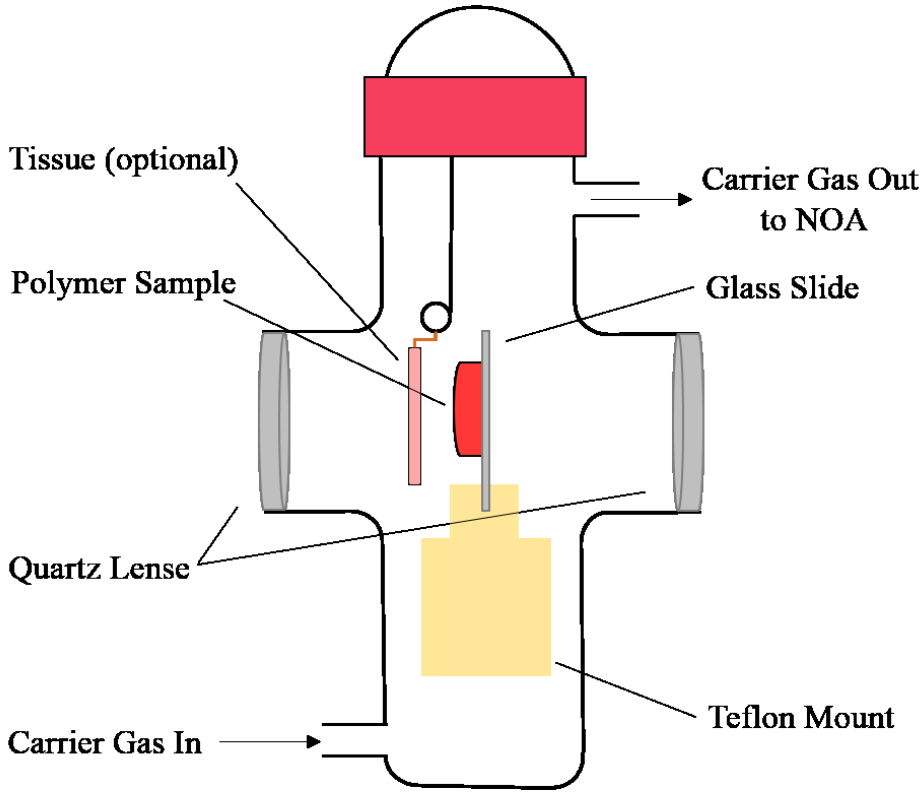

Figure i.2. Cartoon depiction of the solid state NOA chamber.

Appendix ii. Additional Ruthenium Nitrosyls

Aii. Introduction

Several additional compounds have been synthesized and characterized for their ability to release NO upon photo excitation. These compounds were not used due to poor water solubility or discarded as the project shifted focus. However, these compounds are of interest due to their organic solubility and salen and salophen modifications. The phenol or methyl ester modifications could therefore be used in other projects where the functionalized groups can be used to integrate into polymers or chemically linked to a secondary structure. This chapter will encompass the synthesis and NO releasing abilities of phenol and methyl ester modified salens and the synthesis and characterization of the methyl ester salophen ligand along with the synthesis of common ruthenium precursor $Ru(PPh_3)_2$.

Aii.2 Synthesis of Additional Ligands

Aii.2.4 Salen-CO_2CH_3

The synthesis of Salen-CO_2CH_3 [methyl dimethyl 3,3'-((1E,1'E)-(ethane-1,2-diylbis(azanylylidene))bis(methanylylidene))bis(4-hydroxybenzoate)] was completed by a Shiff base reaction of methyl 3-formyl-4-hydroxybenzoate and ethylenediamine.

Methyl 3-formyl-4-hydroxybenzoate was purchased from Sigma Aldrich and was used without further purification. Methyl 3-formyl-4-hydroxybenzoate (0.5013g, 2.7 mmol) was dissolved in approximately 30 mL of ethanol and heated slightly to aid in dissolving the benzaldehyde completely. Ethelenediamine (0.0909g, 1.5 mmol) was dissolved into 5 mL of ethanol and added drop wise to the warm benzaldehyde solution. The solution was heated

slightly with stirring for 30 minutes until the flask had completely turned opaque yellow from the initially clear solution.

The solution was allowed to cool to room temperature and the precipitate was filtered and washed with ethanol to product 0.5090g Salen-CO_2CH_3. To extract additional product, supernatant was concentrated to 5 mL via rotary evaporation and the salen was allowed to settle out of the ethanol solution producing an additional 0.0048g.

Total mass produced of 0.5138 g (1.34 mmol) Salen-MeEs at a 96% yield. Reaction shown is Scheme ii.1. ^{1}H NMR taken on a Varian 400 MHz NMR in deuterated DCM. δ= 8.435 ethylene (s, 2 H), aromatics δ= 6.947 (d, 2H), δ= 7.941 (d, 2H), δ= 7.991 (d, 2H), ethane bridge δ= 3.971 (s, 4H), methyl ester δ= 3.846 (s, 6H). (Figure ii.1) Peaks at δ= 3.406 and δ= 1.586 are attributed to ethanol and water contamination from the reaction.[1] Elemental Analysis C 62.50%, H 5.00%, N 7.20%. Theoretical C 62.49%, H 5.24%, N 7.29%.

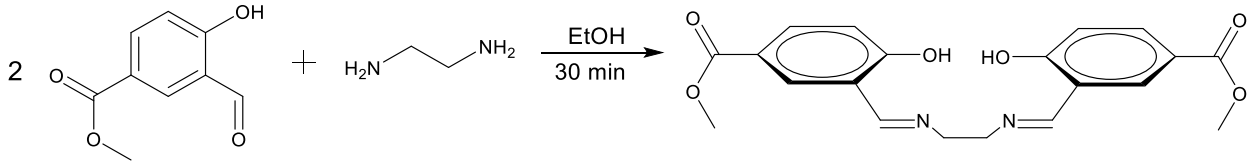

Scheme ii.1. Synthesis of Salen-CO_2CH_3

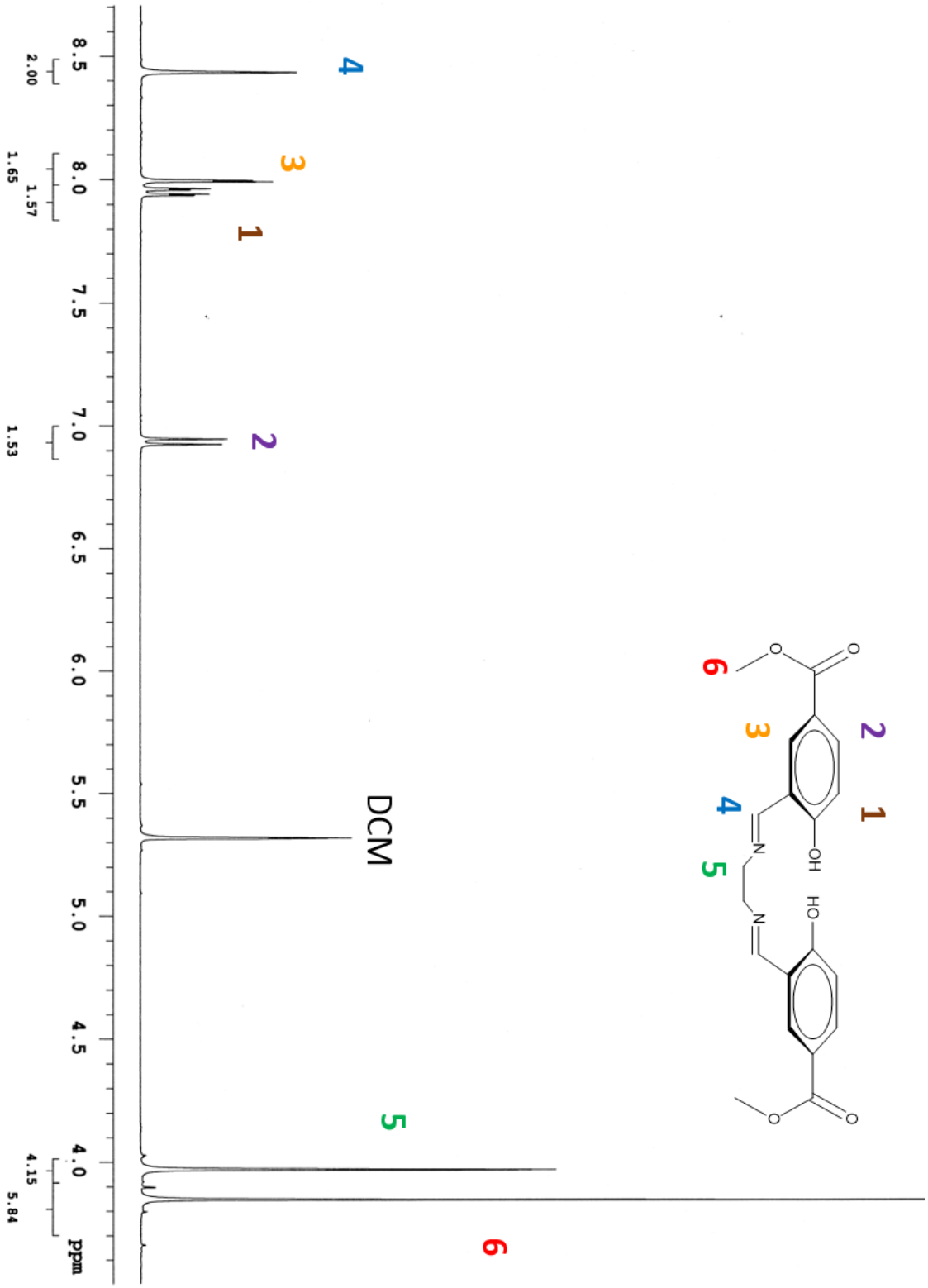

Figure ii.1. ^{1}H NMR of Salen-CO_2CH_3 taken on a Varian 400 MHz NMR in deuterated DCM

Aii.2.5 Salen-OH

Synthesis of salen-OH [N,N'-bis(salicylidene)ethylenediamine-4-hydroxide] was completed by a Shiff base reaction of ethylenediamine and 2,4-dihydroxybenzaldehyde.

The benzaldehyde, 2,4-dihydroxybenzaldehyde (1.0002 g, 7.24 mmoles) was dissolved in approximately 100 mL of ethanol and heated slightly until the 2,4-dihydroxybenzaldehyde fully dissolved. Ethylenediamine (0.2008 g, 3.34 mmoles) was added to the warm solution and the solution was brought up to refluxed and stirred for one hour. The solution was allowed to cool to room temperature before the precipitate was filtered and collected. This produced 0.6286 g of the salen-OH product (Scheme ii.2).

^{1}H-NMR in d^{6} DMSO, methane proton, s (8.36p), aromatic protons, d (7.17, 7.15), d (6.26, 6.24), s (6.14), amine bridge, d (3.77, 3.33) (Figure ii.2). Elemental Analysis; C 63.72%, H 5.38%, N 9.71%. Theoretical; C 63.99%, H 5.37%, N 9.33%.

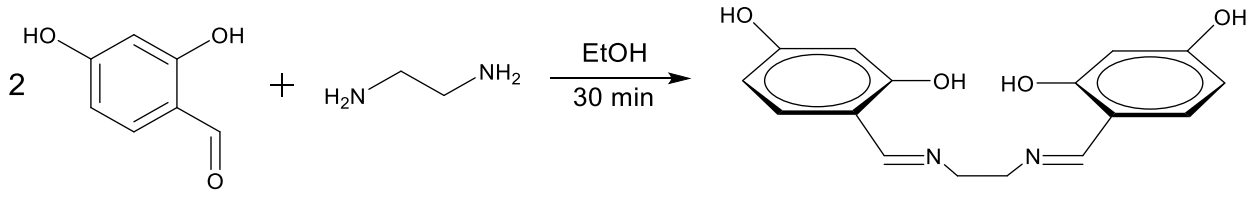

Scheme ii.2. Synthesis of Salen-OH

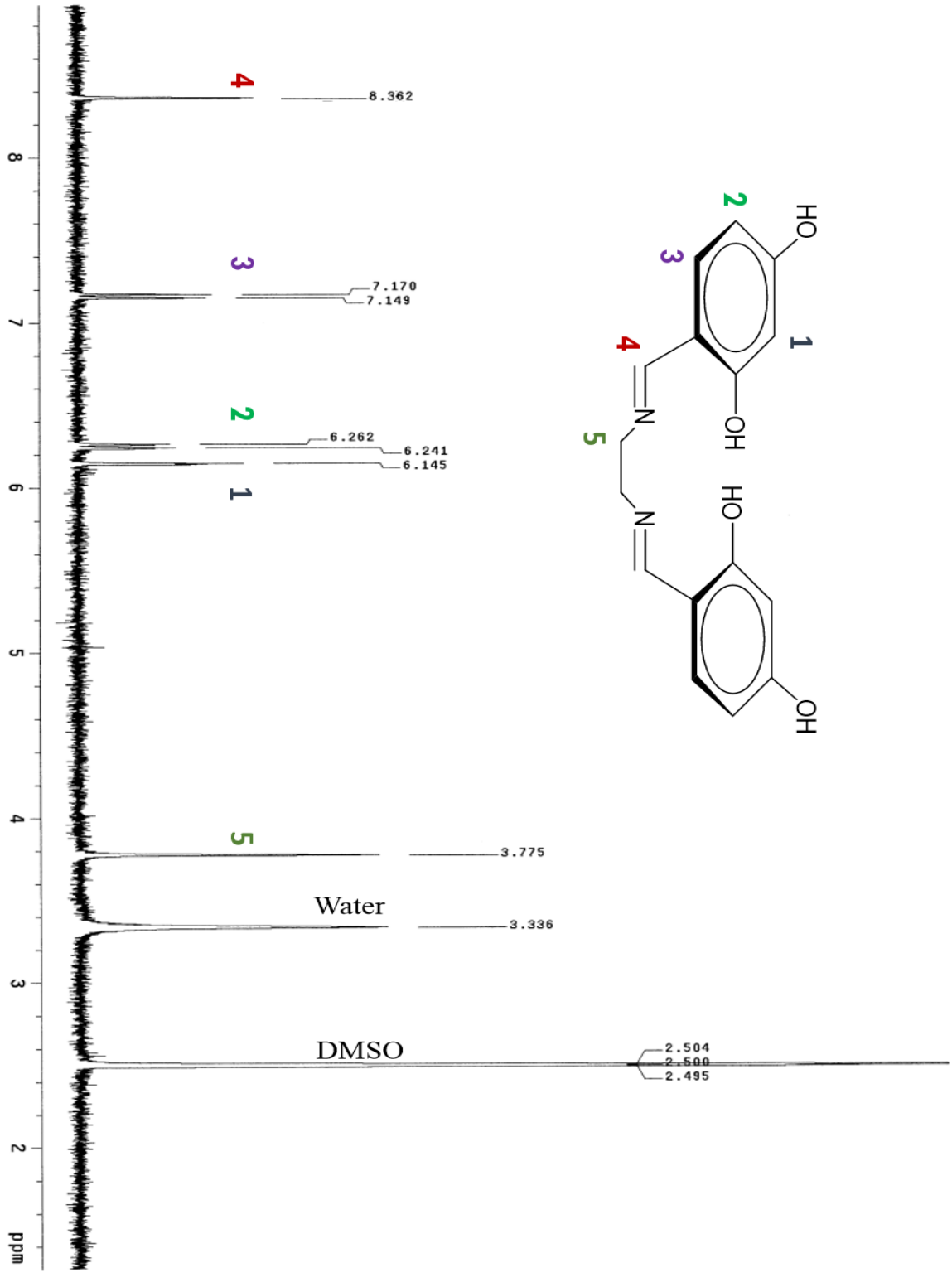

Figure ii.2. ^{1}H NMR of Salen-COH taken on a Varian 400 MHz NMR in $(CD_3)_2SO$.

Aii.2.6 Salophen-MeEs

The synthesis of Salophen-CO_2CH_3 [dimethyl 3,3'-((1E,1'E)-(1,2-phenylenebis(azanylylidene))bis(methanylylidene))bis(4-hydroxybenzoate)] was completed by a Shiff base reaction of o-phenylenediamine and methyl 3-formyl-4-hydroxybenzoate.

The benzaldehyde, methyl 3-formyl-4-hydroxybenzoate (0.3409 g) was dissolved in approximately 25 mL of ethanol with stirring and mild heating. In a separate flask, 0.1025 g o-phenylenediamine was dissolved in 10 mL of ethanol and added drop wise into the benzaldehyde solution. The mixture was heated to reflux and stirred for 45 minutes. The solution was allowed to cool to room temperature and solid precipitate was collected and washed with cold ethanol. Solid product was left under vacuum for 2 hours to remove excess ethanol. ^{1}H NMR in d^2-methylenechloride on a 500 mHz Varian NMR showed the filtered product was pure. Solid was used without further purification (Scheme ii.3). ^{1}H NMR 500 mHz Varian (CD_2Cl_2) δ 8.73 (s, 2H), 8.18 (d, 2H), 8.04 (dd, 2H), 7.42 (ddd, 2H), 7.30 (ddd, 2H), 7.05 (d, 2H), 3.88 (s, 6H), and phenol group at 13.67 (s, 2H) (Figure ii.3). Elemental Analysis C 60.50%, H 3.60%, N 7.40%. Theoretical C 66.66%, H 4.663%, N 6.48%.

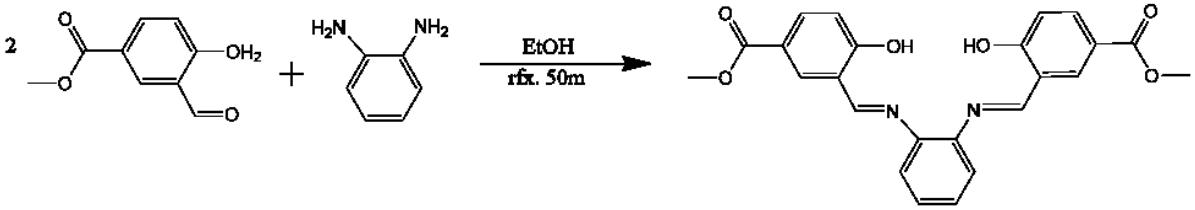

Scheme ii.3. Synthesis of Salophen-CO_2CH_3

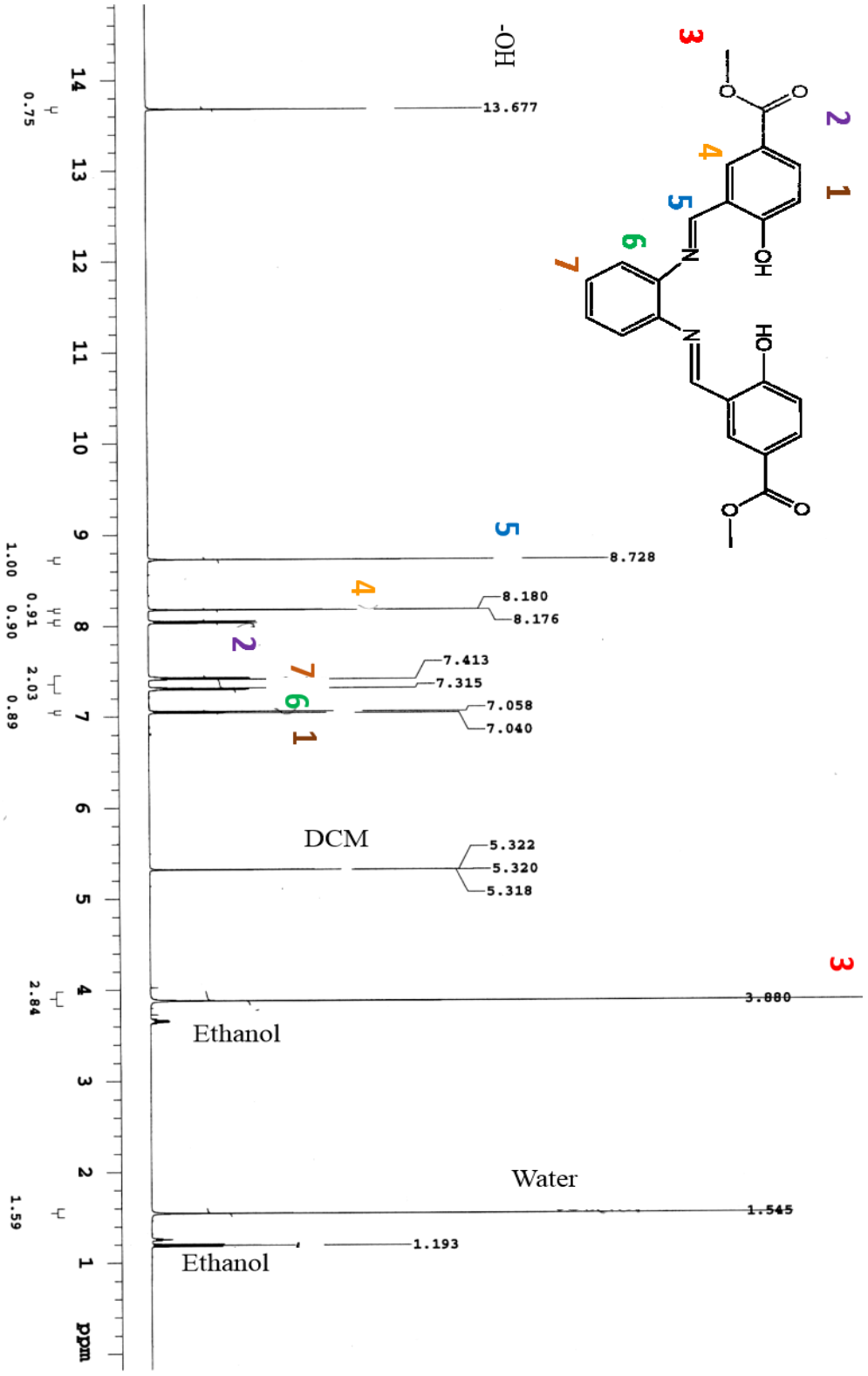

Figure ii.3. ^{1}H NMR of Salophen-CO_2CH_3 in d^2-methylenechloride on a 500 mHz Varian NMR.

Aii.3 Synthesis of Ruthenium Nitrosyls

Aii.3.3 Ru(NO)(Salen-CO_2CH_3)Cl

Salen-CO_3CH_3 (0.0201g, 0.052 mmol, 1 eq.) and NaH (0.0082g, 0.14 mmol, 2.7 eq.) in 57% oil dispersion were degassed and put under argon. Approximately 30 mL of degassed ethanol was cannula transferred into the round bottomed flask and the solution was refluxed and stirred under argon for 1 hour.

In the dark, 0.0135g $RuCl_3(NO)\cdot H_2O$ (0.053 mmol, 1 eq.) was dissolved in approximately 10 mL of degassed THF and cannula transferred into the hot salen solution in the dark. Ruthenium nitrosyl insertion required refluxing under argon in the dark for 3 hours (Scheme ii.4). The reaction mixture was allowed to cool to room temperature and the solution was cannula filtered off, precipitate collected.

If the precipitate is impure, crude product was purified by silica column chromatography run in the dark 60:40 toluene: acetonitrile. Brown fractions removed slightly after the solvent line were shown to be the product by TLC and later by ^{1}H NMR in deuterated acetonitrile. ^{1}H NMR taken on a Varian 500 MHz NMR in deuterated acetonitrile. δ= 8.435 ethylene (s, 2 H), aromatics δ= 7.065 (d, 2H), δ= 8.169 (d, 2H), δ= 8.376 (d, 2H), ethane bridge δ= 3.817, 4.335 (q, qq, 4H), methyl ester δ= 3.860 (s, 6H). Ethane bridge and methyl ester peaks seem to overlap due to the shouldering on the singlet of the methyl ester peak. This can account for slightly skewed integration of the peaks. (Figure ii.4).

Peaks at δ= 2.131 and δ= 1.361 are attributed to water and ethanol contamination from the reaction. Additional peak after silica gel column at δ= 11.305 (s) is indicative of a carboxylic acid proton which is created by the deprotection of the methyl ester when run through the column.

IR spectra taken in deuterated acetonitrile on salt plates. Formation of nitrosyl stretching frequency at 1862 cm^{-1} is observed while other salen-MeEs peaks remain unchanged other than the splitting of the C=N stretch from 1636 to having a 1635 and 1609 cm^{-1}. The extinction coefficient of Ru(NO)(salen-MeEs)Cl was taken in acetonitrile from 800-200nm. UV-vis $\varepsilon = 4.0 \times 10^4$ at $\lambda_{max} = 378$nm.

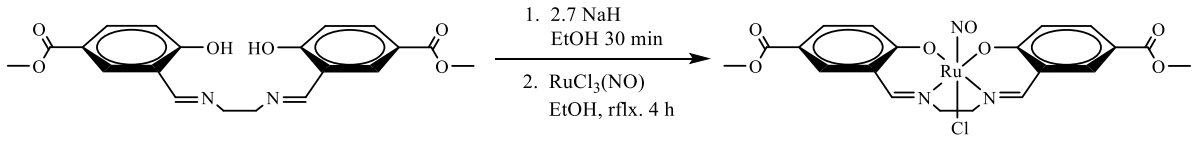

Scheme ii.4. Insertion of the ruthenium nitrosyl into the salophen-CO_2CH_3 ligand structure.

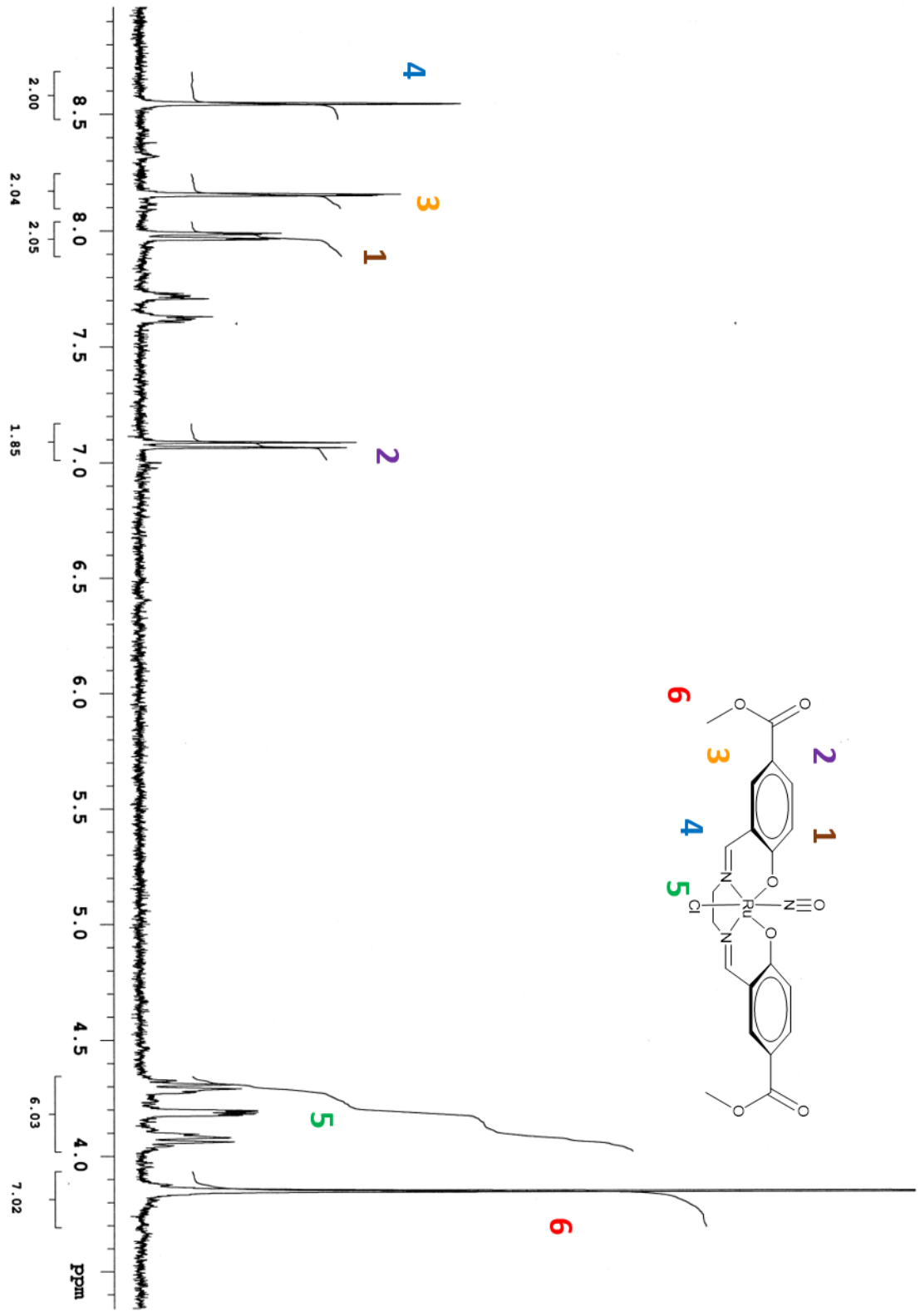

Figure ii.4. ^{1}H NMR of Ru(NO)(Salophen-CO_2CH_3)Cl in acetonitrile on a 500 mHz Varian NMR.

Aii.3.4 Ru(NO)(Salen-OH)Cl

$RuCl_3(NO)\cdot H_2O$ (0.0263 g, 0.103 mmoles) and salen-OH (0.0309 g, 0.103 mmoles) were placed in a three neck flask, vacuumed and back filled with argon three times to assure an air free starting flask. Distilled and degassed THF (30 mL) was added to the solution via cannula and the solution was heated and stirred in the dark. After 20 minutes of heating and stirring, 0.02 mL (0.143 mmoles) of fully degassed triethylamine was added. The solution was refluxed under argon for 3 hours in the dark. The reaction was allowed to cool to room temperature and was filtered under argon via cannula (Scheme ii.5).

^{1}H NMR 400 mHz Varian ($(CD_3)_2SO$) δ 9.7 (s, 2H), 7.51 (d, 2H), 6.51 (d, 2H), 6.33 (s, 2H), 3.54 (q, 4H).). (Figure ii.5). MS(ESI+): m/z (464.9 – H^+) 463.96 is consistent with deprotinated RuCl(NO)(salen-OH) (Figure ii.6). FTIR (KBr) ν_{NO} = 1851 cm^{-1}. UV-vis (acetonitrile) λ_{max} 276nm ($\varepsilon = 3.9 \times 10^4\ M^{-1}\ s^{-1}$).

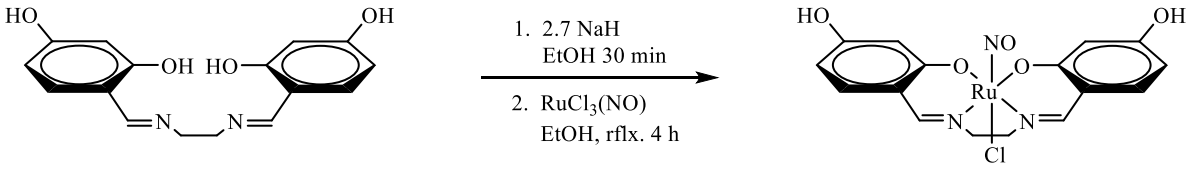

Scheme ii.5. Insertion of the ruthenium nitrosyl into the salen-OH ligand structure. Experiment conducted in the dark.

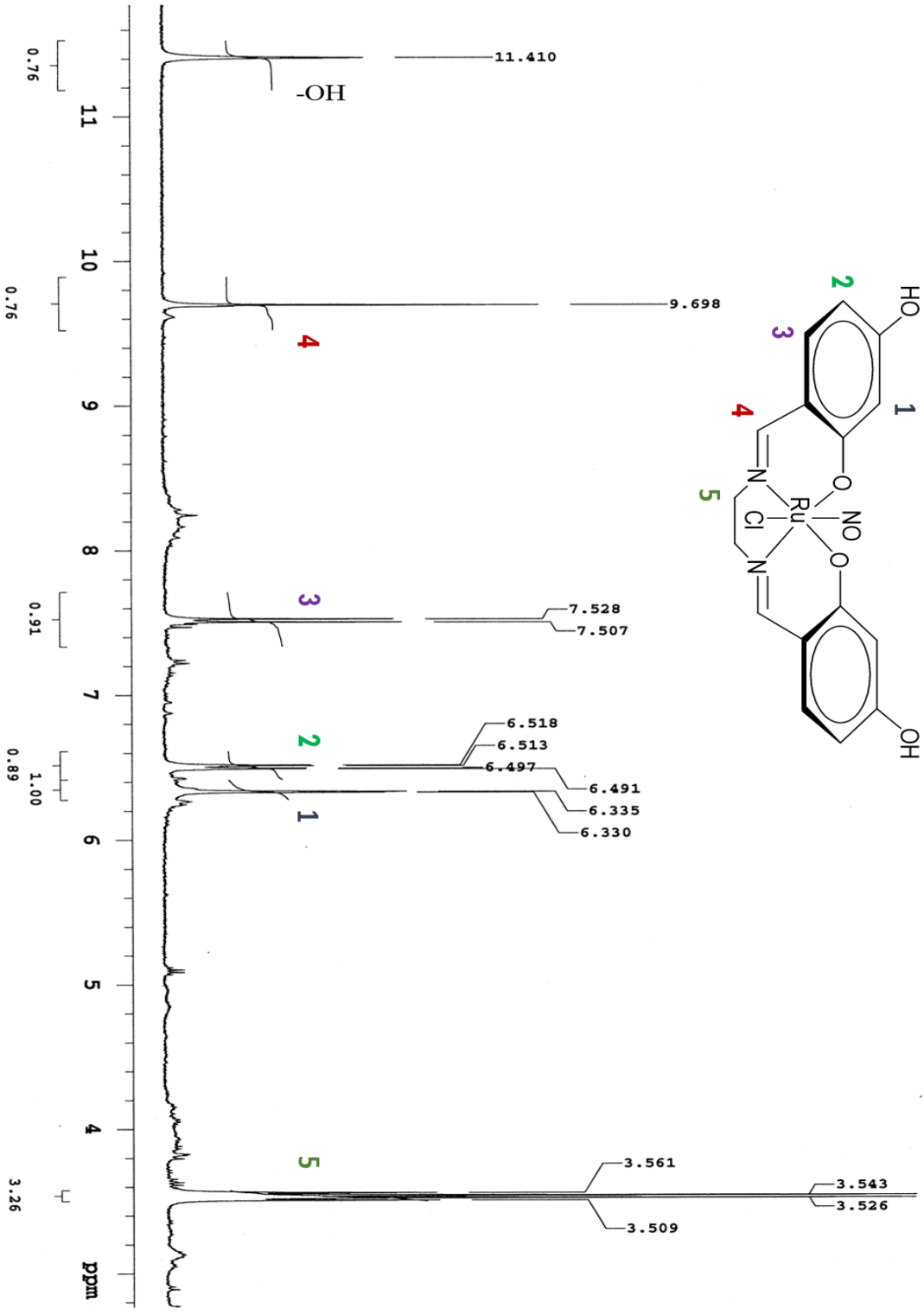

Figure ii.5. ^{1}H NMR of Ru(NO)(Salen-OH)Cl in $(CD_3)_2SO$ on a 400 mHz Varian NMR.

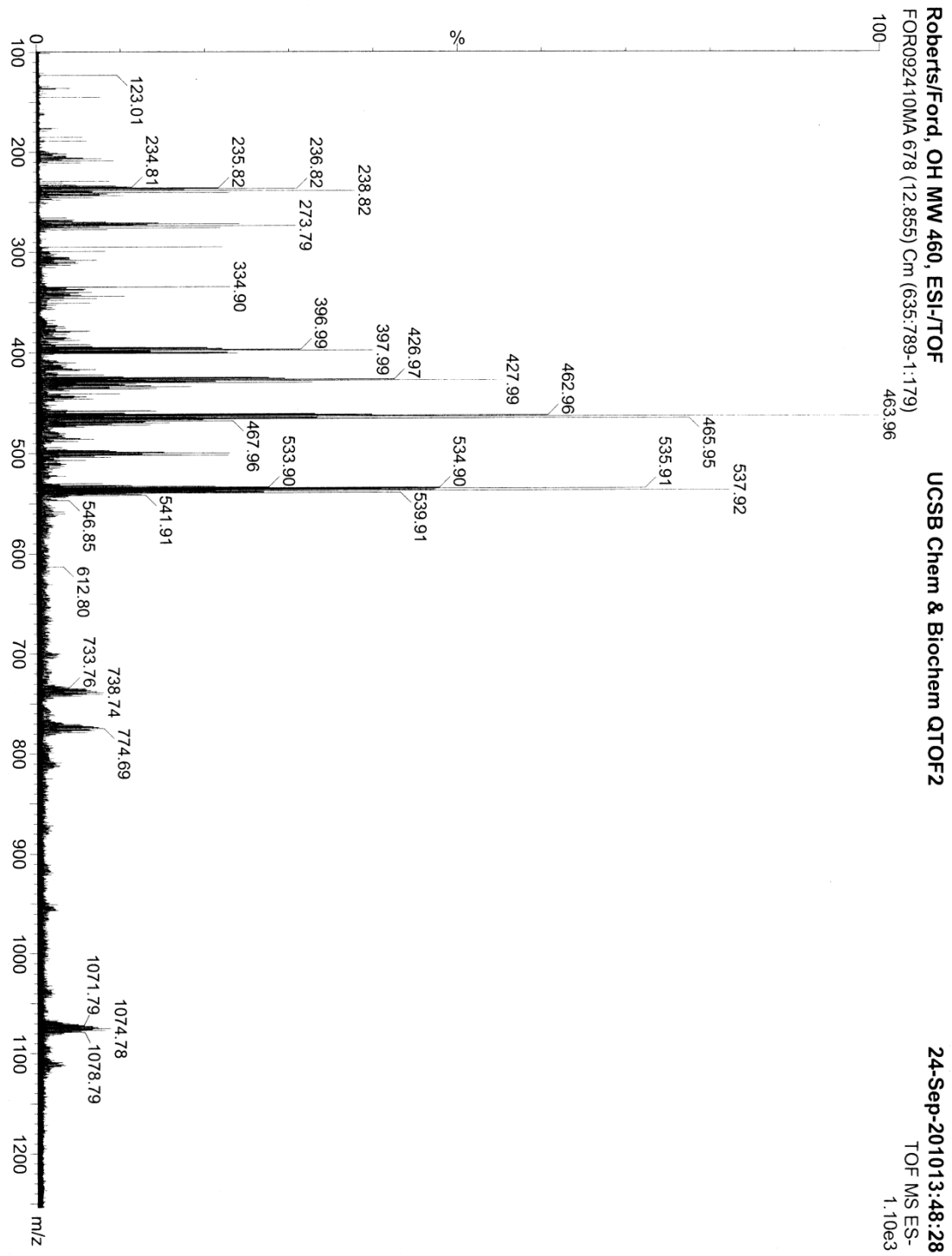

Figure ii.6. Low resolution negative ion mass spectrometry for RuCl(NO)(salen-OH) in water with ammonium hydroxide. A mass of 463.96 is consistent with deprotinated RuCl(NO)(salen-OH).

Aii.3.5 Ru(NO)(Salophen- CO_2CH_3)Cl

0.3009 g salophen-MeEs and 0.0368 g NaH were combined and dissolved in 50 mL ethanol. The sample was sonicated for 5 minutes for the salophen to completely dissolve. The solution was heated and stirred for 30 minutes and purged with argon. 0.1778g $Ru(NO)Cl_3 \cdot H_2O$ was dissolved in 10 mL of ethanol and cannula added to the hot reaction flask in the dark under argon (Scheme ii.6).

The reaction was allowed to progress for 24 hours. The solution was removed from heat and allowed to cool. Stirring stopped and precipitate was allowed to fall out of solution. The solid was dried and ^1H NMR was taken in d^3-acetonitrile. Mass Spec data shows the full compound with a sodium cation with a signal at 622.05. ^1H NMR 500 mHz Varian (CD_3CN) δ 9.23 (s, 2H), 8.44 (d, 2H), 8.20 (m, 2H), 8.04 (dd, 2H), 7.58 (m, 2H), 7.18 (d, 2H), 3.88 (s, 6H) (Figure ii.7). Elemental Analysis C 43.9%, H 2.51%, N 6.58%. Theoretical [Ru(NO)(salophen-CO_2CH_3)Cl•NaCl], C 43.98%, H 2.77%, N 6.41%. MS(ESI+): m/z (596.99 + 23) 620.05 ($M + Na^+$) (Figure ii.8). FTIR (KBr) ν_{NO} = 1829 cm^{-1}. UV-vis (acetonitrile) λ_{max} 284nm ($\varepsilon = 6.0 \times 10^4\ M^{-1}\ s^{-1}$), 433 ($\varepsilon = 1.06 \times 10^4\ M^{-1}\ s^{-1}$) (Figure ii.9).

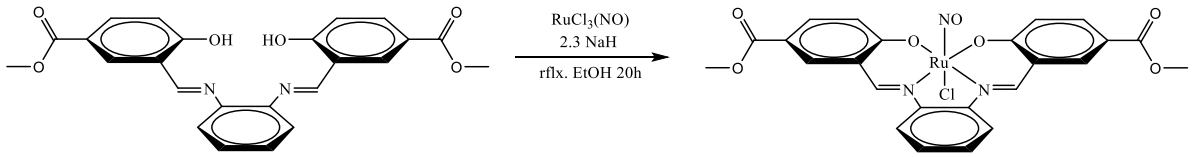

Scheme ii.6. Synthesis of Ru(NO)(Salophen- CO_2CH_3)Cl. Synthesis completed in the dark.

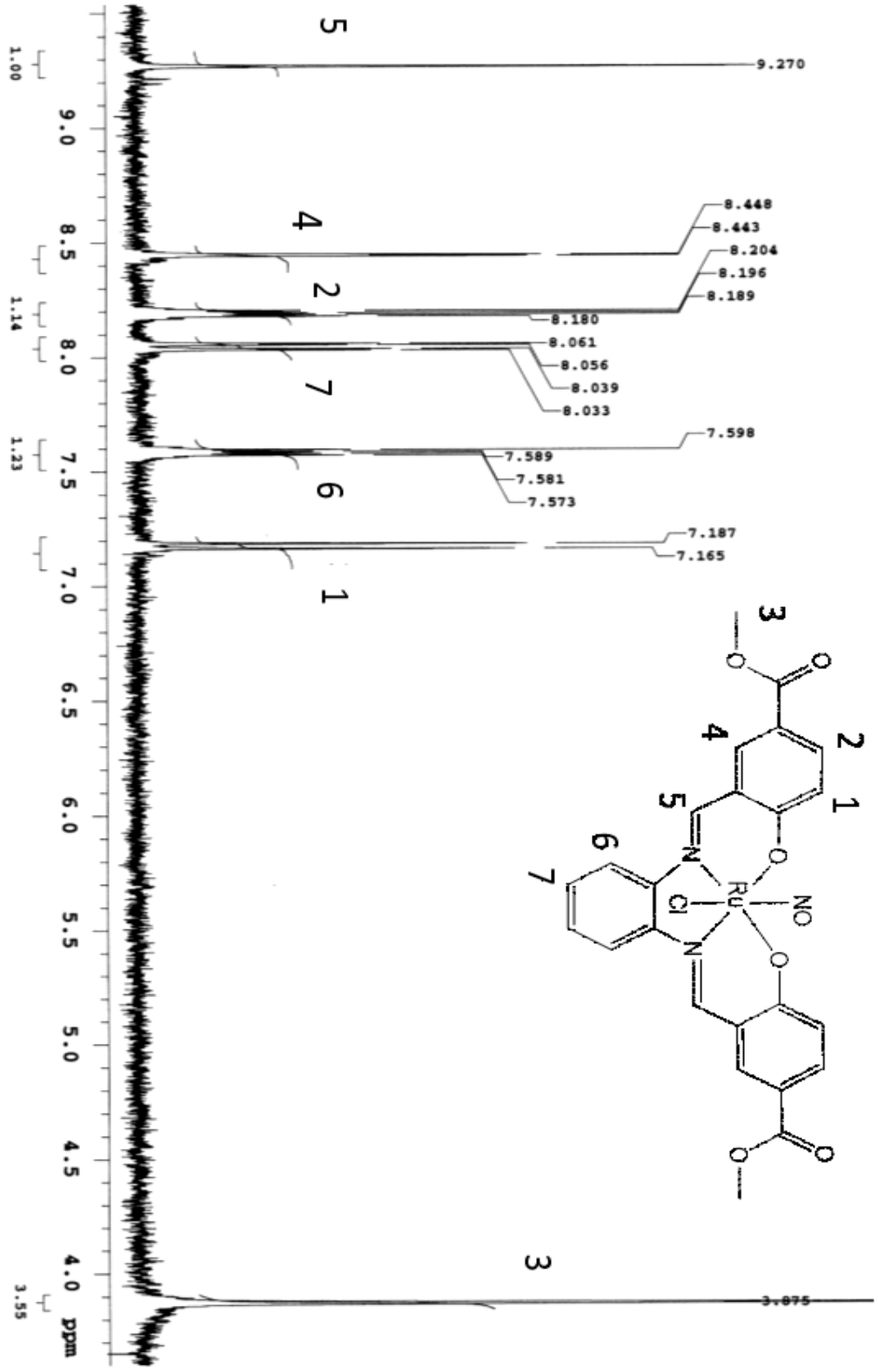

Figure ii.7. ^{1}H NMR of Ru(NO)(salophen-MeEs)Cl in acetonitrile. Protons designations are labeled with corresponding numbers.

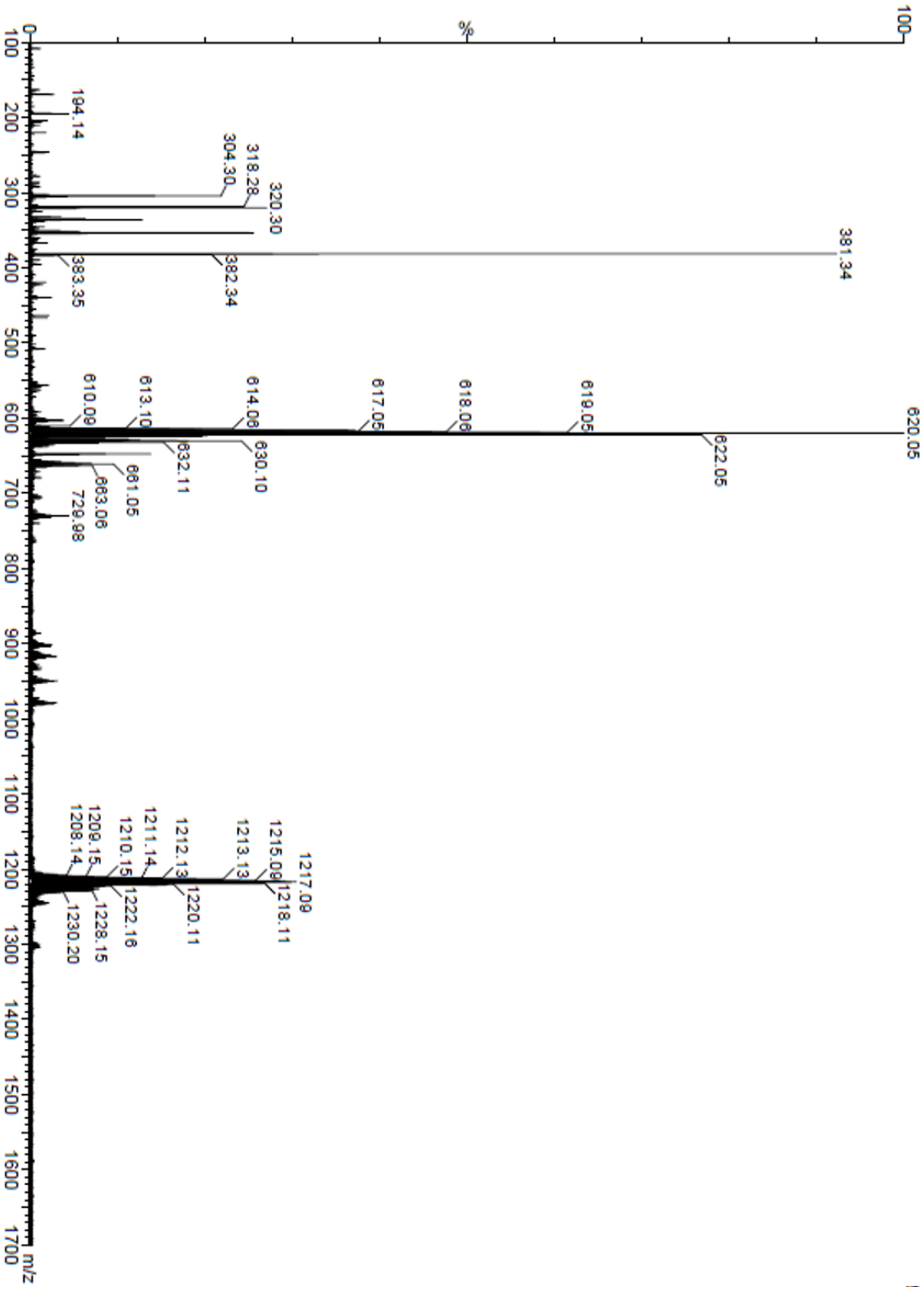

Figure ii.8. Mass spectra, ESI+ for Ru(NO)(salophen-CO_2CH_3)Cl + Na^+ MW= 596.99 + 23.

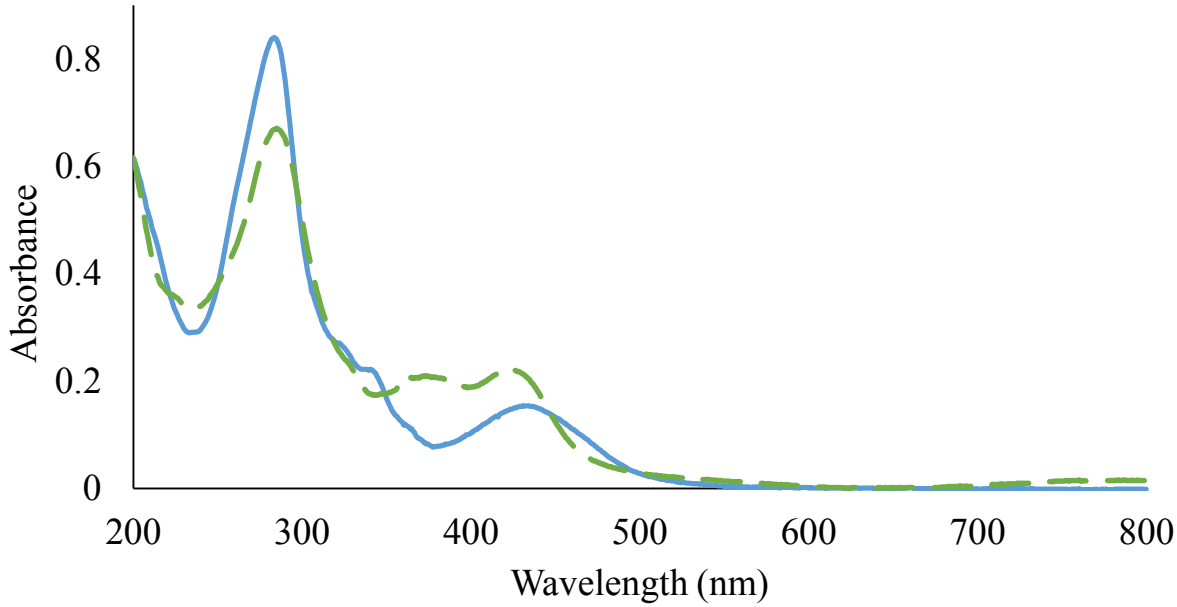

Figure ii.9. Ru(NO)(salophen-MeEs)Cl in acetonitrile before (solid line) and after exposure to UV-lamp (dashed line). The LMCT band shifts from 432 nm to 422 nm after photolysis while the MLCT drops in intensity at 284 nm upon irradiation.

Aii.4 Ruthenium Precursors

Aii.4.6 $RuCl_2(PPh_3)_3$

The synthesis was modified from the published work of T. A. Stephenson and G. Wilkinson.[2] Dichlorotris(triphenylphosphine)ruthenium(II) was synthesized by dissolving 0.0258 g $RuCl_3$ (0.1244 mmol) and into 0.3269 g triphenylphosphine (1.246 mmol) 50mL of degassed methanol. The solution was refluxed under inert atmosphere for 4 hours with stirring. The solution was allowed to cool to room temperature and stirring was stopped to allow for the product to precipitate. The methanol was removed using cannula filtration. The red powder was washed with ethyl ether and allowed to dry on vacuum. (Note: $RuCl_2(PPh_3)_3$ is extremely oxygen sensitive, this will oxidize from red to green at any oxygen exposure.)

Aii.4.7 Ru(salen)(PPh_3)$_2$

In the same flask as the $RuCl_2(PPh_3)_3$ a 1:1 mole ratio of salen (0.065 g, 0.00024 mol) was added. Distilled, degasses THF was cannula transferred into the reaction flask to dissolve compounds and begin heating. The triethylamine was fully deaerated by freeze/pump/thaw of approximately 1mL until there is no air present in the liquid, add 0.04 mL (0.286 mmoles) of triethylamine to the ruthenium solution with a lure lock syringe.

The reaction was allowed to reflux, under inert atmosphere for 3 hours then the solution was removed from heat and allowed to cool to room temperature. Supernatant was removed by cannula filtration and the product was fully dried under vacuum to produce a red solid. Solid was transferred into an inert atmosphere glove box for storage.

Aii.4 Quantum Yield Studies

Quantum yield studies were completed for Ru(NO)(salen-CO_2CH_3)Cl and Ru(NO)(salen-OH)Cl by monitoring the change in UV-visible spectra or by monitoring the production of NO on the Nitric Oxide Analyzer (Sievers 1080i NOA). Both methods underwent the same photochemical conditions of irradiation at λ = 365 nm in acetonitrile under an inert atmosphere, the results of the QY tests are discussed below.

Aii.4.1 Nitric Oxide Quantum yield measurements for Ru(NO)(salen-CO_2CH_3)Cl and Ru(NO)(salen-OH)Cl

For each NO QY experiment, a 0.25 mM solution of either Ru(NO)(salen-CO_2CH_3)Cl or Ru(NO)(salen-OH)Cl was prepared in acetonitrile and an aliquot of 3 mL was used for each individual experiment. The sample was photolyzed in a 4-sided, Y-shaped cuvette which allows the carrier gas (helium, bubbled through 5 mL acetonitrile prior to entering the

photolysis cell) to flow through the cell and purge the experiment as NO is generated. The samples were irradiated at 365 nm with a mercury lamp. Ferrioxolate actinometry was used to calculate the photons of light emitted and the photolysis timing was controlled with a uniblitz optical shutter. After each photolysis, the Nitric Oxide Analyzer (NOA) was allowed to return to baseline for a minimum of 1 minute prior to the next irradiation time point. (A complete description of the Sievers 1080i NOA is described in Appendix 1.)The moles of NO were calculated from the calibration curve established on the NOA.

The moles of NO released versus the photons of light absorbed by the sample is plotted in Figures ii.10 and ii.11. Photolysis of Ru(NO)(salen-CO_2CH_3)Cl at 365 nm resulted in a Φ_{NO} of 0.111 or 11.1% while the electron donating phenol groups lowered the Φ_{NO} for Ru(NO)(salen-OH)Cl with a Φ_{NO} of 0.0073 or 7.3%.

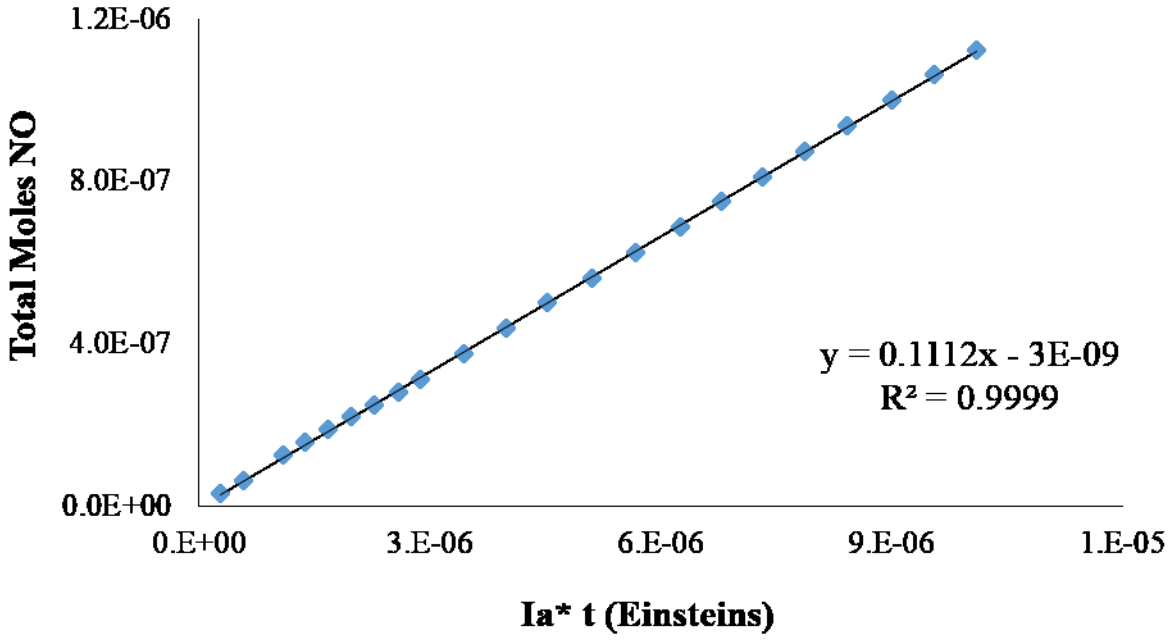

Figure ii.10. QY Ru(NO)(salen-CO_2CH_3)Cl on the NOA irradiating at λ = 365 nm in acetonitrile under inert conditions.

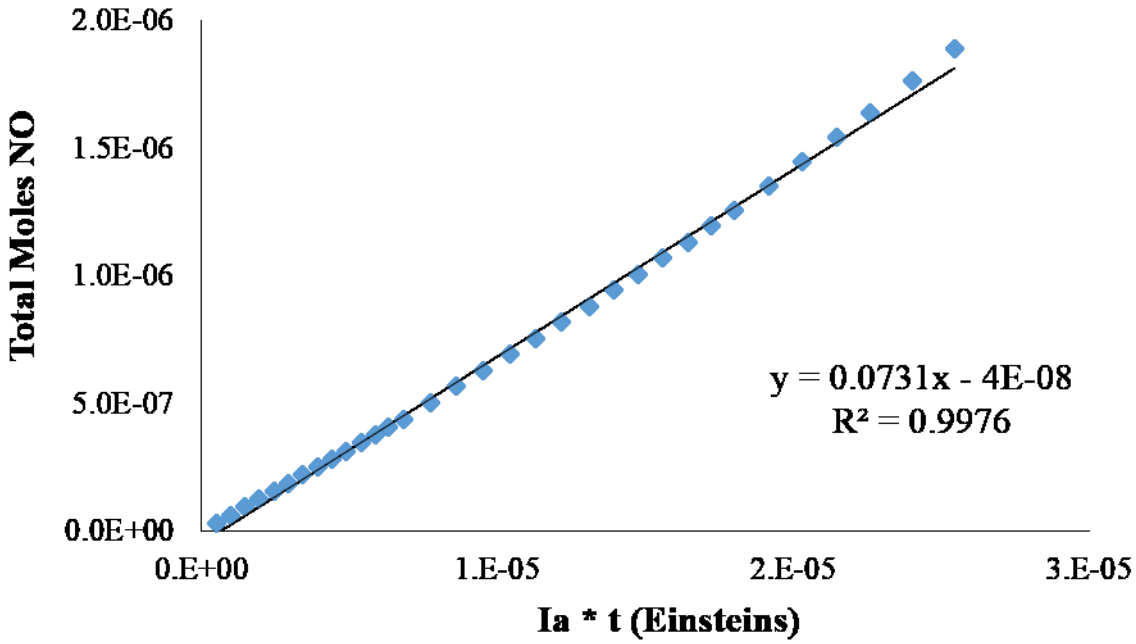

Figure ii.11. QY Ru(NO)(salen-OH) on the NOA irradiating at λ = 365 nm in acetonitrile under inert conditions.

Aii.4.2 Quantum yield measurements for Ru(NO)(salen-CO_2CH_3)Cl and Ru(NO)(salen-OH)Cl

For each QY experiment, a 0.25 mM solution of either Ru(NO)(salen-CO_2CH_3)Cl or Ru(NO)(salen-OH)Cl was prepared in acetonitrile and an aliquot of 3 mL was used for each individual experiment. The sample was photolyzed in a 4-sided, capped cuvette with a stir bar and was purged with argon, the sample was allowed to stir for 30 seconds after photolysis prior to taking the UV-visible spectra to allow the solution to equilibrate prior to measurement. The samples were irradiated at 365 nm with a mercury lamp. Ferrioxolate actinometry was used to calculate the photons of light emitted and the photolysis timing was controlled with a uniblitz optical shutter. The change in absorbance throughout the experiment were collected including the initial absorbance spectra.

The Ru(NO)(salen- CO_2CH_3)Cl had two new bands appear throughout photolysis at 358 nm and 613 nm. The wavelength λ = 613 nm was monitored for the appearance of the

photo product resulting in a Φ_{365} of 0.130 (± 0.04). The Ru(NO)(salen-OH)Cl compound in solution, similarly showed the growth of two absorbance bands during photolysis at 276 nm and 687 nm. The Φ_{365} was measured by monitoring at 687 nm which has no absorbance in the original solution. Therefore, the Φ_{365} of Ru(NO)(salen-OH)Cl was 0.081 (± 0.012).

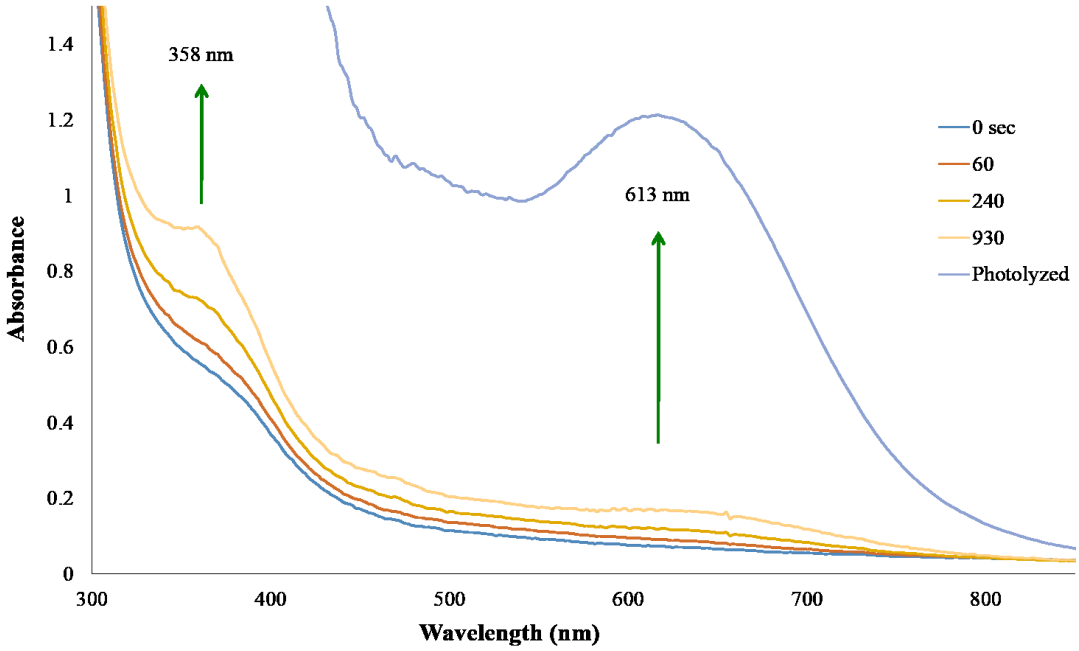

Figure ii.12. Solution of Ru(NO)(salen- CO_2CH_3)Cl in acetonitrile. Upon photolysis and generation of the photoproduct, the growth of two peaks at 358 nm and 613 nm.

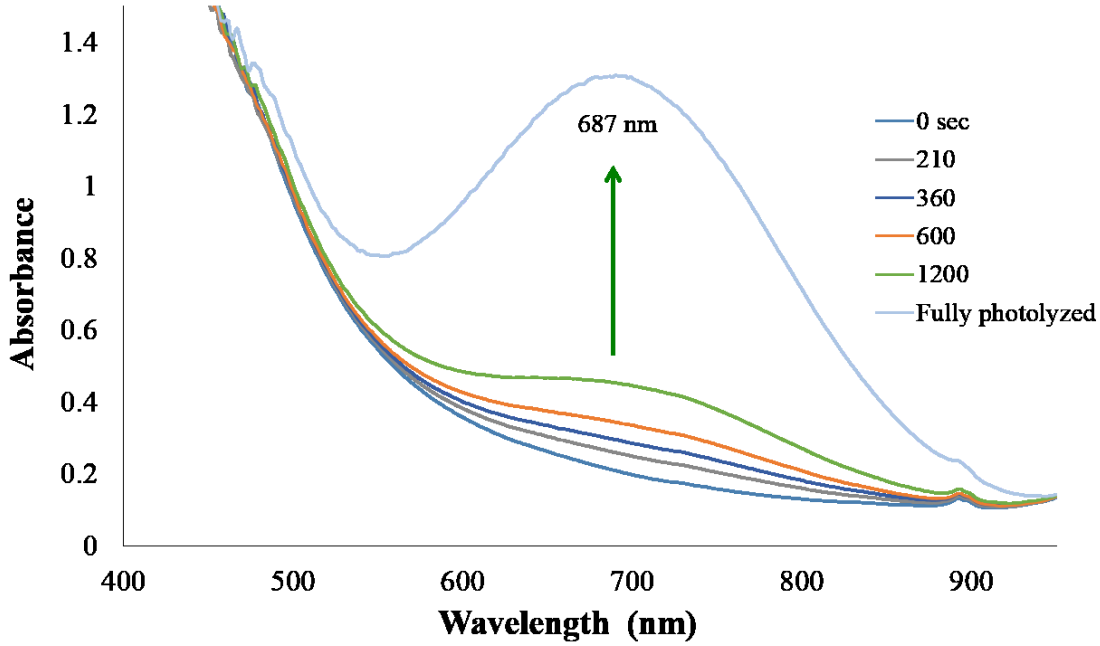

Figure ii.13. Solution of Ru(NO)(salen-OH)Cl in acetonitrile. Upon photolysis and generation of the photoproduct, the growth of a peak at 687 nm.

Aii.4.3 Conclusion for QY Studies

Quantum yield studies have been presented here for two compounds, Ru(NO)(salen-CO_2CH_3)Cl and Ru(NO)(salen-OH)Cl. As there are two products generated (the ruthenium-photo product and the nitric oxide) two methods for calculating QYs have been utilized under inert conditions with irradiation at 365 nm. The first method measured the moles of NO produced while the second method measured the spectral change and formation of the ruthenium photoproduct which has a unique spectra from the unphotolyzed species (depicted in Figures ii.12 and ii.13). The two methods resulted in QY values within standard deviation and are shown in Table ii.1.

	Ru(NO)(salen-CO_2CH_3)Cl	**Ru(NO)(salen-OH)Cl**
$\Phi_{365\ nm}$	0.13 ± 0.04 (monitoring 613 nm)	0.081 ± 0.012 (monitoring 687 nm)
$\Phi_{NO\ 365\ nm}$	0.111 ± 0.001	0.073 ± 0.001

Table ii.1. Quantum yield measurements at 365 nm under inert conditions measured by spectral changes ($\Phi_{365\ nm}$) or measured on the NOA by the release of nitric oxide ($\Phi_{NO\ 365nm}$).

Aii.5 References

[1] Budavari, S.; O'Neil, M.J.; Smith, A.; Heckelman, P.E.; "The Merck Index, an Encyclopediaof Chemicals, Drugs, and Biologicals- Eleventh Edition" Merck Co., Inc. Rahway, NJ, 1989.

[2] Stephenson, T. A.; Wilkinson, G.; "New complexes of Ruthenium (II) and (III) with triphenylphosphine, triphenylarsine, trichlorostannate, pyridine and orther ligands", *J. Inorg. Nucl Chem.*. 1966, **28**, 945-956.